*Article*

# Structures of Annulenes and Model Annulene Systems in the Ground and Lowest Excited States

**Cristina Gellini and Pier Remigio Salvi** ⋆

Dipartimento di Chimica, Università di Firenze, via della Lastruccia 3, 50019 Sesto Fiorentino (Firenze), Italy; E-Mail: cristina.gellini@unifi.it

⋆ Author to whom correspondence should be addressed; E-Mail: piero.salvi@unifi.it.

**Abstract:** The paper introduces general considerations on structural properties of aromatic, antiaromatic and non-aromatic conjugated systems in terms of potential energy along bond length alternation and distortion coordinates, taking as examples benzene, cyclobutadiene and cyclooctatetraene. Pentalene, formally derived from cyclooctatetraene by cross linking, is also considered as a typical antiaromatic system. The main interest is concerned with [$n$]annulenes and model [$n$]annulene molecular systems, $n$ ranging from 10 to 18. The rich variety of conformational and configurational isomers and of dynamical processes among them is described. Specific attention is devoted to bridged [10]- and [14]annulenes in the ground and lowest excited states as well as to $s$-indacene and biphenylene. Experimental data obtained from vibrational and electronic spectroscopies are discussed and compared with *ab initio* calculation results. Finally, porphyrin, tetraoxaporphyrin dication and diprotonated porphyrin are presented as annulene structures adopting planar/non-planar geometries depending on the steric hindrance in the inner macrocycle ring. Radiative and non-radiative relaxation processes from excited state levels have been observed by means of time-resolved fluorescence and femtosecond transient absorption spectroscopy. A short account is also given of porphycene, the structural isomer of porphyrin, and of porphycene properties.

**Keywords:** annulenes; aromaticity; antiaromaticity; symmetry; porphyrins

## 1. Introduction

Annulenes, *i.e.*, conjugated hydrocarbon monocycles of general formula $C_{2n}H_{2n}$, form a class of organic molecules for which the experimental ingenuity of synthetic chemistry [1–3] and the internal robustness of quantum chemistry [4,5] have fully displayed their best qualities. For instance, benzene has represented along the years one of the preferred reference systems in order to validate new *ab initio* theoretical procedures. Higher annulenes, on the other hand, have allowed to investigate about isomeric rearrangements by means of advanced experimental techniques [6] and theoretical methods [7–9]. Comprehensive treatments of annulene preparation, structure and properties are available in textbooks [4,10,11], thematic issues [12,13] and review articles [14,15].

According to the Hückel rule conjugated monocycles with $(4n + 2)$ $\pi$ electrons are more stable than the corresponding open-chain polyenes and should be associated with a set of structural and chemical properties (bond equalized geometries, substitution reactivity) collectively known as aromatic [4,10]. However, the experimental difficulties under which the next higher homologues of benzene, [10]- and [14]annulene, have been synthesized [1] and the ease of thermal rearrangements [6] are in stark contrast with the stability of the first component of the $(4n + 2)$ series. Additional steric factors related to the cycle geometry and size not explicitly considered by the Hückel theory obscure the energetic and structural manifestations of aromaticity. Therefrom two main strategies have been apparently developed. On one hand, aromaticity has been recovered lowering as much as possible the molecular flexibility by the introduction of chemical bridges between opposite ends of the annulene ring [16] or by replacement of double with triple bonds along the cycle [1]. On the other, the theoretical foundations responsible for the delocalized arrangement of the $\pi$ electrons in aromatic systems have been critically reexamined leading to the view of $\pi$ propensity to distortion in benzene and cyclobutadiene [17]. In addition, it has been found that the transition from bond equalized to bond alternating structures in $(4n + 2)$ $\pi$ systems, theoretically predicted long ago [18], may occur for rings of 30 C atoms [19] or lower [20].

Monocycles with $4n$ $\pi$ electrons are the second large group of conjugated hydrocarbons, the antiaromatic systems [21,22], characterized by the instability with respect to acyclic polyenes and the tendency toward bond alternating geometries [4]. Cyclobutadiene has been considered the reference antiaromatic system [23,24] though recently criticism has been advanced to this view [25,26]. Going up with the ring size, while cyclooctatetraene is characterized by a non planar arrangement of the four $\pi$ bonds [4,10,11], pentalene, where the ring is forced to planarity by crosslink [27,28], is equally well suited to model antiaromatic properties [29]. On the contrary, the more complex and formally antiaromatic structure of *s*-indacene peculiarly shows a bond equalized ring geometry [30,31].

It is the purpose of this review to report on the experimental and computational activity of our group in the field of aromatic as well as antiaromatic systems in the last years with particular attention to molecular structures of the ground and lowest excited states. Further, it has been thought to be useful to associate to our results an updated outline of the aromaticity/antiaromaticity theory [17] and a short description of isomeric structures up to [18]annulene [10,15,32,33]. The paper is organized in two Sections, one dedicated to basic aromatic/antiaromatic systems and the second to higher annulenes and model annulene systems to which the research activity of our group has mostly contributed.

## 2.  Archetypal Conjugated Monocycles: Cyclobutadiene, Benzene and Cyclooctatetraene

This Section deals with the three simplest monocyclic conjugated hydrocarbons, cyclobutadiene, benzene and cyclooctatetraene. These molecules may be considered as reference systems to introduce the structural properties of ring geometries characterizing also higher annulenes. Review articles on cyclobutadiene [23,24,26], benzene [34,35] and cycloctatetraene [36,37] are well known references of the past years.

### 2.1.  π-electron Approximation

In the $\pi$-electron approximation both the Hückel molecular orbital (HMO) method and the simple valence bond (VB) theory predict that displacing the planar cyclic structures from the bond equalized to the bond alternating configurations the ground state energy is lowered [38,39].

For instance, in the VB treatment of benzene [38] the two equivalent Kekule' structures $K_A$ and $K_B$ at the bond equalized $D_{6h}$ geometry are degenerate with energy $Q + (3/2)J_o$, $Q$ and $J_o$ being the classical VB coulomb and exchange integrals [40], respectively. The interaction between the $K_A$ and $K_B$ functions split their energies by $(9/10)J_o$ and $-(3/2)J_o$, thus giving origin to the ground and lowest excited states. The evolution from the bond equalized to the bond alternating structure, *i.e.*, the $D_{6h} \rightarrow D_{3h}$ process described by the displacement parameter $\delta$, increases the energy gap between the two states. For small $\delta$ values the two levels further shift by the amount $\pm(9/4)J_o\delta^2$. Therefore, since $J_o < 0$ the total $\pi$ energy of benzene in $D_{3h}$ geometry is lower in the ground and higher in the excited state than in the $D_{6h}$ geometry. Similar considerations apply to cyclobutadiene when distorted along the $D_{4h} \rightarrow D_{2h}$ trajectory. As it is summarized in **Table I, top**, the negative resonance energies of the two molecules, $J_o$ and $(9/10)J_o$, respectively, imply that the $\pi$-electron systems are stabilized with respect to the Kekule' structures. Nevertheless, the $\pi$ energies are lower in the bond alternating than in the bond equalized configuration.

In the Hückel theory the MO energies for monocycles $C_{2n}H_{2n}$ with conjugated double/single bonds [41] were adapted to the bond alternation case [38]

$$\epsilon_j = \pm\beta_o\sqrt{2\left[1 + \cos\left(\frac{2j\pi}{n}\right) + \delta^2\left(1 - \cos\left(\frac{2j\pi}{n}\right)\right)\right]} \qquad j = 0, 1, \ldots (n-1)$$

where $\beta_o < 0$ is the resonance integral. In this expression the $\pm$ and $j$ labels are combined to give rise to the $2n$ orbital energies. At $\delta = 0$ the traditional expression for the orbital energies of fully symmetrical monocycles is recovered. All $(4n + 2)$ $\pi$-electron rings have a closed shell ground state. On the other hand, $4n$ $\pi$-electron rings are open shell systems, due to the occurrence of two non bonding orbitals and to their occupancy with two electrons. The alternation shifts all bonding orbitals (except the lowest) downward and all antibonding orbitals (except the highest) upward so that the $\pi$ energy at $\delta \neq 0$ is lower than at $\delta = 0$. To first order in $\delta$, the shift dependence on bond alternation of the bonding and antibonding energies (except the lowest and the highest) is quadratic in $\delta$ for both $4n$ and $(4n + 2)$ $\pi$ systems. However, the non bonding orbitals of the $4n$ $\pi$ systems shift linearly with $\delta$. As a result the variation of the $\pi$ energy, $\Delta E_\pi$, with $\delta$ is different for cyclobutadiene and benzene as reported in **Table 1, bottom**.

**Table 1.** Valence bond (VB) and molecular orbital (MO) energies of cyclobutadiene and benzene [38,39]. Upper, VB theory: under $K_A$, $K_B$; energies of the Kekule' structures at the most symmetrical geometries, $D_{4h}$ for cyclobutadiene and $D_{6h}$ for benzene; under $G$; $E_\pi(0)$ ground state $\pi$ energy after $K_A$, $K_B$ mixing at the undistorted geometries, $D_{4h}$ and $D_{6h}$, respectively, $\Delta E_\pi(\delta)$ $\pi$ energy change as a function of the displacement parameter $\delta$; under $Exc$; the same quantities for the excited state. $Q$, $J_0$, coulomb and exchange integrals, both negative [40]. Lower, MO theory: under $E_{b.eq.}$, $\pi$ energies of cyclobutadiene and benzene in the Hückel approximation; under $\Delta E_\pi(\delta)$, $\pi$ energy change as a function of the displacement parameter $\delta$; under $\Delta E_\sigma(\delta)$, $\sigma$ energy change as a function of the displacement parameter $\delta$. $\beta_0$, $\beta_0'$ resonance integral and slope at the symmetrical configuration; $k$, force constant of the CC $\sigma$ bond.

| | | VB theory | | | | |
|---|---|---|---|---|---|---|
| | $K_A$; $K_B$ | | $G$ | | $Exc$ | |
| | | $E_\pi(0)$ | $\Delta E_\pi(\delta)$ | | $E_\pi(0)$ | $\Delta E_\pi(\delta)$ |
| $C_4H_4$ | $Q + J_0$ | $J_0$ | $3J_0\ \delta^2$ | | $-3J_0$ | $-3J_0\ \delta^2$ |
| $C_6H_6$ | $Q + \frac{3}{2}J_0$ | $\frac{9}{10}J_0$ | $\frac{9}{4}J_0\ \delta^2$ | | $-\frac{3}{2}J_0$ | $-\frac{9}{4}J_0\ \delta^2$ |

| | MO theory | | |
|---|---|---|---|
| | bond equalized $\rightarrow$ bond alternating configuration | | |
| | $E_{b.eq.}$ | $\Delta E_\pi(\delta)$ | $\Delta E_\sigma(\delta)$ |
| $C_4H_4$ | $4\,\beta_0$ | $4\,\beta_0\,\lvert\,\delta\,\rvert$ | $2k(\beta_0/\beta')^2\delta^2$ |
| $C_6H_6$ | $8\,\beta_0$ | $6\,\beta_0\delta^2$ | $3k(\beta_0/\beta')^2\delta^2$ |

## 2.2.   *The Role of σ Electrons*

Comparing the VB and MO data on benzene it is seen that the $\pi$ energies depend in both cases on $\delta^2$. In the harmonic approximation the quadratic dependence holds also for the $\sigma$ energy [39]. The relative weight of the $\sigma$ and $\pi$ contributions to the total energy determines the condition under which the delocalized structure is the ground state minimum. Since in the Hückel approximation $E_{tot}(\delta) = E_\sigma(\delta) + E_\pi(\delta)$, the following expression is obtained for benzene [39]

$$E_{tot}(\delta) = E_{tot}(0) + 3\mid\beta_o\mid[k\mid\beta_o\mid/(\beta_o')^2 - 2]\delta^2$$

where the subscript index $o$ refers to the equilibrium geometry of the delocalized structure, $k > 0$ is the stretching force constant of the CC $\sigma$ bond and $\beta_o' = (d\beta/d\delta)\mid_o$ is the slope of $\beta$ at equilibrium. From this expression a criterion may be established: if $k\mid\beta_o\mid/(\beta_o')^2 - 2 > 0$ benzene takes on the delocalized $D_{6h}$ geometry while in the opposite, $k\mid\beta_o\mid/(\beta_o')^2 - 2 < 0$, benzene shifts to the localized $D_{3h}$ geometry. Since for benzene this quantity is positive [39], the $D_{6h}$ structure is the equilibrium geometry. Thus, for a given $\beta_o$ and $\beta_o'$ the ultimate reason of the bond equalized geometry of benzene is the high rigidity of the $\sigma$ skeleton. Applying the same treatment to cyclobutadiene, the distortion to geometries less symmetrical than $D_{4h}$ follows directly within the HMO model. In fact, the total ground state energy

at $\delta \neq 0$ of cyclobutadiene and, more in general, of $4n$ $\pi$-electron systems contains a linear term in $\delta$ as seen in **Table 1**. This means that all these systems are prone to distortion in their fully symmetrical geometries. The distortion in $(4n + 2)$ $\pi$-electron rings is less obvious. Increasing the annulene size $n$, the HOMO-LUMO energy gap becomes smaller and as a result also the energy difference between the ground and the lowest excited state. Due to second order Jahn-Teller effect [42], electronic states close to each other may interact and for $n$ sufficiently large a structure with bond alternation may be energetically advantageous even for the higher annulenes satisfying the Hückel rule [43,44].

Following early recognitions of the propensity of $\pi$ electrons to distortivity [18,45], the rather surprising statement was advanced in a series of important papers [17,46–53]. The delocalized structure of benzene was seen as intermediate configuration between the localized $K_A$ and $K_B$ structures in the bond exchange process $K_A \rightarrow K_B$ along the distortion mode where CC stretchings alternate with CC shrinkings. As illustrated in **Figure 1**, there are two possibilities for this process. On the left, the high energy gap between ground $K_A$, $K_B$ and excited $K_B^*$, $K_A^*$ states leads to localization of double bonds. If the gap is small as in **Figure 1b**, the delocalized geometry is preferred. The vertical gap $(VG)$ is related to the energy required to unpair the $\pi$ electrons, which is roughly three times the singlet-triplet excitation energy of the C=C system [49]. Then, a strong bond favors localization while a weak bond favors delocalization. Since the C=C bond is relatively strong it was concluded [48] that the $\pi$ electrons are distortive in benzene and that the crucial factor for symmetrization is the $\sigma$ propensity to bond equalization.

**Figure 1.** The bond exchange process between the two alternating structures of benzene: $K_A$, $K_B$ ground state $(G)$ structures; $K_A^*$, $K_B^*$ excited state $(E)$ structures conserving electron pairing. $\Psi_G$ and $\Psi_E$: wave functions after $K_A$ and $K_B$ mixing. Light and heavy lines: unperturbed and perturbed energy profiles. For the sake of clarity the correlation diagrams between the Kekule' structures have been assumed to be linearly dependent on the bond alternating coordinate $\delta$. Bond alternating (**1a**) and bond equalized (**1b**) structures are stabilized according to the height of the vertical gap $(VG)$. $QMRE$: quantum mechanical resonance energy, equal in both cases.
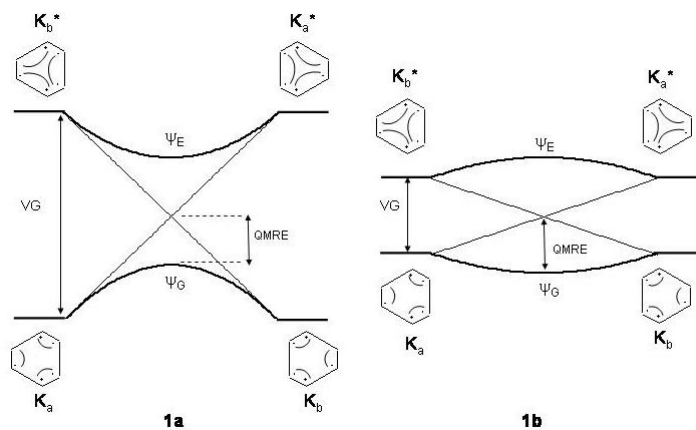


Several *ab initio* strategies have been applied in order to confirm the qualitative model [17,50,51,53]. The total distortion energy $\Delta E_{\pi\sigma}$ was partitioned into components, $\Delta E_{\pi\sigma} = \Delta E_\sigma + \Delta E_\pi$, displacing

the C atoms in such a manner that the nuclear repulsion term between these atoms is independent of distortion. The pure $\sigma$ contribution $\Delta E_\sigma$ was determined either for the $\pi$-septuplet state of benzene (where the $\pi$ delocalization is intentionally eliminated) or for the bare $\sigma$ framework $(C^+)_6H_6$. Since $\Delta E_{\pi\sigma}$ of benzene is easily calculated, the comparison shows that $\Delta E_\sigma > \Delta E_{\pi\sigma} > 0$ and therefore that $\Delta E_\pi$ adds negatively to $\Delta E_\sigma$. The restoring tendency to symmetrization decreases when $\pi$ electrons are present [17]. The same conclusion was reached also starting from different partition schemes where the nuclear repulsion term is not kept constant [54]. As to cyclobutadiene, $\Delta E_{\pi\sigma}$ is negative and $\Delta E_\sigma$ positive [49]. It follows that $\Delta E_\pi$ is negative and $| \Delta E_\pi | > \Delta E_\sigma$. The rigidity of the $\sigma$ framework is not sufficient to constrain cyclobutadiene to a square geometry and the molecule shifts toward a rectangular geometry in the ground state. The quantities $\Delta E_{\pi\sigma}$, $\Delta E_\sigma$ and $\Delta E_\pi$ for the two molecules are collected in **Table 2**, shown later on for sake of clarity. The response to distortion is qualitatively illustrated in **Figure 2**. For benzene, the negative $\Delta E_\pi$ curvature at the symmetrical equilibrium configuration is overcompensated by the positive curvature of $\Delta E_\sigma$; the opposite occurs for cyclobutadiene.

> **Figure 2.** Schematic representation of the $\sigma$ and $\pi$ response to distortion in benzene (left) and cyclobutadiene (right). $\Delta E_\sigma$ and $\Delta E_\pi$ are the energy changes as a result of the bond alternating distortion and $\Delta E_{\pi\sigma} = \Delta E_\sigma + \Delta E_\pi$.
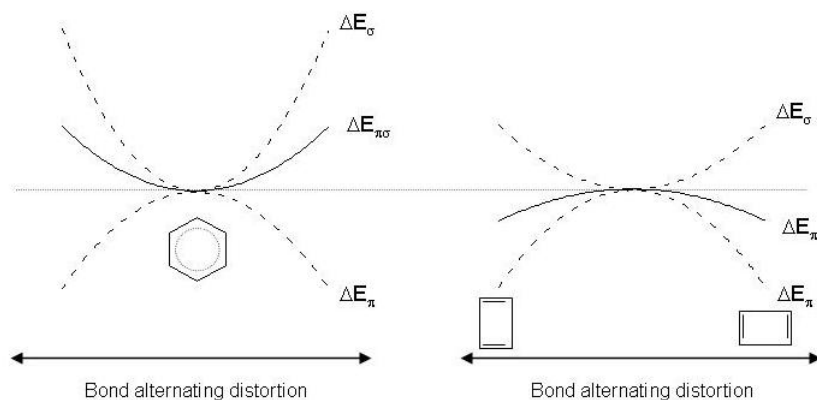


### 2.3. Quantum Mechanical and Thermochemical Resonance Energy

The stability of the $(4n + 2)\pi$-electron conjugated monocycles and instability of the $4n\pi$ counterparts is commonly expressed by the Hückel rule [4,10]. A strong support to this rule is given by the chemical stability of benzene and by the elusive nature of cyclobutadiene. The Hückel rule has therefore become one of the most powerful paradigms of chemistry: aromatic species are associated with (i) delocalized arrangements of the $\pi$ electrons, (ii) bond equalized geometries and (iii) special stability relative to an open-chain polyenic reference with the same number of C atoms [55–57]. In the converse, antiaromatic species are associated with bond localization/alternation and high reactivity [21]. A correlation has been assumed between $\pi$ delocalization and geometry and this has led to the concept that geometries with equal bond lengths, such as in benzene, are due to the inherent tendency of the $\pi$ electrons to delocalization. As this view is opposed by theoretical evidences about the $\pi$ propensity to distortion in benzene and in cyclobutadiene [17,48–51,53], arguments were advanced to reconcile the new structural

approach with the Hückel rule and with well-known aromatic properties including thermochemical stability and substitution reactivity. This essential point has been discussed in detail [17] and will be shortly reviewed in the following paragraphs. To this purpose let us first recall the types of resonance energies pertinent to the discussion.

The quantum mechanical resonance energy ($QMRE$) is the energy lowering due to the linear mixing of the $K_A$ and $K_B$ wave functions with respect to the energy of the Kekule' structures at the same nuclear geometry. As made evident in **Figure 3**, no $\pi$ conjugation among C=C bonds is associated with the Kekule' structures. The $QMRE$'s of cyclobutadiene and benzene are largely different, being for instance $QMRE(C_4H_4) \approx (1/3) QMRE(C_6H_6)$ in a VBSCF/6-31G calculation [17]. The difference reflects the essence of the Hückel rule and indicates that $\pi$ delocalization in benzene is favored over $\pi$ delocalization in cyclobutadiene.

**Figure 3.** Quantum mechanical energy resonance ($QMRE$) in benzene and cyclobutadiene at the bond equalized geometries of $D_{6h}$ and $D_{4h}$ symmetry, respectively (VBSCF/6-31G calculation [17]).
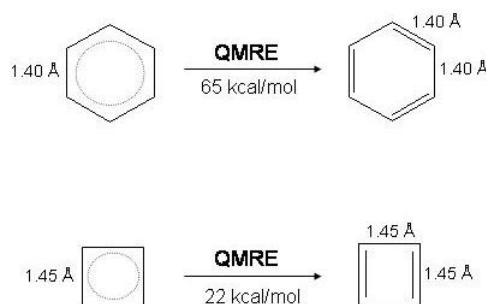


A second resonance energy is adiabatic ($ARE$) where the Kekule' structures at the bond-equalized geometries are substituted by the optimized bond-alternating geometries in absence of all $\pi$ conjugation. Taking as example benzene in **Figure 4**, $ARE$ and $QMRE$ are related according to the equation [58]

$QMRE = ARE + E_c$

where $E_c$ is the compression energy from the non-conjugated optimized to the non-conjugated bond-equalized geometry.

Finally, the thermochemical, Dewar-type, resonance energy ($TRE$) is defined as the energy difference between the conjugated monocycle and an appropriate reference system $R$ [59–63]. In the present case $R$ is the hypothetical cyclic hexatriene or cyclic butadiene with the same amount of $\pi$-conjugation as in the open-chain polyene, as sketched in **Figure 5**. $TRE$ is referred to also as aromatic stabilization energy ($ASE$) for benzene [58] while it is a sum of two contributions for cyclobutadiene, the (negative) $ASE$ term due only to the antiaromatic destabilization and the angular strain term [64]. Since the resonance energies of open polyenes depend linearly on the number $n$ of conjugative interactions between formal double bonds [65], $ASE$ may be evaluated by subtracting the contribution of the hypothetical reference molecule from $ARE$ [4,58]

$ASE = ARE - n$ x $ARE$ (butadiene)

where $n = 2, 3$ for cyclic butadiene and hexatriene, respectively.

**Figure 4.** Relation between $ARE$ and $QMRE$ in benzene. $E_c$ represents the compression energy from the non-conjugated optimized to the non-conjugated bond-equalized geometry.
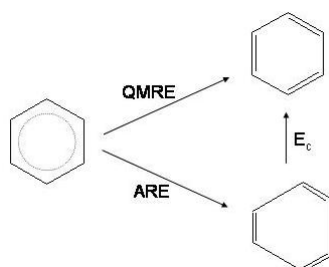


**Figure 5.** Thermochemical resonance energy ($TRE$) of benzene and cyclobutadiene with respect to the cyclic reference of polyenic origin, *i.e.*, cyclic hexatriene and cyclic butadiene.
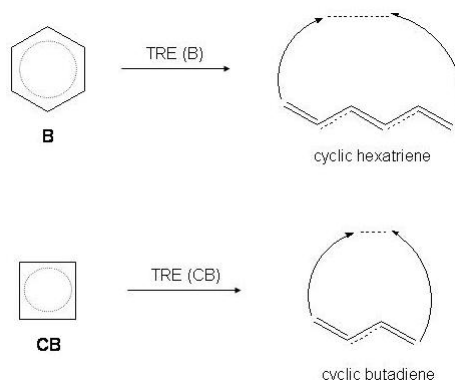


Empirical estimates of resonance energies are obtained by means of isodesmic and homodesmotic reactions [66,67] or heats of formation [68,69]. The isodesmic reaction $C_6H_6 + 6CH_4 \rightarrow 3(H_2C = CH_2) + 3(H_3C - CH_3)$, having equal numbers of formal single and double CC bonds in reactants and products, gives an approximate determination of $ARE$ ($C_6H_6$) since it compares the energy of benzene with that of three ethylene molecules. In a homodesmotic reaction the previous condition is strengthened, further demanding for reactants and products equal numbers of (i) C atoms in the same hybridization state and (ii) $sp^2$ and $sp^3$ C atoms with one, two or three hydrogen atoms attached. Examples of homodesmotic reactions for benzene and cyclobutadienes are reported in **Figure 6** where the cyclic standards are 3 and 2 molecules, respectively, of *s-trans-* or *s-cis*-butadiene.

Due to the proper number of conjugative interaction in the acyclic reference, the enthalpies of these reactions are easily related to $ASE$. In the case of benzene, $ASE$ is 21.6 kcal/mol and 28.8 kcal/mol with respect to *s-trans-* and *s-cis*-butadiene, respectively [58,68]. $ASE$ (cyclobutadiene) has been recently investigated in detail and determined to be -42 kcal/mol and -37 kcal/mol with respect to *s-trans-* and *s-cis*-butadiene [64]. It has been further noted that the intrinsic $ASE$ value of cyclobutadiene, *i.e.*, resulting from separating the $\pi$ repulsion effect from the total $ASE$ with respect to the *s-cis*-butadiene is -12 kcal/mol [64].

**Figure 6.** Examples of homodesmotic reactions of benzene and cyclobutadiene.
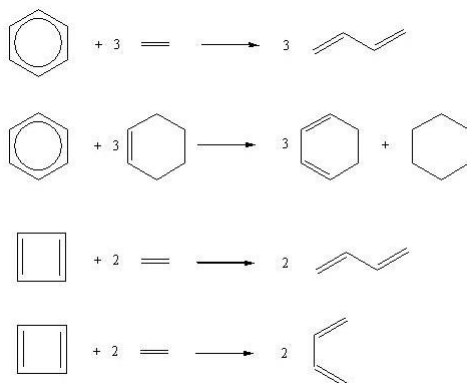


Going back to the point in discussion, $TRE$ may be derived [17] coupling the $\pi$-distortive model of benzene and cyclobutadiene with a thermochemical cycle involving benzene/cyclobutadiene ($B$; $CB$), distorted benzene / distorted cyclobutadiene ($DB$; $DCB$), Kekule' structures of distorted benzene /cyclobutadiene ($DKB$; $DKCB$) and the reference molecule $R$, *i.e.*, cyclic hexatriene/cyclic butadiene. Consider the cycle for benzene in **Figure 7**, upper. In the first step, $B \rightarrow DB$, the $D_{6h}$ structure is distorted to $D_{3h}$ structure and the energy change is $\Delta E_{\pi\sigma}$. Therefore $\Delta E_1 = \Delta E_{\pi\sigma} = 7.2$ kcal/mol from **Table 2**.

**Table 2.** Summary of distortion energies $\Delta E_\sigma$, $\Delta E_\pi$, $\Delta E_{\pi\sigma} = \Delta E_\sigma + \Delta E_\pi$, quantum mechanical resonance energies [$QMRE$, cyclobutadiene and benzene; $QMRE(D)$, distorted cyclobutadiene and distorted benzene; $QMRE(R)$, reference, cyclic butadiene and cyclic hexatriene], relaxation energy $\Delta E_{rel}$ and thermochemical resonance energy $TRE$ (all values in kcal/mol, VBSCF/6-31G calculation [17]).

|        | $\Delta E_\sigma$ | $\Delta E_\pi$ | $\Delta E_{\pi\sigma}$ | $QMRE$ | $QMRE(D)$ | $QMRE(R)$ | $\Delta E_{rel}$ | $TRE$ |
|--------|------|-------|------|------|------|------|-------|-------|
| $C_4H_4$ | 7.0 | −10.4 | −3.4 | 22. | 8.3 | 17.9 | −57.0 | −70.0 |
| $C_6H_6$ | 16.3 | −9.1 | 7.2 | 65. | 39.9 | 26.7 | | 20.4 |

In the second, $DB \rightarrow DKB$ at the $DB$ geometry, $\Delta E_2 = QMRE(DB) = 39.9$ kcal/mol [17]. The third step, from $DKB$ to the reference molecule, restores partially the $\pi$-conjugation. Since $QMRE$ of polyenes is found to be nearly additive, the resonance energy of the reference molecule, which is cyclic hexatriene, is 3/2 that of hexatriene, 26.7 kcal/mol [17]. Therefore, $\Delta E_3 = -QMRE(R) = -26.7$ kcal/mol. Overall, $TRE(B) = \Delta E_1 + \Delta E_2 + \Delta E_3 = 20.4$ kcal/mol, in agreement with the accepted $TRE$ value [4,68].

In the analogous cycle for cyclobutadiene, **Figure 7** lower, $DKCB$ and $R$ ( see **Figure 5**) are substantially different structures for in one case, $DKCB$, (i) the $\pi$ bonds face one another and (ii) the ring is strained while in the second, $R$, the first effect is greatly reduced and the second is absent. In the third step not only partial $\pi$ restoration occurs with resonance energy 17.9 kcal/mol [48] but

in addition a relaxation term must be considered due to the decrease of the two effects. All recently reported values of angular strain are between 32 and 35 kcal/mol [64,70–72]. $\Delta E_{rel}$ is estimated to be largely negative, $-59$ kcal/mol from the strain energy of 34 kcal/mol [64] and the repulsion energy between $\pi$ bonds of 25 kcal/mol c. Then, $\Delta E_3 = -QMRE(R) + \Delta E_{rel} = -76.9$ kcal/mol. The other two terms are $\Delta E_1 = \Delta E_{\pi\sigma} = -3.4$ kcal/mol (from **Table 2**) and $\Delta E_2 = QMRE(DCB) = 8.3$ kcal/mol [17]. It results $TRE(CB) = \Delta E_1 + \Delta E_2 + \Delta E_3 = -72.0$ kcal/mol, in good agreement with the reported value of $TRE$ [17]. Further, if the strain and $\pi$ repulsion energies are left aside, the portion of $TRE(CB)$ associated with delocalization is only -13 kcal/mol, closely matching the intrinsic $ASE(CB)$ value [64]. The thermochemical instability (with respect to the reference molecule) of $CB$ is related to the instability of the Kekule' structure and not to absence of $QMRE$ at the square geometry. The distortive $\pi$ propensity of benzene and cyclobutadiene is consistent with the stability/instability of the hexagonal/square geometry with respect to the reference molecules [49].

**Figure 7.** The thermochemical cycle for benzene ($B$, upper) and cyclobutadiene ($CB$, lower): $DB/DCB$ distorted $B/CB$; $DKB/DKCB$ Kekule' structures of distorted $DB/DCB$ (see text for explanation of these acronyms); $R$ reference molecule, cyclic hexatriene and cyclic butadiene. $TRE$ and $QMRE$: thermal and quantum mechanical resonance energies. $\Delta E_{rel}$: relaxation energy due to angle strain and $\pi$ overlap in cyclobutadiene; this term is not considered for benzene [17]. The energy values (kcal/mol) characterizing the thermochemical cycle of benzene and cyclobutadiene are indicated.
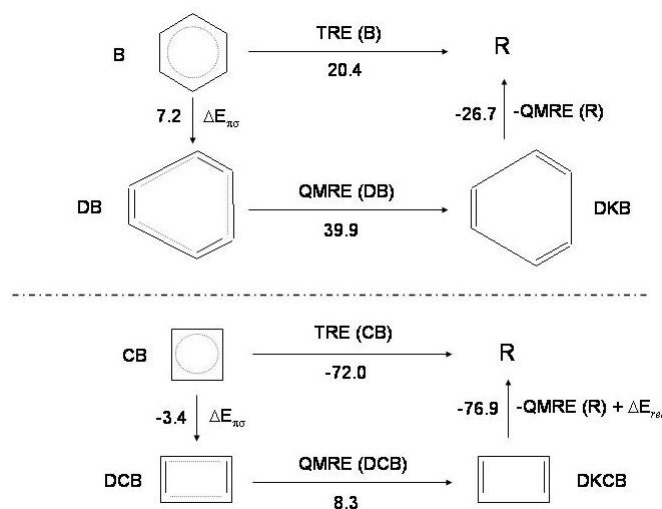


Because of the $\sigma$-imposed rigidity of the C framework, benzene has geometries restricted to those close to perfect hexagons even at non-equilibrium configurations. Since the resonance energy is only moderately affected by small displacements from $D_{6h}$ symmetry, the aromatic stability is conserved in all experiments probing near equilibrium properties such as reactivity, UV spectroscopy and magnetism. Much less common are experiments on $\pi$-distortivity. The unusually low infrared frequency of the $b_{2u}$ bond alternating mode was an early evidence of $\pi$-distortivity related to the fact that the $b_{2u}$ vibrating molecule spends a non vanishing fraction of time distorted as cyclohexatriene [45]. More recently, two-photon spectroscopy on the lowest excited $B_{2u}$ state has supported this conclusion [73–75]. As

the frequency of the $b_{2u}$ mode, which is strongly active as vibronically induced two-photon $B_{2u} \times b_{2u}$ transition, is considerably increased with respect to the ground state value, this result fits nicely the model of **Figure 1** since the $\pi$ curvature adds to the $\sigma$ curvature in the $B_{2u}$ state while subtracts in the ground state. This behaviour is documented also for other aromatic hydrocarbons [76–83].

### 2.4.   Cyclobutadiene: Ground and Lowest Excited States

Cyclobutadiene in Square Geometry

In the MO theory the four $\pi$ orbitals of square $D_{4h}$ cyclobutadiene are classified into the $a_{2u}$, $e_g$ and $b_{1u}$ symmetry species in order of increasing nodal planes [84,85]. All the MO's are determined by symmetry with the two degenerate $e_g$ orbitals characterized by one nodal plane and distributed either over the whole ring, $\phi_2$ and $\phi_3$, or, equivalently, localized on opposite ring atoms, $\phi'_2$ and $\phi'_3$ .

**Figure 8.** Upper: $\pi$ molecular orbitals of cyclobutadiene with energies, symmetry labels ($D_{4h}$ symmetry) and representation in terms of atomic $p_z$ orbitals. Lower: valence bond configurations contributing to the low energy states of cyclobutadiene.
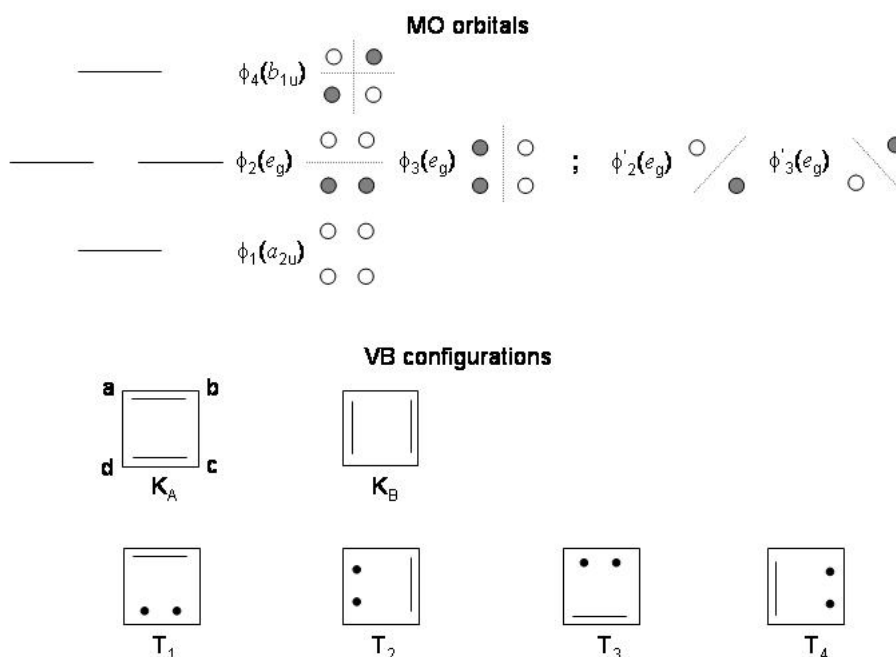


The two alternatives are shown in the schematic representation of **Figure 8**. The four $\pi$ electrons fill the lowest $a_{2u}$ orbital and partly the $e_g$ pair. With two orbitals containing altogether two electrons, six electronic configurations are possible, $| \phi_2\overline{\phi_2} |$, $| \phi_3\overline{\phi_3} |$, $| \phi_2\overline{\phi_3} |$, $| \overline{\phi_2}\phi_3 |$, $| \phi_2\phi_3 |$, $| \overline{\phi_2}\overline{\phi_3} |$. Since the $a_{2u}$ orbital is doubly occupied, the $a_{2u}^2 \times e_g^2$ representation is reduced to $^1A_{1g} + {}^3A_{2g} + {}^1B_{1g} + {}^1B_{2g}$. The four states, expressed in terms of only the $\phi_2$ and $\phi_3$ orbitals, *i.e.*, omitting for simplicity the inner $\sigma$ electrons and the lowest $a_{2u}$ orbital, and the corresponding HF energies are [85]

$$\Phi(^3A_{2g}) = (\phi_2\phi_3 - \phi_3\phi_2)(\alpha\beta + \beta\alpha) \qquad E(^3A_{2g}) = J_{23} - K_{23}$$

$$\Phi(^1B_{2g}) = (\phi_2\phi_3 + \phi_3\phi_2)(\alpha\beta - \beta\alpha) \qquad E(^1B_{2g}) = J_{23} + K_{23}$$
$$\Phi(^1B_{1g}) = (\phi_2^2 - \phi_3^2)(\alpha\beta - \beta\alpha) \qquad E(^1B_{1g}) = J_{22} - K_{23}$$
$$\Phi(^1A_{1g}) = (\phi_2^2 + \phi_3^2)(\alpha\beta - \beta\alpha) \qquad E(^1A_{1g}) = J_{22} + K_{23}$$

where $\Phi(^3A_{2g})$ is the $M_s = 0$ component of the triplet state. Since coulomb and exchange two-electron repulsion integrals are always positive, $\Phi(^3A_{2g})$ lies below $\Phi(^1B_{2g})$ and $\Phi(^1B_{1g})$ below $\Phi(^1A_{1g})$; further, since $J_{22} > J_{23}$, $\Phi(^3A_{2g})$ is the lowest state and $\Phi(^1A_{1g})$ the highest among the four states. It may be also verified [85] that $E(^1B_{1g}) < E(^1B_{2g})$ when $\phi_2$ and $\phi_3$ are expressed in terms of the localized orbitals $\phi_2'$ and $\phi_3'$, *i.e.*, $\phi_{2,3}' = (1/\sqrt{2})[\phi_2 \pm \phi_3]$.

In the VB formalism the two lowest singlet states are described by mixing the two Kekule' configurations $K_A$ and $K_B$. Given the $a$, $b$, $c$, and $d$ atomic orbitals, $K_A$ and $K_B$ are expressed as

$$\phi_{ab,cd} \equiv K_A = \mathcal{A}[abcd(\alpha\beta - \beta\alpha)(\alpha\beta - \beta\alpha)]$$
$$\phi_{ad,bc} \equiv K_B = \mathcal{A}[adbc(\alpha\beta - \beta\alpha)(\alpha\beta - \beta\alpha)]$$

where $\mathcal{A}$ is the antisymmetry operator. Their variational mixing leads to the $^1B_{1g}$ state as the minus and to the $^1A_{1g}$ state as the plus combination

$$\Phi(^1B_{1g}) = K_A - K_B$$
$$\Phi(^1A_{1g}) = K_A + K_B$$

Four equivalent configurations with one $\pi$ bond broken (see **Figure 8**) contribute to the two lowest triplet states. For instance, the $T_1$ configuration is defined as

$$\phi_{ab} \equiv T_1 = \mathcal{A}[abcd(\alpha\beta - \beta\alpha)(\alpha\alpha)]$$

and similarly for the other three triplet configurations $T_2$, $T_3$, $T_4$. Two states, $^3A_{2g}$ and $^3E_u$, result from the linear combination of the four configurations

$$\Phi(^3A_{2g}) = T_1 + T_2 + T_3 + T_4$$
$$\Phi(^3E_u) = T_1 - T_3 \; ; \; T_2 - T_4$$

since only three linearly independent combinations are possible for a system of four electrons in four orbitals [40]. Overall, the singlet pair, *i.e.*, one resonant $^1B_{1g}$ and one antiresonant $^1A_{1g}$ state, and the triplet pair, *i.e.*, one resonant $^3A_{2g}$ and one antiresonant $^3E_u$ state, are obtained. Considering that $E(T_1) > E(\phi_{ab,cd})$ and reasonably assuming that the resonance energy of the $^3A_{2g}$ triplet is not much greater than that of the $^1B_{1g}$ singlet, the ground state is predicted to be singlet and the first excited state to be triplet [85]. Qualitatively, both theories account for low-lying $^1B_{1g}$ and $^3A_{2g}$ states, however in reverse order. The relative energies of **Table 3** obtained from *ab initio* SCF calculations [85] are in agreement with these considerations and indicate that at the HF/VB calculation level the lowest state of square cyclobutadiene is $1^3A_{2g}/1^1B_{1g}$.

Let us now consider the effect of configuration interaction on the MO energies of the singlet $1^1B_{1g}$ and triplet $1^3A_{2g}$ states. Singly-excited configurations within the $\pi\pi^*$ space may arise from three different promotions, $a_{2u}^2 \to a_{2u}^1b_{1u}^1$ , $a_{2u}^2e_g^2 \to a_{2u}^1e_g^3$ and $e_g^2 \to e_g^1b_{1u}^1$. The only excited states interacting with the

$1^1A_{1g}$, $1^3A_{2g}$, $1^1B_{1g}$, $1^1B_{2g}$ states originate from the single $a_{2u}^2 \rightarrow a_{2u}^1 b_{1u}^1$ excitation, being $a_{2u}^1 \times e_g^2 \times b_{1u}^1$ = $A_{1g} + A_{2g} + B_{1g} + B_{2g}$. Out of the total 24 $a_{2u}^1 \times e_g^2 \times b_{1u}^1$ configurations, 16 have a single occupancy of each $\pi$ orbital and 8 a double occupancy of one of the two $e_g$ orbitals (and zero of the other) [92]. The 16 configurations are combined to six states, $^5B_{1g}$, $2^3B_{1g}$, $^3A_{2g}$, $^1B_{1g}$, $^1A_{2g}$ while the other 8 configurations to four states, $2^1A_{1g}$ and $2^3B_{2g}$. The lowest triplet, $1^3A_{2g}$, interacts with one singly excited state $^3A_{2g}$ and the lowest singlet, $1^1B_{1g}$, with one singly excited $^1B_{1g}$ state. Since the corresponding matrix elements differ approximately by a $\sqrt{3}$ factor in favor of the lowest singlet [93], the stabilization energy of $1^1B_{1g}$ is three times that of $1^3A_{2g}$ and may be larger than the unperturbed $\mid E(1^1B_{1g}) - E(1^3A_{2g}) \mid$ energy gap. In principle, the singlet $1^1B_{1g}$ may become the ground state for square cyclobutadiene, thus settling the difference with the VB results. As to the other pair of states, $1^1B_{2g}$ and $1^1A_{1g}$, no $^1B_{2g}$ within the $\pi\pi^*$ space is available for interaction while $1^1A_{1g}$ may interact with the pair of singly-excited $^1A_{1g}$ states. The $^1A_{1g}$ energy may decrease until inversion with respect to $SCF$ results. In fact, there is a large number of calculations made with increasingly refined methods, from full $\pi$-CI to MC/CASSCF to MRCC, which corroborate the two predictions [85–91,93,94]. It may be seen from **Table 3** that $1^1B_{1g}$ lies 6 - 10 kcal/mol below $1^3A_{2g}$ and that $1^1A_{1g}$ is energetically lower than $1^1B_{2g}$.

**Table 3.** Energies (kcal/mol) of the lowest excited states of square cyclobutadiene relative to that of $1^1B_{1g}$.

|          | SCF[a] | GRVB[a,b] | $\pi$-CI[c] | $\pi$-CI[d] | $\pi$-CI[e] |
|----------|--------|-----------|-------------|-------------|-------------|
| $^1A_{1g}$ | 57.1   | 55.2      | 53.2        | 49          | 50          |
| $^1B_{2g}$ | 52.0   | –         | 50.2        | 74          | 83          |
| $^1B_{1g}$ | 0      | 0         | 0           | 0           | 0           |
| $^3A_{2g}$ | –4.4   | 12.9      | –4.4        | 6.4         | 10.2        |

|          | MCSCF[f] | MCSCF[g] | MRCCSD(T)[h] | MR-AQCC[i] |
|----------|----------|----------|--------------|------------|
| $^1A_{1g}$ | 55.3     | 55.8     | 40.9         | 30.7       |
| $^1B_{2g}$ | 80.6     | 95.4     | 52.6         | 41.6       |
| $^1B_{1g}$ | 0        | 0        | 0            | 0          |
| $^3A_{2g}$ | 15.9     | 12.6     | 6.9          | 5.4        |

[a] Dunning double-$\zeta$ basis set [85]. [b] Generalized Resonating Valence Bond; $1B_{2g}$ state described by ionic configurations (not considered in [85]). [c] limited $\pi$-CIS; 3-21G basis set [86]. [d] full $\pi$-CI; 6-31G* basis set [87]. [e] full $\pi$-CI; Dunning double-$\zeta$ basis set [85]. [f] Dunning double-$\zeta$ basis set [88]. [g] CAS(4,4); 6-31G basis set [89]. [h] Multireference coupled cluster calculation with single and double excitations augmented non-iteratively by triple excitations; DZP basis set [90]. [i] Multireference average-quadratic coupled cluster calculation; aug'-cc-pVTZ basis set [91].

The stabilization of $1^1B_{1g}$ state with respect to $1^3A_{2g}$ in the configuration interaction approach is also known as dynamic spin polarization of cyclobutadiene [93]. Shortly, the spin polarization of the two paired $a_{2u}^2$ electrons depends on the spin state of the two unpaired $e_g$ electrons. Resorting to the $\phi_2'$ and $\phi_3'$ description of the $e_g$ orbitals it may be seen [93] that when two antiparallel electrons occupy $\phi_2'$ and $\phi_3'$ the $a_{2u}$ electrons are easily polarized by mixing $a_{2u}$ with the antibonding $b_{1u}$ MO. On the contrary,

with parallel electrons in $\phi_2'$ and $\phi_3'$ virtual orbitals of much higher energy are required for mixing, giving a smaller polarization contribution to the lowering of the $1^3A_{2g}$ energy.

Structural Instabilities

Molecular geometries of non-degenerate electronic states may be unstable due to coupling with higher excited states through non-totally symmetric distortions [42,43]. The effect has been called second-order (or vibronic) Jahn-Teller effect and is distinguished from the first-order effect, relative to degenerate states [95]. For instance, the $1^1B_{1g}$ state of square cyclobutadiene couples with $1^1A_{1g}$ when the molecule is distorted along the rectangular $b_{1g}$ mode consisting of adjacent in- and out-of-phase CC bond stretchings around the ring. For a sufficiently strong coupling term the square $(D_{4h}) \rightarrow$ rectangular $(D_{2h})$ structural change occurs. The consequent state correlation is $1^1B_{1g} \rightarrow 1^1A_g$; $1^1A_{1g} \rightarrow 2^1A_g$. This process may be viewed also as a bond shifting reaction interconverting two equivalent $D_{2h}$ structures (see **Figure 9**) through the transition structure of $D_{4h}$ symmetry [87].

**Figure 9.** The valence isomerization or bond shifting process in cyclobutadiene.
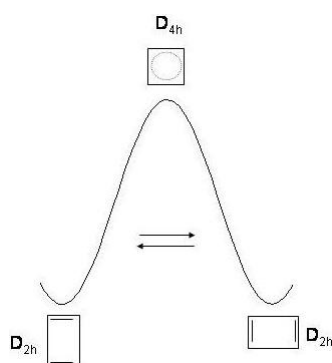


The barrier height has been measured to be in the range 1.6–10 kcal/mol [96,97]. The stabilization energy $\Delta E(1^1B_{1g} - 1^1A_g)$ going from square to rectangular geometry has been calcultated [85–91,93, 94,98] between 5 and 13 kcal/mol according to the results of **Table 4**.

Recent estimates including $ZPE$ correction [89–91] lower the height to 3–6 kcal/mol. In these calculations accurate ground state structures of cyclobutadiene have been also reported exhibiting geometrical parameters "very close to the true equilibrium bond distances" [91]. *Ab initio* normal mode calculations on the $1^1B_{1g}(D_{4h})$ state confirm its saddle point character given that imaginary frequencies, $990i$, $803i$, $1579i$ cm$^{-1}$, are found for the bond alternating $b_{1g}$ vibration [89–91]. On the other hand, the $1^1A_g(D_{2h})$ state is associated with a minimum structure since all the vibrational modes have real frequencies. Geometries and frequencies [89–91,99] are reported in **Table 5** while the calculated [90] potential energy profile is shown in **Figure 10**, left.

**Table 4.** $\Delta E(1^1B_{1g} - 1^1A_g)$ energy barrier (kcal/mol) for the interconversion process square $D_{4h} \rightarrow$ rectangular $D_{2h}$ (first two rows) and for the process square $D_{4h} \rightarrow$ rhombic $D_{2h}$ process (last row). Values in parentheses include the Zero Point Energy ($ZPE$) correction.

| | SCF/IEPA[a] | GRVB[b] | $\pi$-CI[c] | $(\sigma + \pi)$-CI[d] | $(\sigma + \pi)$-CI[e] |
|---|---|---|---|---|---|
| $\Delta E(1^1B_{1g} - 1^1A_g)$ | 7.3 | 4.8 | 8.7 | 8.3 | 12 |
| | GVB/CISD[f] | MCSCF[g] | MCSCF[h] | MRCCSD[i] | MR-AQCC[l] |
| $\Delta E(1^1B_{1g} - 1^1A_g)$ | 9 | 6.2 | 4.8(3.2) | 6.6(4.0) | 8.3(5.8) |
| | MCSCF[h] | MRCCSD[i] | | | |
| $\Delta E(1^1A_{1g} - 1^1A_g(rh.))$ | 3.2(3.3) | 3.6(1.8) | | | |

[a] Dunning double-$\zeta$ basis set [93]. [b] Generalized Resonating Valence Bond; Dunning double-$\zeta$ basis set [85]. [c] limited $\pi$-CIS; 3-21G basis set [86]. [d] STO-3G [94]. [e] 6-31G* basis set [87]. [f] Dunning double-$\zeta$ basis set [98]. [g] Dunning double-$\zeta$ basis set [88]. [h] CAS(4,4); 6-31G basis set [89]. [i] Multireference coupled cluster calculation with single and double excitations augmented non-iteratively by triple excitations; DZP basis set [90]. [l] Multireference coupled cluster average-quadratic calculation; aug′-cc-pVTZ basis set [91].

**Table 5.** Bondlengths (Å) and bond angles (degrees) of cyclobutadiene in the $D_{4h}$, $D_{2h}$ (rectangular) and $D_{2h}$ (rhombic) structures. Structural data indicated but not reported are determined by symmetry. Imaginary frequencies $\nu$ (cm$^{-1}$) of the $1^1B_{1g}$ ($D_{4h}$) ground state, of the $1^1A_{1g}$ ($D_{4h}$) and $1^1A_g$ ($D_{2h}$) (rhombic symmetry) excited singlet states.

| | ground state $S_o$ | | | | | | |
|---|---|---|---|---|---|---|---|
| | $1^1B_{1g}$ ($D_{4h}$) | | | | $1^1A_g$ (rect. $D_{2h}$) | | |
| $C_1$-$C_2$ | 1.452[a] | 1.467[b] | 1.447[c] | | 1.553[a] | 1.570[b] | 1.562[c] | 1.566[d] |
| $C_3$-$C_4$ | | | | | 1.365 | 1.366 | 1.350 | 1.343 |
| $C_1$-H | 1.067 | 1.104 | 1.076 | | 1.068 | 1.097 | 1.077 | 1.074 |
| $\nu(b_{1g})$ | 990$i$ | 803$i$ | 1579$i$ | | | | | |

| | lowest singlet $S_1$ | | | | | | |
|---|---|---|---|---|---|---|---|
| | $1^1A_{1g}$ ($D_{4h}$) | | | | $1^1A_g$ (rh. $D_{2h}$) | | |
| $C_1$-$C_2$ | 1.458[a] | 1.457[b] | 1.447[c] | | 1.450[a] | | 1.454[b] |
| $C_1$-H | 1.066 | 1.101 | 1.076 | | 1.073 | | 1.111 |
| $C_2$-H | | | | | 1.061 | | 1.094 |
| $\angle$ $C_1C_2C_3$ | | | | | 85.8 | | 95.0 |
| $\nu(b_{1g})$ | 2125 | 1783 | | | | | |
| $\nu(b_{2g})$ | 9423$i$ | 1104$i$ | | $\nu(b_{2g})$ | 459$i$ | | 506$i$ |
| | | | | $\nu(b_{1u})$ | 247$i$ | | 404$i$ |

| | lowest triplet $T_1$ | | | | second excited singlet $S_2$ | | |
|---|---|---|---|---|---|---|---|
| | $1^3A_{2g}$ ($D_{4h}$) | | | | $1^1B_{2g}$ ($D_{4h}$) | | |
| $C_1$-$C_2$ | 1.449[a] | 1.456[b] | 1.442[c] | 1.439[d] | 1.431[a] | 1.447[b] | 1.436[c] |
| $C_1$-H | 1.067 | 1.102 | 1.076 | 1.073 | 1.066 | 1.101 | 1.076 |

[a] MCSCF/CAS(4,4)/6-31G results [89]. [b] Multireference coupled cluster calculation with single and double excitations augmented non-iteratively by triple excitations; DZP basis set [90]. [c] Multireference coupled cluster average-quadratic calculation; aug′-cc-pVTZ basis set [91]. [d] Equation-of-motion coupled-cluster (EOM-CC) calculation, cc-pVTZ basis set [99].

The distortions of cyclobutadiene (other than rectangular) to geometries lower than square may be guessed considering that a square $X_4$ ring has, in addition to the $b_{1g}$ mode, three non-totally symmetric

normal displacements, $1b_{2g} + 1b_{1u} + 1e_u$. The $b_{1u}$ out-of-plane mode cannot couple the lowest excited $\pi\pi^*$ states of cyclobutadiene which are all symmetric with respect to the molecular plane. The $b_{2g}$ CCC bending mode couples $1^1A_{1g}$ with $1^1B_{2g}$ and is responsible of the square ($D_{4h}$) $\rightarrow$ rhomboidal ($D_{2h}$) distortion. The consequent state correlation is $1^1A_{1g} \rightarrow 1^1A_g$; $1^1B_{2g} \rightarrow 2^1A_g$. The $1^1A_g$ state of rhombus cyclobutadiene is stabilized with respect to $1^1A_{1g}$ of square cyclobutadiene by $\approx 3$ kcal/mol. The rhomboidal stabilization (see **Figure 10, right**) is triggered by the $b_{2g}$ bending mode with imaginary frequency, $9423i$ cm$^{-1}$ (overestimated [89]) and $1104i$ cm$^{-1}$ [90]. As to the $1^1A_{1g}$ state (square geometry) it should be added [89] that in correspondence of the ground state stabilization along the rectangular distortion, this state is destabilized along the same coordinate. In other words, the $b_{1g}$ frequency is considerably strengthened in $1^1A_{1g}$ (square geometry), up to 2125/1783 cm$^{-1}$ [89,90]. Second, the rhomboidal structure of the $1^1A_g$ state is not a true minimum structure. Two modes of $b_{2g}$ and $b_{1u}$ symmetry retain imaginary frequencies (see **Table 5**) and suggest the occurrence of a minimum structure with symmetry lower than rhomboidal [89,91]. Closely related potential energy curves have been documented for the cyclopentadienyl cation along the $D_{5h} \rightarrow C_{2v}$ distortion mode [100].

**Figure 10.** Energy profiles (a.u.) of the lowest four states of cyclobutadiene ($^1B_{1g}$, $^3A_{2g}$, $^1A_{1g}$, $^1B_{2g}$ in $D_{4h}$ symmetry in order of increasing energy) as a function of the rectangular and rhomboidal distortion. Adapted MRCCSD(T) results [90]. The state correlation for the square ($D_{4h}$) $\rightarrow$ rectangular ($D_{2h}$) distortion is $B_{1g} \rightarrow A_g$, $A_{2g} \rightarrow B_{1g}$, $A_{1g} \rightarrow A_g$ and $B_{2g} \rightarrow B_{1g}$. The state correlation for the square ($D_{4h}$) $\rightarrow$ rhomboidal ($D_{2h}$) distortion is $B_{1g} \rightarrow B_{1g}$, $A_{2g} \rightarrow B_{1g}$, $A_{1g} \rightarrow A_g$ and $B_{2g} \rightarrow A_g$.
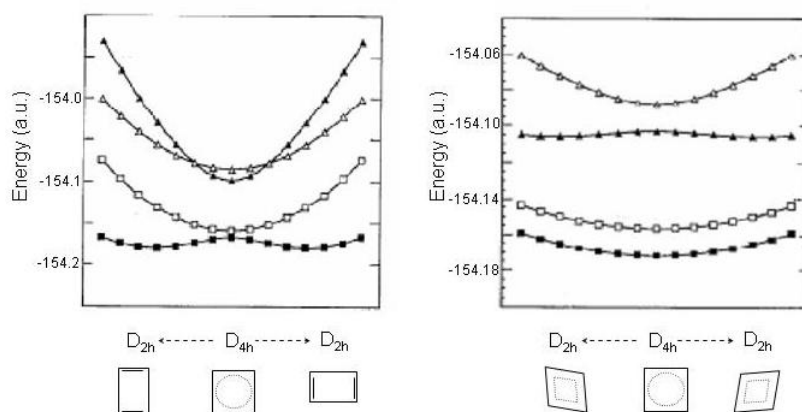


Finally, the $e_u$ mode, where one CC bond lengthens and the opposite shortens, may cause a square ($D_{4h}$) $\rightarrow$ trapezoidal ($C_{2v}$) distortion coupling $1^1B_{1g}$, $1^1A_{1g}$ and $1^1B_{2g}$ with higher excited $^1E_u$ states. The state correlation is $A_{1g}$, $B_{1g} \rightarrow A_1$; $A_{2g}$, $B_{2g} \rightarrow B_1$; $E_u \rightarrow A_1 + B_1$. However, with the $E_u$ states high in energy, the coupling is expected to be weak and a trapezoidal equilibrium geometry is not reached in any of these states [87]. By the same argument applied to $1^3A_{2g}$ it follows that, due to the large energy gap with respect to the next nearest state, $1^3E_u$, the lowest triplet is stable toward trapezoidal and *a fortiori* all types of planar deformations [94]. The minimum $D_{4h}$ structure of the $1^3A_{2g}$ state in **Table 5** is confirmed by the absence of imaginary frequencies in all *ab initio* vibrational calculations [89–91]. The square triplet structure of cyclobutadiene agrees with the reversal of the

$(4n + 2)/4n$ rule [22,101] according to which $4n$ $\pi$-electron rings with bond alternating geometry in the lowest singlet have bond equalized structures in the lowest triplet. Triplet aromaticity of cyclobutadiene and more in general of $4n$ $\pi$-electron annulenes up to the cyclononatetraenyl cation has been quantitatively estimated by high-level *ab initio* calculations in terms of aromatic stabilization energies and of geometric and magnetic properties [102].

### 2.5. Benzene: Ground and Lowest Excited States

**Table 6.** Bondlengths (Å) and bond angles (degrees) of benzene in the $D_{6h}$, $D_{2h}$ (quinoidal and antiquinoidal) and $C_s$ structures. Structural data indicated but not reported are determined by symmetry. Imaginary frequencies $\nu$ (cm$^{-1}$) of the $1^3B_{1u}(D_{6h})$ and $1^3B_{1u}(D_{2h})$ triplet states. $\Delta E$ (kcal/mol) is the energy barrier between minima.

| | ground state $1^1A_{1g}(D_{6h})$ | | | | | | | | | |
|---|---|---|---|---|---|---|---|---|---|---|
| | exp$^{(a-d)}$ | | | | calc$^{(e-l)}$ | | | | | |
| C-C | 1.392 | 1.398 | 1.399 | 1.397 | 1.398 | 1.388 | 1.407 | 1.386 | 1.388 | 1.389 |
| C-H | | 1.090 | 1.085 | 1.084 | 1.086 | 1.073 | 1.092 | 1.075 | 1.073 | 1.084 |

| | lowest triplet T$_1$ | | | | | |
|---|---|---|---|---|---|---|
| | $1^3B_{1u}$ $(D_{6h})$ | | $1^3B_{1u}$ $(D_{2h}; \sigma \equiv yz)$ | | | |
| | | | A$^{(m)}$ | Q$^{(m)}$ | A$^{(n)}$ | Q$^{(n)}$ |
| C$_1$-C$_2$ | 1.432$^{(m)}$ | 1.440$^{(n)}$ | 1.404 | 1.466 | 1.403 | 1.477 |
| C$_2$-C$_3$ | | | 1.494 | 1.370 | 1.514 | 1.366 |
| C$_1$-H | 1.072 | | 1.074 | 1.071 | | |
| C$_2$-H | | | 1.072 | 1.073 | | |
| $\nu(e_{2g})$ | 924$i$ | | $\nu(a_g)$ 1108 | 1213 | | |
| | | | $\nu(b_{2g})$ 369$i$ | 541 | | |
| $\Delta E$ | 0 | 0 | -1.0 | -1.4 | -2.3 | -2.3 |

| | lowest excited singlet $1^1B_{2u}(D_{6h})$ | | | | | second excited singlet S$_2$ $^{(t-v)}$ | | |
|---|---|---|---|---|---|---|---|---|
| | exp$^{(o,p)}$ | | calc$^{(q,r,s)}$ | | | $1B_{1u}(D_{6h})$ | $1B_{1u}(D_{2h})$ | $1A'(C_s)$ |
| C$_1$-C$_2$ | 1.435 | 1.432 | 1.449 | 1.416 | 1.428 | 1.438 | 1.358/1.432 | 1.46 |
| C$_2$-C$_3$ | | | | | | | 1.469/1.321 | 1.37 |
| C$_3$-C$_4$ | | | | | | | | 1.45 |
| C$_1$-H | 1.07 | 1.084 | 1.082 | 1.071 | | 1.079 | | |
| C$_2$-H | | | | | | | | |

$^{(a)}$ X-ray data [103]. $^{(b)}$ neutron diffraction data [104]. $^{(c)}$ electron diffraction results [105]. $^{(d)}$ rotational Raman results [106]. $^{(e)}$ MP2/6-311++G** results [113]. $^{(f)}$ MCSCF/CI/6-31G results [115]. $^{(g)}$ calculated values, Feynman path integral method [116]. $^{(h)}$ HF/MO *ab initio* results [111]. $^{(i)}$ HF/6-31G results [112]. $^{(l)}$ MP2/TZ2P+f calculation [114]. $^{(m)}$ MCSCF/6-31G results [119]. $^{(n)}$ MRDCI results [120]. $^{(o)}$ experimental determination [121]. $^{(p)}$ experimental determination [122]. $^{(q)}$ MCSCF/CAS(6,6)/STO-3G results [123]. $^{(r)}$ MCSCF/CIS/6-31-3G results [115]. $^{(s)}$ SCF/MO results [124]. $^{(t)}$ SINDO/CI calculation [125]. $^{(u)}$ MRDCI results [120]. $^{(v)}$ SCF/CI/4-31G calculation. Two angles are in addition defined for the $C_s$ structure: $\alpha = 44°$, $\beta = 67°$, $\alpha$ and $\beta$ being the angle between planes $C_1C_2C_6$ and $C_3C_4C_5$ with the plane $C_2C_3C_5C_6$ [126].

All the structural determinations from X-ray [103], neutron [104] and electron [105] diffraction studies to rotational Raman spectroscopy [106] converge on a regular hexagonal $D_{6h}$ geometry for the structure of benzene in the ground state. However, it has been acutely noted [107] that the X-ray structural data are compatible not only with an ordered crystal of $D_{6h}$ molecules but also with one

disordered with $D_{3h}$ molecules overimposed and rotated $60°$. With a 0.10 Å difference between C-C and C=C bondlengths the crystal disorder would be far below the resolving power of the X-ray diffraction technique. Since all other diffraction techniques are equally unable to resolve the $D_{6h}/D_{3h}$ dilemma [107], this means that there are strong experimental indications in favor of the $D_{6h}$ geometry which nevertheless do not allow to discard unequivocally the $D_{3h}$ alternative. In spite of this, support to the $D_{6h}$ geometry has been more recently provided by the analysis of the temperature dependence of the neutron diffraction data relative to the $C_6D_6$ crystal [108,109]. Based on the atomic displacement parameters of the C atoms at 15 and 123 K [109], the model shows that the small in-plane temperature independent contribution to these parameters is due to the zero-point intramolecular motion and not to the disorder between Kekule' structures.

The theoretical calculations take on great significance [110]. *Ab initio* calculations [111–117] point to the $D_{6h}$ structure as that of minimum energy for benzene on the ground state energy surface. The data [111–116] are collected in **Table 6** and compared with the most important structural results. However, anomalous results such as the occurrence of imaginary frequencies in $D_{6h}$ symmetry have been reported when incomplete basis sets are used in conjunction with correlated calculation methods [118].

In order of increasing number of nodal planes the six $\pi$ orbitals of $D_{6h}$ benzene are classified into the $a_{2u}$, $e_{1g}$, $e_{2u}$ and $b_{2g}$ symmetry species. The $\pi\pi^*$ HOMO $\rightarrow$ LUMO excitation, *i.e.*, $e_{1g}^4 \rightarrow e_{1g}^3 e_{2u}^1$, gives origin to six $\pi\pi^*$ states, three singlets, $^1B_{2u}$, $^1B_{1u}$ and $^1E_{1u}$, and three triplets, $^3B_{2u}$, $^3B_{1u}$ and $^3E_{1u}$. In addition, both the $a_{2u}^2 \rightarrow a_{2u}^1 e_{2u}^1$ and the $e_{1g}^4 \rightarrow e_{1g}^3 b_{2g}^1$ promotions contribute to the $^1E_{2g}$ and $^3E_{2g}$ $\pi\pi^*$ states. The energy level diagram established on the basis of the assignment of the observed excitation energies [35,127] is summarized in **Table 7**. All the excited state calculations [116,128–132] are consistent with the energy ordering $^1B_{2u} <^1 B_{1u} <^1 E_{1u}$ and $^3B_{1u} <^3 E_{1u} <^3 B_{2u}$. From the point of view of the VB theory these states may be classified into two groups, covalent and ionic [128,129,133]. States with covalent character are $^1B_{2u}$, $^3B_{1u}$ and $^3E_{1u}$ described by Kekule', Dewar and quinoidal structures $a$ - $c$ of **Figure 11**. Structures with charge separations [for instance, $(d)$ in **Figure 11**] predominantly contribute to $^1B_{1u}$, $^1E_{1u}$ and $^3B_{2u}$, thus imparting ionic character to these states [133]. The excitation energies to covalent states are fairly well reproduced even in less extended *ab initio* calculations while more sophisticated calculation methods are needed for the calculation of the excitation energies to ionic states [129].

The equilibrium geometries of the lowest $\pi\pi^*$ states have been the object of several studies [119,120,126,134]. For the lowest triplet, $^3B_{1u}$, a structure with symmetry lower than $D_{6h}$ is expected on the basis of the reversal of the $(4n + 2)/4n$ rule [101]. Due to the coupling of $^3B_{1u}$ with the close lying $^3E_{1u}$ state, benzene shifts from hexagonal to structures of quinoidal $Q$ and antiquinoidal $AQ$ character sketched in **Figure 11** (four long, two short bonds for $Q$; four short, two long bonds, for $AQ$). Both have $D_{2h}$ symmetry.

The calculation indicates that $^3B_{1u}(D_{6h})$ is the transition state between $AQ$ and $Q$ minima whose energies are $\approx 2.3$ kcal/mol below the transition state [120,134]. The saddle point nature of the $^3B_{1u}(D_{6h})$ state is confirmed by the occurrence of one imaginary $\nu_8(e_{2g})$ frequency $924i$ cm$^{-1}$ in the normal mode calculation [119]. The structures of $^3B_{1u}(D_{6h})$ and of the $AQ$ and $Q$ states are reported in **Table 6**. Evidence of $^3B_{1u}/^3E_{1u}$ coupling comes from low-temperature EPR experiments according to which the lowest triplet of benzene is non hexagonal [135,136]. Further, the phosphorescence

excitation spectrum [137] shows an intense doublet 239/252 cm$^{-1}$ above (0-0) assigned [138] as the lowest vibrational transition of the $\nu_8(e_{2g})$ vibration. This vibration has frequency 1584 cm$^{-1}$ in the ground state. The strongly anharmonic potential well around the $Q$ and $AQ$ minima sets a value of 220 cm$^{-1}$ for the vibrational transition $0 \to 1$ of the $\nu_8(e_{2g})$ mode [134].

**Table 7.** Lowest singlet and triplet excited states of benzene: experimental $S_0 \to S_n$ and $S_0 \to T_n$ band maxima (eV) and calculated transition energies (eV).

| | exp[a] | calc | | | | | |
|---|---|---|---|---|---|---|---|
| $1^1B_{2u}$ | 4.8 | 5.0[c] | 4.9[d] | 5.25[e] | 5.02[f] | 6.32[g] | 5.02[h] |
| $1^1B_{1u}$ | 6.2 | 7.64 | 7.4 | 6.60 | | 6.53 | |
| $1^1E_{1u}$ | 6.9 | 8.34 | 7.8 | 7.47 | | 8.53 | |
| $1^1E_{2g}$ | 7.8[b] | 8.33 | 8.1 | | | | |
| | | | | | | | |
| $1^3B_{1u}$ | 3.9 | 3.83 | 3.9 | 4.06 | 4.16 | | 4.18 |
| $1^3E_{1u}$ | 4.85 | 4.98 | 4.9 | 5.02 | 4.83 | | 4.86 |
| $1^3B_{2u}$ | 5.7 | 7.0 | 6.7 | 6.02 | 6.02 | | 5.69 |
| $1^3E_{2g}$ | | 7.28 | 7.2 | | | | |

[a,b] observed band maxima [35], [127]. [c-h] calculation methods: [c] SCF-CISD [128], [d] CASSCF-CCI [129], [e] SAC-CI [130], [f] GVVPT2 [132], [g] Feynman path integral [116], [h] CASPT2 [131].

**Figure 11.** Upper row: valence bond configurations contributing to covalent and ionic states of benzene. Lower row: quinoidal ($Q$) and antiquinoidal ($AQ$) structures of the second excited singlet of benzene.
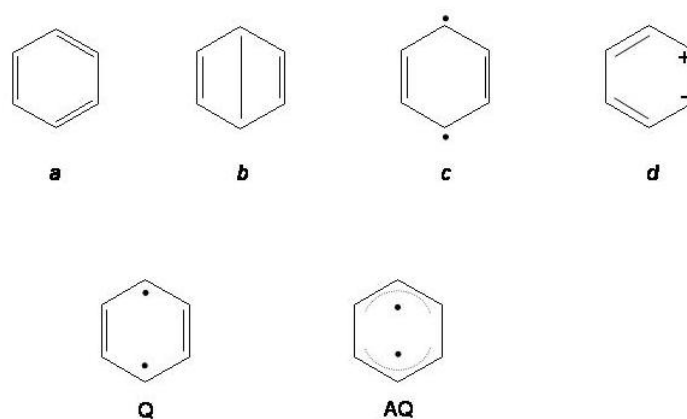


According to experiment [35,121,122] and calculation data [115,123,124] the $1^1B_{2u}$ state retains hexagonal symmetry with uniform expansion of the carbon ring and CC bondlength increase of $\approx 0.04$ Å with respect to the ground state. As to the second excited singlet, $1^1B_{1u}$, a SINDO calculation predicts a mere increase of CC bond lengths [125]. In contrast, *ab initio* calculations indicate [120] that $1^1B_{1u}$, similarly to $1^3B_{1u}$, distorts toward a quinoidal/antiquinoidal structure. The behaviour was

justified noting the similarity of energy gaps between the singlet $1^1B_{1u}/1^1E_{1u}$ and triplet $1^3B_{1u}/1^3E_{1u}$ pairs and the independence of the vibronic coupling on the spin state. A biradicaloid structure of $C_s$ symmetry has been also reported for $1^1B_{1u}$ on the basis of *ab initio*, limited CI, calculations, as intermediate structure in the photochemical conversion benzene → Dewar benzene [126].

### 2.6.   *Cyclooctatraene: A Non Planar Cyclic Conjugated System*

Due to angular strain cyclooctatetraene, the next higher homologue in the annulene series, is a non aromatic molecule with a non planar structural arrangement of four weakly interacting $\pi$ bonds [4,10,11]. It is known from electron [139–141] and X-ray diffraction [142,143] data and recent results of femtosecond spectroscopy [144] that the molecule adopts a tub-shaped structure of $D_{2d}$ symmetry, as shown in **Figure 12**.

Two basic dynamical processes characterize the molecule [145] (see **Figure 13**), (i) ring inversion ($RI$), $a \to d$, $b \to c$ and (ii) bond shifting ($BS$), $a \to b$, $c \to d$, $a \to c$, $b \to d$.

**Figure 12.** The molecular structure of cyclooctatetraene in $D_{2d}$ symmetry, femtosecond measurement [144] and electron diffraction data (in parentheses) [141].
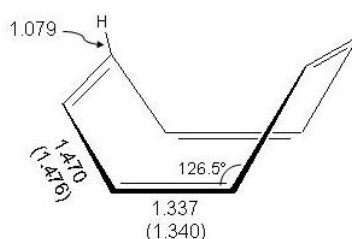


**Figure 13.** Ring inversion ($RI$) and bond shifting ($BS$) between the four conformational isomers of cyclooctatetraene.
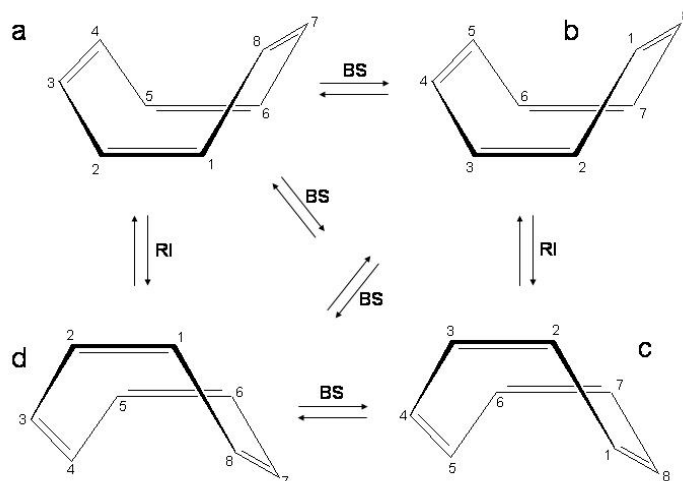
The four equienergetic $D_{2d}$ conformations $a$, $b$, $c$, $d$ are interconverted passing through transition states of $D_{4h}$ symmetry for $RI$ and $D_{8h}$ symmetry for $BS$. In cyclooctatetraene only $BS$ is probed by $NMR$ spectroscopy [6]. The transition state is $\approx$ 14 kcal/mol above the tub structure [6,146]. In monoalkyl derivatives both processes are observed and the energy barriers are $\approx$ 11 kcal/mol for $RI$ and 15 kcal/mol for $BS$ [6]. The larger energy involved in the $BS$ process is due to the fact that ring flattening is accompanied by bond length changes in order to have a $D_{8h}$ transition state. The $RI/BS$ barriers have been calculated for cyclooctatetraene with *ab initio* methods, $\approx$ 10/16.4 kcal/mol and 17.1/19.3 kcal/mol, respectively [147,148]. The mode responsible for ring inversion is the $b_{2u}$ out-of-plane mode with frequency $139i$ cm$^{-1}$ in $D_{4h}$ symmetry while that for bond shift is the bond alternating $b_{1g}$ mode with frequency $1962i/2363i$ cm$^{-1}$ in $D_{8h}$ symmetry [147,148].

The structures and energies (relative to the tub minimum) of the $D_{4h}$ and $D_{8h}$ stationary points and of one selected isomer and two conformers (bicyclo[4.2.0]octa-2,4,7-triene, crown and chair; $C_s$, $D_4$ and $C_{2h}$ symmetry) are reported in **Figure 14**. The chair and crown conformers are stable species 56.5 and 171.1 kcal/mol above the tub conformation [148]. They are obtained from the tub by rotation of two and four CC double bonds so that the $\pi$ orbitals are directed toward the internal part of the cyclic structure, thus increasing the repulsion among $\pi$ electrons [148]. The tub and bicyclo isomers are only a small fraction of the total number of (CH)$_8$ valence isomers, 21 including stereoisomers [149,150]. Disregarding H atoms, they correspond to regular graphs of degree three [150], *i.e.*, their formulas are drawn under the condition that (i) three lines (bonds) always meet at each vertex (C atom) and (ii) no two of these lines cross. If these conditions are relaxed additional (CH)$_8$ isomers can be derived.

**Figure 14.** On the left, $D_{2d}$ cyclooctatetraene and $BS$, $RI$ transition states of $D_{8h}$ and $D_{4h}$ symmetry; on the right cyclooctatetraene isomers (crown, chair and bicyclo[4.2.0]octa-2,4,7-triene, $D_4$,$C_{2h}$ and $C_s$ symmetry, respectively). Structural parameters (Å) and energies (kcal/mol) relative to $D_{2d}$ minimum, reported results [148] (MP2-CASSCF//CASSCF/6-31G* calculations). Experimental energy values (kcal/mol) of the $D_{8h}$ and $D_{4h}$ transition states are given in parentheses [151].
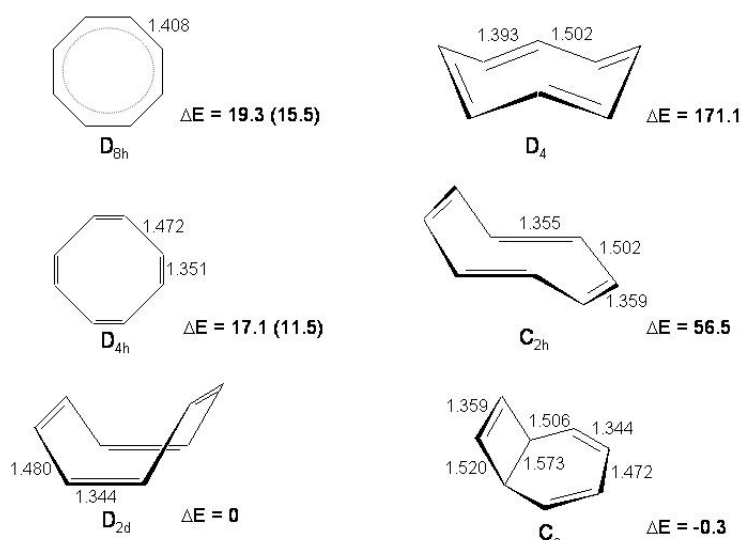
The properties of these isomers have been reviewed [36] and the isomerization reactions, such as those shown in **Figure 15**, have been discussed by means of extensive computational studies [152–155]. In particular, the relaxation pathways relevant to the photochemical reactivity of cyclooctatetraene after excitation into $S_2[1E(D_{2d})]$ have been described in terms of radiationless decay from $S_2$ into the $S_1$–excited planar minimum of $D_{8h}$ symmetry and internal conversion to $S_0$ through $S_1/S_0$ conical intersections [156].

**Figure 15.** Photochemical and thermal isomerization processes in cyclooctatetraene.
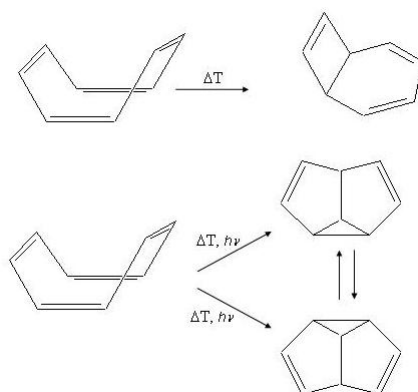


As to the transition structures of $D_{4h}$ and $D_{8h}$ symmetry, their occurrence has been provided by photodetachment experiments on the radical cyclooctatetraene anion [151]. Two states have been observed, $1^1A_{1g}(D_{4h})$, *i.e.*, the ground state of the $D_{4h}$ transition structure and $1^3A_{2u}(D_{8h})$, the lowest triplet state of the $D_{8h}$ transition structure. Their energies with respect to the $D_{2d}$ minimum have been determined, $E[1^1A_{1g}(D_{4h})] - E[1^1A_1(D_{2d})] \approx 11.5$ kcal/mol and $E[1^3A_{2u}(D_{8h})] - E[1^1A_1(D_{2d})] \approx 23.5$ kcal/mol. Since the difference between the $RI$ and $BS$ energy barriers is $\approx 4$ kcal/mol [6], this is experimental evidence [151] that the lowest $D_{8h}$ singlet, *i.e.*, $1^1B_{1g}(D_{8h})$, lies $\approx 8$ kcal/mol below the lowest $D_{8h}$ triplet, $1^3A_{2u}(D_{8h})$.

Pentalene

Pentalene (**Figure 16**) is formally derived from the regular octagonal $\pi$ perimeter of cyclooctatetraene by cross-linking opposite atomic centers [157]. Due to the reduction of molecular symmetry from $D_{8h}$ to $D_{2h}$, all the $\pi$ orbitals of pentalene are non degenerate and the lowest four are occupied by eight $\pi$ electrons. Simple arguments based on the second-order bond fixation in conjugated molecules [43,44] indicate that the symmetrical bond equalized $D_{2h}$ structure corresponds to a maximum on the ground state energy surface and that the molecule distorts to $C_{2h}$ symmetry with alternating single and double bonds. Bond alternation of the order of $\approx 0.15$ Å has been calculated by all *ab initio* methods for ground state $C_{2h}$ pentalene [28,29,158] (see **Table 8**).

The highly reactive molecule is generated by photochemical cleavage of pentalene dimers with 254-nm light at 20 K [28]. Infrared and electronic spectra of pentalene have been measured and interpreted on the basis of *ab initio* calculations on $C_{2h}$ molecular symmetry [28]. The three absorption bands at 3.48, 3.94 and 4.80 eV are assigned to the lowest allowed $S_0 \rightarrow nB_u$ ($n = 1, 2, 3$) transitions.

At lower energy two states of $A_g$ symmetry are predicted with spectral activity too weak to be observed in the unsubstituted system. Their occurrence is due to the fact that in pentalene the $HOMO \rightarrow LUMO$ singly and doubly excited configurations are of $a_g$ symmetry and comparable energy [28].

**Table 8.** Upper: bond lengths (Å) of pentalene ($D_{2h}$ and $C_{2h}$ equilibrium structures, numbering as in **Figure16**) and of 1,3,5-tri-*tert*-butylpentalene ($C_s$ equilibrium structure) in the ground state. Structural data indicated but not reported are determined by symmetry. Imaginary frequency $\nu$ (cm$^{-1}$) of the $1^1B_{1g}(D_{2h})$ state. $\Delta E$ (kcal/mol) is the energy barrier between minima of $C_{2h}$ symmetry. Lower: bond lengths (Å) of pentalene in the lowest excited states, from $S_1$ to $S_4$. Imaginary frequency $\nu$ (cm$^{-1}$) of the $2^1A_g(D_{2h})$ state. $\Delta E$ (kcal/mol) is the energy barrier between minima of $C_{2v}$ symmetry.

| | ground state | | | | | | | |
| --- | --- | --- | --- | --- | --- | --- | --- | --- |
| | $D_{2h}$ | | $1A_g(C_{2h})$ | | | | $1A'(C_s)$ | |
| | $1^1B_{1g}^{(a)}$ | TS$^{(c)}$ | calc$^{(a-c)}$ | | | exp$^{(d)}$ | calc$^{(f)}$ | exp$^{(e)}$ |
| r$_{1,6a}$ | 1.404 | 1.422 | 1.352 | 1.369 | 1.355 | 1.360/1.357 | 1.354/1.358 | 1.34/1.41 |
| r$_{1,2}$ | 1.426 | 1.414 | 1.500 | 1.504 | 1.497 | 1.478/1.500 | 1.504/1.506 | 1.54/1.50 |
| r$_{2,3}$ | | | 1.357 | 1.369 | 1.356 | 1.351/1.358 | 1.360/1.361 | 1.32/1.28 |
| r$_{3,3a}$ | | | 1.472 | 1.482 | 1.474 | 1.496/1.465 | 1.485/1.470 | 1.46/1.52 |
| r$_{3a,6a}$ | 1.490 | 1.413 | 1.468 | 1.468 | 1.461 | 1.460 | 1.465 | 1.43 |
| $\nu(b_{1g})$ | 2726$i$ | | | | | | | |
| $\Delta E$ | 9.7 | 6.6 | 0 | | | 0 | | |

| | excited states$^{(a)}$ | | | | |
| --- | --- | --- | --- | --- | --- |
| | $S_1[A_g(D_{2h})]$ | $S_2$ | | $S_3[B_{2u}(D_{2h})]$ | $S_4[B_{3u}(D_{2h}]$ |
| | | $2^1A_g(D_{2h})$ | $1^1A_1(C_{2v})$ | | |
| r$_{1,6a}$ | 1.431 | 1.405 | 1.400 | 1.444 | 1.435 |
| r$_{1,2}$ | 1.411 | 1.427 | 1.482 | 1.434 | 1.428 |
| r$_{2,3}$ | | | 1.387 | | |
| r$_{3,3a}$ | | | 1.435 | | |
| r$_{3a,6a}$ | 1.390 | 1.502 | 1.479 | 1.401 | 1.459 |
| $\nu(b_{2u})$ | | 1262$i$ | | | |
| $\Delta E$ | | 1.6 | 0 | | |

$^{(a)}$ MCSCF/CAS(8,8)/6-31G$^*$ results except for the second excited state, $S_2$, for which the 3-21G basis set has been used [29]. $^{(b)}$ B3LYP/6-31G$^*$ results [28]. $^{(c)}$ B3LYP/6-31G$^*$ results [158]. $^{(d)}$ X-ray structural data of dimethyl-4,6-di-*tert*-butyl-1,2-dicarboxylate [159] (pair of values relative to symmetrically equivalent distances assuming a $C_{2h}$ structure). $^{(e)}$ X-ray data of 1,3,5-tri-*tert*-butylpentalene [159] (pair of values relative to symmetrically equivalent distances assuming a $C_{2h}$ structure). $^{(f)}$ MCSCF/CAS(8,8)/6-31G$^*$ results [160] (pair of values relative to symmetrically equivalent distances assuming a $C_{2h}$ structure).

The first stable derivative at room temperature, 1,3,5-tri-*tert*-butylpentalene, was synthesized hindering sterically the dimerization [27]. The ring geometry was determined by X-ray diffraction [159]. Low energy absorption bands have been observed at 1.50 and 2.14 eV in the low temperature spectrum of the *tert*-butyl derivative and assigned to the two $A_g$ states previously mentioned [161]. Further, the derivative fluoresces from the lowest $B_u$ state at 3.17 eV ($\approx$ 25550 cm$^{-1}$) with quantum yield 0.002 and decay time 13 ps [29,160]. This band has been assigned as the emission counterpart of the 3.67 eV ($\approx$ 29600 cm$^{-1}$) absorption band (see **Figure 17**). Other two absorption bands are observed with maxima

at 4.52 ($\approx$ 36500 cm$^{-1}$) and 5.76 eV (not shown in **Figure 17**). Calculated transition energies of the tri-*tert*-butyl derivative are in good agreement with experiment [160].

**Figure 16.** Pentalene: upper (a), atomic numbering and reference axes; lower (b), valence isomerization between $C_{2h}$ structures.



(a)

(b)
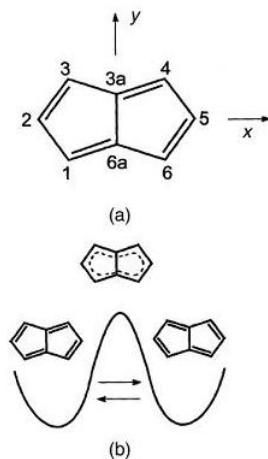
**Figure 17.** Absorption and fluorescence ($\lambda_{exc}$ = 313 nm, 10$^{-4}$ M in cyclohexane) spectra of 1,3,5-tri-*tert*-butylpentalene at room temperature.
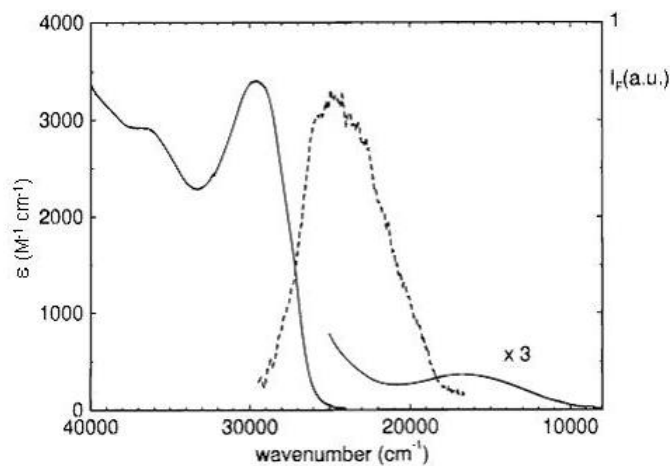


Similarly to cyclobutadiene and cyclooctatetraene, pentalene interconverts between $C_{2h}$ isomers. In 1,3,5-tri-*tert*-butylpentalene the energy barrier was found to be $\approx$ 4 kcal/mol [162]. The calculated barrier height amounts to 9.7 kcal/mol [29] and 6.6 kcal/mol (including $ZPE$) [158]. Another structural rearrangement from $D_{2h}$ to $C_{2v}$ symmetry occurs in the second excited state due to the $2A_g/1B_{2u}$, *i.e.*, $S_2/S_3$, vibronic coupling promoted by a $b_{2u}$ vibration [29]. Overall, the energy diagram of the ground and of the lowest three excited states of pentalene is shown in **Figure 18** as a function of the deviation from $D_{2h}$ geometry. The excited state equilibrium geometries are reported in **Table 8**.

**Figure 18.** Energy profiles of the lowest four states of pentalene ($^1B_{1g}$, $1^1A_g$, $2^1A_g$, $^1B_{2u}$ in $D_{2h}$ symmetry) as a function of the displacement from $D_{2h}$ geometry (vertical dotted line). Adapted MCSCF/CAS(8,8)/3-21G results [29]. For the sake of clarity the $S_0$ and $S_2$ structures of pentalene displaced from $D_{2h}$ symmetry have strongly exaggerated differences. Actually, the $S_0$ minimum has $C_{2h}$ symmetry ($C_2$ normal to the molecular plane) while the $S_2$ minimum has $C_{2v}$ symmetry ($C_2$ along the short in-plane axis).
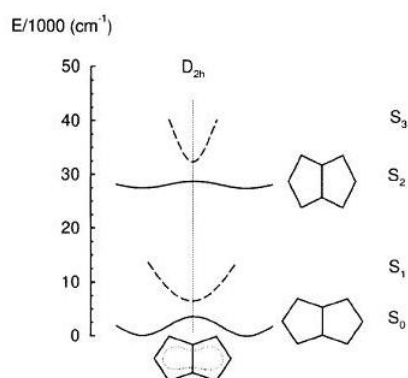


## 3. Higher Annulenes

In this Section the structural properties of fully conjugated monocyclic hydrocarbons, from [10]- to [18]annulenes, will be reviewed together with those of their most significant derivatives. Historical landmarks in the chemistry of these molecules are the synthesis of monocycles up to [30]annulene [163,164] and of the first bridged [10]annulene [165,166]. Due to angle strain and/or steric interactions between hydrogen atoms higher annulenes are characterized by a rich variety of non planar conformational and configurational isomers and of interconversion processes between them [6]. As a consequence, *cis/trans* isomerization takes place among configurations and several isomers usually exist in solution. A second important factor on which the annulene structures depend is the decreasing energy difference between localized and delocalized geometries as the ring size increases [18]. For annulenes containing more than 30 C atoms the localized arrangement of double bonds has been predicted to become energetically favored [19]. Limiting the attention to medium size annulenes, the insertion of atoms (or groups of atoms) as bridges between opposite C atoms or the introduction of triple bonds along the cycle in place of the alkene unit stiffens the ring framework. Bridged and dehydroannulenes are then formed with planar (or approximately planar) ring geometries and considerably reduced bond alternation.

### 3.1. [10]Annulene

Conformational Isomers

[10]-annulene was first trapped in a reaction mixture [167] and later isolated as two distinct crystalline isomers [168,169]. The first, (**A**), showed a single line in the $^{13}C$ and $^1H\ NMR$ spectra even down to $-160\ °C$; on cooling the second, (**B**), below $-100\ °C$ a five line $^{13}C\ NMR$ spectrum was observed.

Based on these experiments and chemical evidence, **A** was assigned the all-*cis* and **B** the mono-*trans* configuration, in both cases in non planar conformation [169]. From the theoretical point of view the determination and the energy ordering of the $C_{10}H_{10}$ isomers have represented a difficult task for the most advanced *ab initio* treatments [112,170–177]. Five conformational structures have been identified as the lowest energy forms of [10]annulene, three of them non planar and two quasi planar, schematically shown in **Figure 19**. The three non planar isomers are all-*cis* or boat, mono-*trans* or twist, di-*trans* or naphthalene-like and the two quasi planar are azulene-like and heart, with the indication of the symmetry group.

**Figure 19.** The low energy isomers of [10]annulene. The symmetry group, usual names and bondlengths (Å, CCSD/DZd and MP2/DZd results [174]) are indicated. Boat, twist and naphthalene-like isomers are non planar, azulene-like and heart are quasi planar.
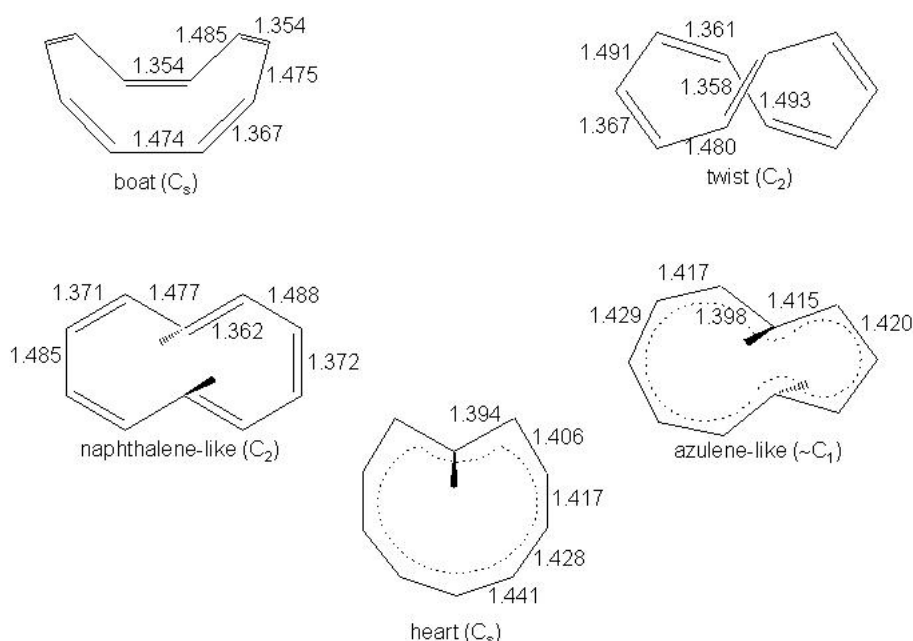


At the HF calculation level these structures are local minima [170,171] except the heart isomer which originally [169] was proposed as the transition state between equivalent twist structures. The HF results of **Table 9** are in good agreement with the assignment, being the twist and boat isomers the lowest energy conformers. On the other hand, correlated calculation methods such as density functional and MP2 assign the lowest minimum to the heart isomer[172]. This approach, however, has been shown to overestimate [173] the stability of the heart with respect to the twist isomer: In fact, the calculation at the correlated geometries using the high-level CCSD(T) method shifts the twist structure below heart by 3–7 kcal/mol. The result was subsequently confirmed starting with twist, naphthalene-like and heart structures optimized at the CCSD(T)/DZd level [174]. The final reference values, *i.e.*, CCSD(T) single-point energies with the triple-$\zeta$ polarized TZ2P basis set at these geometries are 0, 1.4 and 4.24 kcal/mol, respectively (see **Table 9**). The $^{13}C\ NMR$ spectrum calculated with this method supports the assignment of the $NMR$ spectrum of **B** to the twist form while the calculation does not help in the

assignment of the **A** spectrum [175]. Replacing one CH pair with one nitrogen atom in aza[10]annulenes and thus lowering the repulsive interaction of the inner hydrogen atom with the ring in the heart isomer (refer to **Figure 19** for clarity), heart becomes energetically competitive with twist. Nevertheless, this is not enough: the CCSD(T) calculation indicates that twist aza[10]annulene remains more stable than heart aza[10]annulene by $\approx$ 2.1 kcal/mol [178].

**Table 9.** Energy [174] (kcal/mol) of the [10]annulene isomers of **Figure 19**. DZd and TZ2P: double-$\zeta$ polarized and triple-$\zeta$ polarized basis sets. HF: uncorrelated Hartree/Fock, B3LYP and MP2: correlated density functional and Moller-Plesset, CCSD(T): coupled cluster calculation including singles, doubles and perturbatively connected triple excitations. (//) single-point energy calculation with the method indicated before the double slash at the optimized structures determined after the double slash.

|  | HF/DZd | B3LYP/DZd | MP2/DZd | CCSD(T)/DZd //MP2/DZd | CCSD(T)/DZd | CCSD(T)/TZ2P //CCSD(T)/DZd |
|---|---|---|---|---|---|---|
| $C_s$ boat | 1.84 | 2.47 | 7.12 | 5.66 | | |
| $C_2$ azulene-like | 8.13 | -2.96 | -1.14 | 8.61 | | |
| $C_s$ heart | 11.77 | -9.11 | -4.22 | 5.99 | 6.29 | 4.24 |
| $C_2$ naphthalene-like | 2.87 | -2.89 | 1.23 | 2.04 | 1.74 | 1.40 |
| $C_2$ twist | 0 | 0 | 0 | 0 | 0 | 0 |

Among [10]annulene isomers the *all-trans* isomer, *i.e.*, *all-trans*-cyclodecapentaene not shown in **Figure 19** but similar to $D_4$ (crown) cyclooctatetraene (or [8]trannulene according to this classification) of **Figure 14**, has the remarkable property of $p$ orbital overlap parallel to the average ring plane ("in-plane" conjugation). For a schematic depiction of the trannulene principle, see "Structure B" in **Figure 42**. While in planar (or nearly planar) [10]annulene geometries the $p$ orbitals are oriented perpendicular to the ring plane, the *all-trans* configuration forces the $p$ orbitals in the direction toward the ring center [179]. At the B3LYP/6-31G* calculation level, the *all-trans*[10]annulene, the first member of the group of *all-trans*[n]annulenes or [n] trannulenes, has $D_{5d}$ symmetry with equal C-C bond lengths, 1.412 Å [179]. It has been verified that [4n + 2] trannulenes have aromatic character on the basis of geometric and magnetic criteria. [4n] trannulenes, on the other hand, show pronounced bond alternation, for instance 1.393/1.502 Å in $D_4$ (crown) cyclooctatetraene of **Figure 14**, indicating antiaromatic behaviour. Although the [n]trannulenes are considerably higher in energy than the [n]annulene counterparts, a supporting molecular framework may provide a three-dimensional cage to sustain the "in-plane" conjugation in the case of the [4n + 2] trannulenes. Thus, [18]trannulene structures are stable within the 60-fullerene architecture [180–183] and are part of donor-acceptor dyads for light harvesting [180,184].

The fully delocalized $D_{10h}$ and the bond alternating $D_{5h}$ planar structures are local maxima lying 31.9 and 31.2 kcal/mol above the twist isomer (SCF/DZP values) on a quite flat energy surface in the vicinity of the two maxima [170,171]. The instability of these structures is due to the fact that the energy gain of the planar arrangement is overwhelmed by the energy required to deform the CCC angle to 144°. A strategy has been proposed [185] to generate planar [10]annulenes analogues of benzene where cyclopropene or cyclobutene units are fused with the $D_{10h}$ ring. Density functional results indicate that

derivatives with attached five cyclopropene or cyclobutene units arrange as planar $D_{5h}$ structures that are local minima on the energy surface [185].

Introducing one alkyne moiety, 1,2-didehydro[10]annulene is formed, characterized by several conformational minima and transition states [186]. The isomer resembling [10]annulene heart is the lowest energy conformer with a nearly planar and approximately bond equalized structure. Evidently, the replacement of one double with one triple bond relaxes the angle strain in this form. The CCSD(T) calculation at the MP2/cc-pVDZ optimized geometries identifies other three low energy isomers. The next-to-heart isomer, 6.8 kcal/mol higher, has a non planar $C_2$ structure similar to the [10]annulene twist. A second planar $C_{2v}$ isomer with CC distances between 1.372 and 1.434 Å lies 16.6 kcal/mol above heart. The third is a boat structure of $C_s$ symmetry with energy $\approx 17.7$ kcal/mol above heart. All other conformational minima are at much higher energies.

Bridged [10] Annulenes

Experimentally, three types of tautomeric structures have been reported for bridged [10]annulenes, aromatic, polyolefinic and norcaradienic (see **Figure 20**). According to X-ray diffraction studies [187–190] 1,6-methano- and 1,6-epoxy[10]annulene have bond equalized $C_{2v}$ geometries. As to 1,6-methano[10]annulene in particular the maximum value of the torsional angles along the ring is 35° indicating that the structure is appreciably displaced from planarity [187].

**Figure 20.** Top: atomic numbering of bridged [10]annulenes and molecular reference system. Bottom: structures of bridged [10]annulenes: aromatic (left), polyolefinic (center), norcaradienic (right).
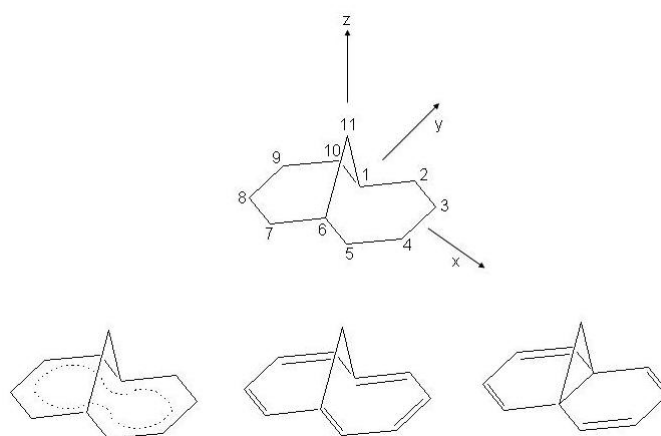


Substituting the hydrogen atoms of the $> CH_2$ group with $\pi$ acceptor units like $-CN$ the 11,11-dicyano derivative takes on the norcaradienic structure [191–193]. Finally, the bulky trimethylsilyl substituent, $-Me_3Si$, in the 2,5,7,10 positions favors the polyolefinic tautomer [194]. The structural data on 1,6-methano-, 1,6-epoxy[10]annulene and on the 11,11-dicyano derivative are in agreement with density functional calculations [195]. The geometries of **Table 10** are minima on the potential energy surface, all the vibrational modes having real frequencies. In particular, the norcaradienic minimum of the dicyano derivative has a $C_1 \cdots C_6$ distance 1.542 Å (1.558 Å, exp [193]) and enhanced bond

alternancy $\approx$ 0.13 Å (0.14 Å, exp [193]). The delicate balance between aromatic and norcaradienic geometries depends on the nature of the bridging groups [196]. As the strain energy decreases from the $> CH_2, > O, > NH$ triplet to the $> PH$ and $> S$ pair, due to the reduction of the bridge angle, the transannular interaction increases and stabilizes the norcaradienic geometry. The valence aromatic/norcaradienic tautomerism has been modelled as a function of the $C_1 \cdots C_6$ distance considering different substituents of the bridge H atoms [197]. The results have been related to minima of the cyclopropane and trimethylene fragments.

**Table 10.** Structural and spectral data characterizing 1,6-methano- (**A**) and 1,6-epoxy[10]annulene (**B**). Upper: ground state geometries (bondlengths, Å), including those of the 11,11-dicyano (**C**) and 11,11-dimethyl (**D**) derivatives of 1,6-methano[10]annulene. Center: geometries of the ground and of the lowest excited state of **A** and **B** (bondlengths, Å). Lower: vertical excitation energies (eV), oscillator strengths ($f$) and relative two-photon intensities ($I$) of the transitions to the lowest excited states of **A**.

| | ground state | | | | | | | |
| | $\mathbf{A}^{(a,e)}$ | | $\mathbf{B}^{(b,e)}$ | | $\mathbf{C}^{(c,e)}$ | | $\mathbf{D}^{(d,e)}$ | |
| | calc | exp | calc | exp | calc | exp | calc | exp |
|---|---|---|---|---|---|---|---|---|
| $C_1$-$C_2$ | 1.410 | 1.402 | 1.400 | 1.39 | 1.478 | 1.474 | 1.426 | 1.459 |
| $C_2$-$C_3$ | 1.393 | 1.378 | 1.396 | 1.39 | 1.348 | 1.334 | 1.382 | 1.357 |
| $C_3$-$C_4$ | 1.426 | 1.417 | 1.416 | 1.39 | 1.455 | 1.439 | 1.427 | 1.432 |
| $C_1$-$C_{11}$ | 1.493 | 1.484 | | | 1.580 | 1.566 | 1.515 | 1.510 |
| $C_1$-O | | | 1.392 | 1.43 | | | | |
| $C_1 \cdots C_6$ | 2.284 | 2.235 | 2.214 | 2.22 | 1.558 | 1.542 | 2.167 | 1.827 |

| | $\mathbf{A}^{(f)}$ | | $\mathbf{B}^{(f)}$ | |
| | $S_0$ | $S_1$ | $S_0$ | $S_1$ |
|---|---|---|---|---|
| $C_1$-$C_2$ | 1.406 | 1.422 | 1.391 | 1.404 |
| $C_2$-$C_3$ | 1.379 | 1.424 | 1.399 | 1.417 |
| $C_3$-$C_4$ | 1.423 | 1.432 | 1.417 | 1.423 |
| $C_1$-$C_{11}$ | 1.487 | 1.500 | | |
| $C_1 \cdots C_6$ | 2.244 | 2.424 | 2.273 | 2.365 |

| | **A** | | | | | | |
| | one-photon$^{(g)}$ | | two-photon$^{(h)}$ | | calc$^{(h)}$ | | |
| | $\Delta E$ | $f$ | $\Delta E$ | $I$ | $\Delta E$ | $f$ | $I$ |
|---|---|---|---|---|---|---|---|
| $S_1(L_b)$ | 3.44 | 0.003 | 3.47 | 0.08 | 3.33 | 5.E-6 | 0.337 |
| $S_2(L_a)$ | 4.16 | 0.107 | 4.09 | | 4.39 | 3.E-3 | 1.E-3 |
| $S_3(B_b)$ | 4.87 | 1.04 | | | 4.65 | 1.64 | 0.024 |
| $S_4(A_1)$ | | | 4.87 | 1 | 4.89 | 8.E-6 | 1 |

[a] X-ray data [187]. [b] X-ray data [190]. [c] X-ray data [193]. [d] X-ray data [191]. [e] B3LYP/6-31G** results [195]. [f] MCSCF/CAS(10,10)/6-31G results [198,199]. [g] spectral data [200]. [h] spectral data and MCSCF/CAS(10,10)/6-31G results [83].

Spectroscopic measurements on 1,6-methano[10]annulene, including absorption, fluorescence and magnetic circular dichroism [200–202], were reported since the synthesis [165] and discussed in relation to the transannular interaction. The molecule was viewed as an example of "arrested transition state" along the electrocyclic path of the ring closure [201]. The UV spectrum was assigned to the aromatic $L_b$, $L_a$, $B_b$ transitions, the absorption bands being at 3.44, 4.16 and 4.87 eV [200]. In the last years the vibrational and electronic properties of 1,6-methano- and 1,6-epoxy[10]annulene have been subjected to

additional scrutiny and the two molecules have been characterized in more detail [83,195,198,199,203]. The infrared and Raman spectra of both molecules have been measured and a complete vibrational assignment was reported on the basis of *ab initio* density functional calculations of frequencies and infrared and Raman intensities [195]. The good agreement between the observed and calculated Raman spectrum is seen in **Figure 21** for 1,6-epoxy[10]annulene.

**Figure 21.** Experimental (lower, polycrystalline sample, room temperature, 647.1 nm excitation wavelength) and calculated (DF/B3LYP/6-31G$^{**}$ basis set) Raman spectra of 1,6-epoxy[10]annulene.
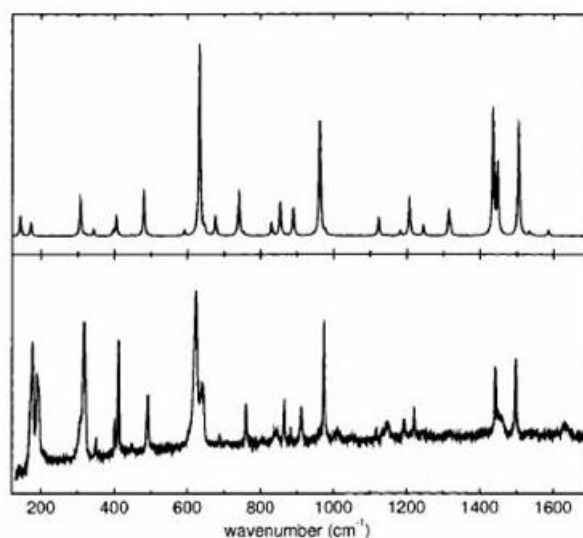


Without going into the full detail of the vibrational analysis, noteworthy are the assignment of the three peaks, 400(ir)/402(R), 862(ir)/865(R) and 982(ir) cm$^{-1}$, to modes of the epoxide bridge with translational parentage (401, 868, 993 cm$^{-1}$, calculated values) and, relatively to the assignment of ring modes, that of the 1319 cm$^{-1}$ band to the $b_1$ bond alternating mode with Kekulean character (1336 cm$^{-1}$, calc).

Medium resolution fluorescence spectra of 1,6-methano[10]annulene have been observed by means of the site selection technique exciting on the onset of the $L_b$ absorption band (origin and the lowest three vibronic bands, see **Figure 22**) [198]. With electronic origin at 25081 cm$^{-1}$ the most active vibronic bands of the fluorescence spectrum lie at 323, 614 and 778 cm$^{-1}$ from the origin. From these bandheads overtones and combination bands extend with clear Franck-Condon profiles.

The analysis has allowed to make inferences on the $L_b$ equilibrium structure on the basis of the common feature of these modes, *i.e.*, the large atomic displacements on $C_1$ and $C_6$. Therefore, it was proposed that upon electronic excitation the $C_1 \cdots C_6$ distance increases so that the transannular interaction as well as the bond alternancy along the ring is reduced. Similar conclusions hold for 1,6-epoxy[10]annulene considering the fluorescence excitation spectrum under supersonic jet expansion [199]. The allowed contribution to the spectrum is due to totally symmetric modes (290, 652, 677 cm$^{-1}$) mostly involving the epoxide bridge. The calculated equilibrium structures of 1,6-methano- and 1,6-epoxy[10]annulene in the $L_b$ state are reported in **Table 10**.

**Figure 22.** Fluorescence spectra of 1,6-methano[10]annulene in isopentane/ether solution ($c = 10^{-3}$ M) at 15 K exciting into the $S_0 \rightarrow S_1$ origin and the lowest three vibronic bands, as shown in the inset.
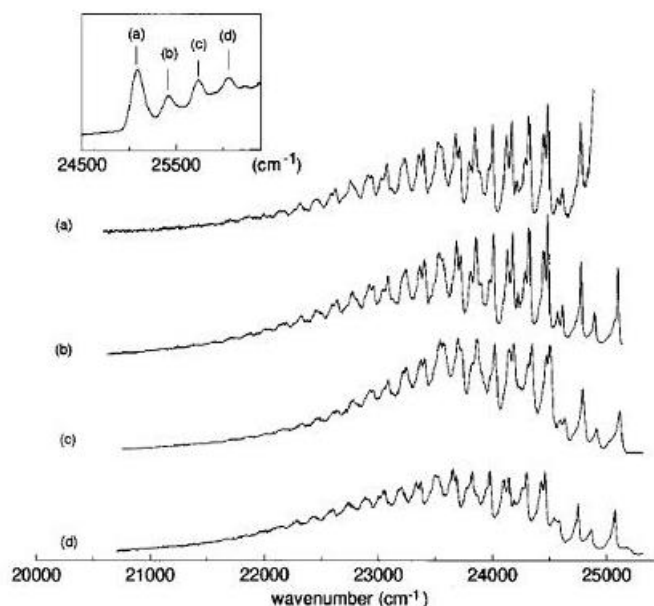


The fluorescence excitation spectrum of 1,6-methano[10]annulene has been measured under supersonic expansion and consists of a rich vibronic band structure with rotational substructure starting from the electronic origin at 25154 cm$^{-1}$ up to 4000 cm$^{-1}$ excess energy [203]. On the basis of the rotational envelope it has been experimentally verified that the $S_0 \rightarrow L_b$ transition dipole oscillates along the molecular long $x$ axis. By a careful analysis of the highly resolved spectrum the assignment has been made of 13 fundamental vibrations of $a_1$ symmetry and 11 of $a_2$ symmetry, these latter being active through $L_b - L_a$ coupling. According to this analysis the observed/calculated frequencies of the ground [195] and lowest excited state form two linearly correlated sets of values, thus enforcing the assignment.

The two-photon fluorescence excitation spectrum of 1,6-methano[10]annulene gives additional information on excited states below 5 eV [83]. The strong one-photon $B_b$ band is almost degenerate with an equally strong two-photon band, as shown in **Figure 23**.

The latter however cannot be similarly assigned. The vertical excitation energies of **Figure 24** have been obtained with MCSCF/CAS(10,10)/6-31G calculations including the MC/QDPT perturbation treatment [204]. The complete set of one- and two-photon data reported in **Table 10** show the remarkably good agreement with experiment if the strong two-photon absorption band is attributed to a fourth $\pi\pi^*$ excited state of $A_1$ symmetry, $S_4(A_1)$.

**Figure 23.** Two-photon excitation spectrum [(a), left, linear polarization] and polarization ratio $\Omega$ of 1,6-methano[10]annulene $10^{-2}$ M in isopentane/ether at room temperature. For the sake of comparison, also the one-photon solution spectrum [(b), right] $10^{-3}$ M in cyclohexane is shown. The one-photon absorption region around $27000$ cm$^{-1}$ is too weak to be observed in these experimental conditions.
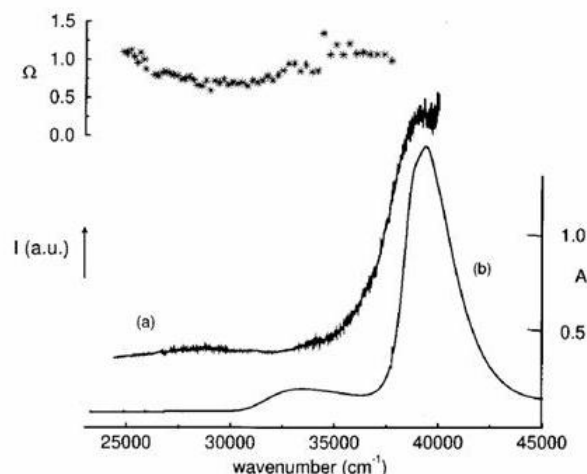


**Figure 24.** Calculated and observed vertical transition energies (eV) of 1,6-methano[10]annulene. Left: MCSCF/CAS(10,10)/6-31G results; center: results from MC/QDPT perturbation treatment [204]; right: observed one- and two-photon transitions.
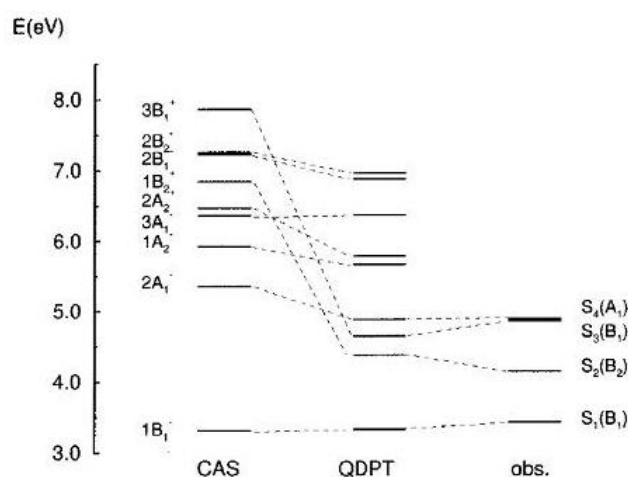


A second interesting point is raised by the observation of the Kekule' mode of $b_1$ symmetry, favoring the bond alternancy in the excited state. This mode increases from 1355 cm$^{-1}$ (ground state value [195]) to 1540 cm$^{-1}$, as expected from the $\pi$ distortive model of cyclic conjugated systems [52]. A steeper potential occurs along the distortion mode in the excited state justifying the occurrence of the equilibrium $C_{2v}$ geometry [198].

### 3.2. [12]Annulene

The synthesis of the elusive [12]annulene as $CTCTCT$ or tri-*trans* isomer was reported almost 40 years ago [205,206]. More recently, the $CCTCCT$ or di-*trans* isomer has been formed as dianion [207]. At the CCSD(T)/cc-pVDZ calculation level on the BHHLYP/6-311+G** optimized geometries (CCSD(T)/cc-pVDZ//BHHLYP/6-311+G**) five minima have been located on the [12]annulene hypersurface within 5-6 kcal/mol above the absolute minimum, which is the $CCCCCT$ or mono-*trans* isomer [208,209]. The five structures, their symmetries and relative energies are shown in **Figure 25**.

**Figure 25.** The five low energy isomers of [12]annulene with the indication of *cis/trans* configuration around double bond, symmetry group, relative energies (kcal/mol) with respect to the $CTCTCT$ isomer and CC bondlengths (Å) on selected structures. CCSD(T)/cc-pVDZ//BHHLYP/6-311+G** results [208,209].
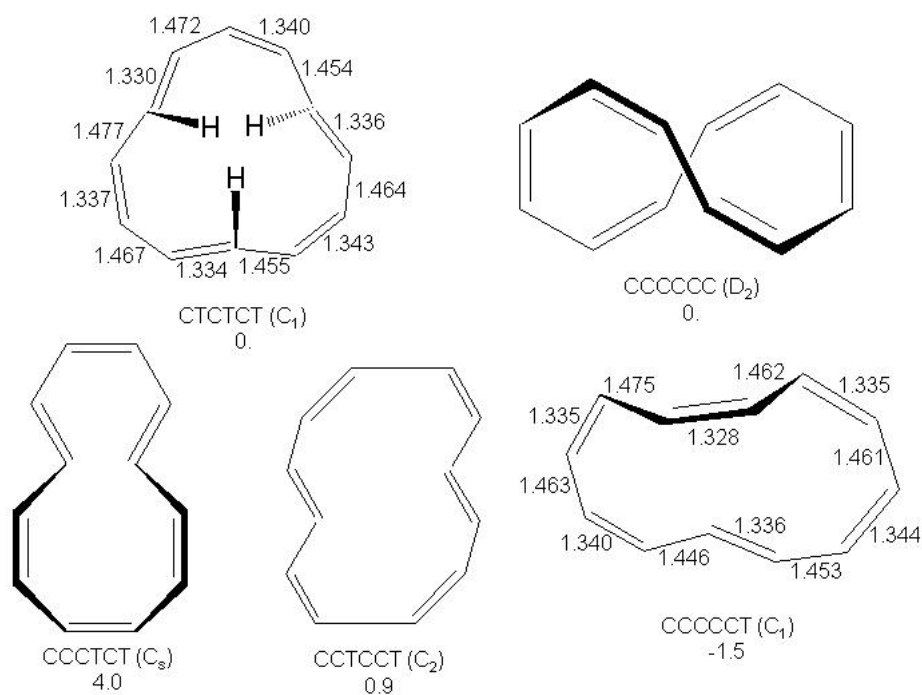


Note that the tri-*trans* isomer has two inner hydrogen atoms above and one below the average ring plane. Among the conformational processes occurring in the tri-*trans* isomer those of **Figure 26**, *i.e.*, (a) the exchange **1a** $\rightleftharpoons$ **1a′** of the three inner with the three outer *trans* hydrogen atoms and (b) the enantiomeric process of the three inner hydrogens **1a** $\rightleftharpoons$ **1a″**, have been investigated in detail [208].

Two transition states have been identified, $TS2$ and $TS3$ of **Figure 27**, 4.5 and 2.7 kcal/mol above $CTCTCT$. $TS2$ is a $C_2$-symmetric transition state with an energy in close agreement with the observed [206] activation energy of the (a) process, 4.1 kcal/mol. The $TS3$ transition state has $C_1$ symmetry and is responsible of the (b) process. The conformation **1b** of **Figure 27**, obtained by simultaneous rotation around all single bonds ($D_3$ symmetry, three *trans* C=C bonds perpendicular to the ring plane), suggested earlier as the transition state for this process [206], is a rather shallow minimum which may be reached crossing

the $TS1$ transition state.  $TS1$ has $C_1$ structure not appreciably modified with respect to **1b** [208].

**Figure 26.** Upper: interconversion of the three inner with the three outer *trans* hydrogen atoms, **1a** $\rightarrow$ **1a$'$**. Lower: conversion of the tri-*trans*[12]annulene to the enantiomer, **1a** $\rightarrow$ **1a$''$**.
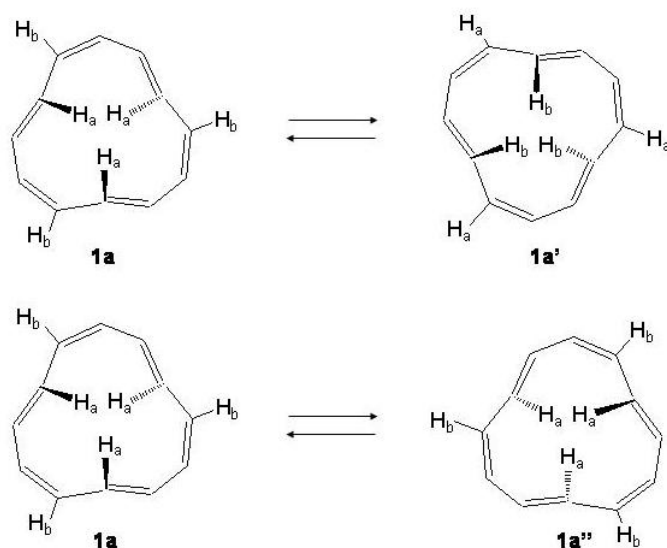


**Figure 27.** Energy profiles of the **1a** $\rightarrow$ **1a$'$** and **1a** $\rightarrow$ **1a$''$** reaction paths, adapted CCSD(T)/cc-pVDZ//BHHLYP/6-311+G$^{**}$ results [208].
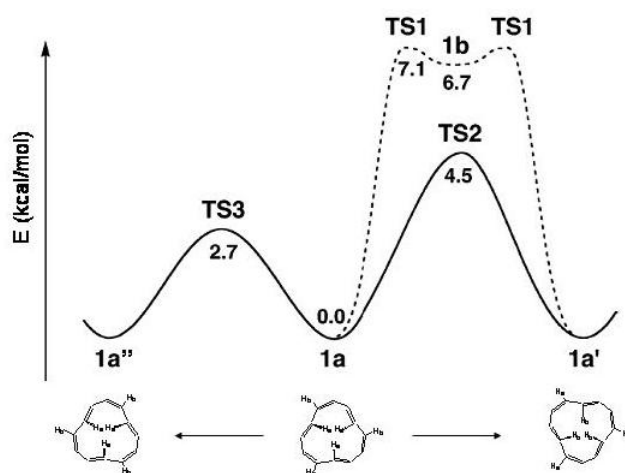


12 $\pi$-electron Systems: Indacene and Biphenylene

$S$-("symmetric")indacene, $as$-("asymmetric")indacene (see **Figure 28**) and biphenylene are planar cyclic conjugated systems with 12 $\pi$ electrons formally derived from $D_{12h}$ [12]annulene and, according to the Hückel rule, antiaromatic systems.

**Figure 28.** Bond alternating and bond equalized structures of *s*-indacene (**2a, 2b, 3**) and *as*-indacene (**4a, 4b, 5**) with atomic numbering.
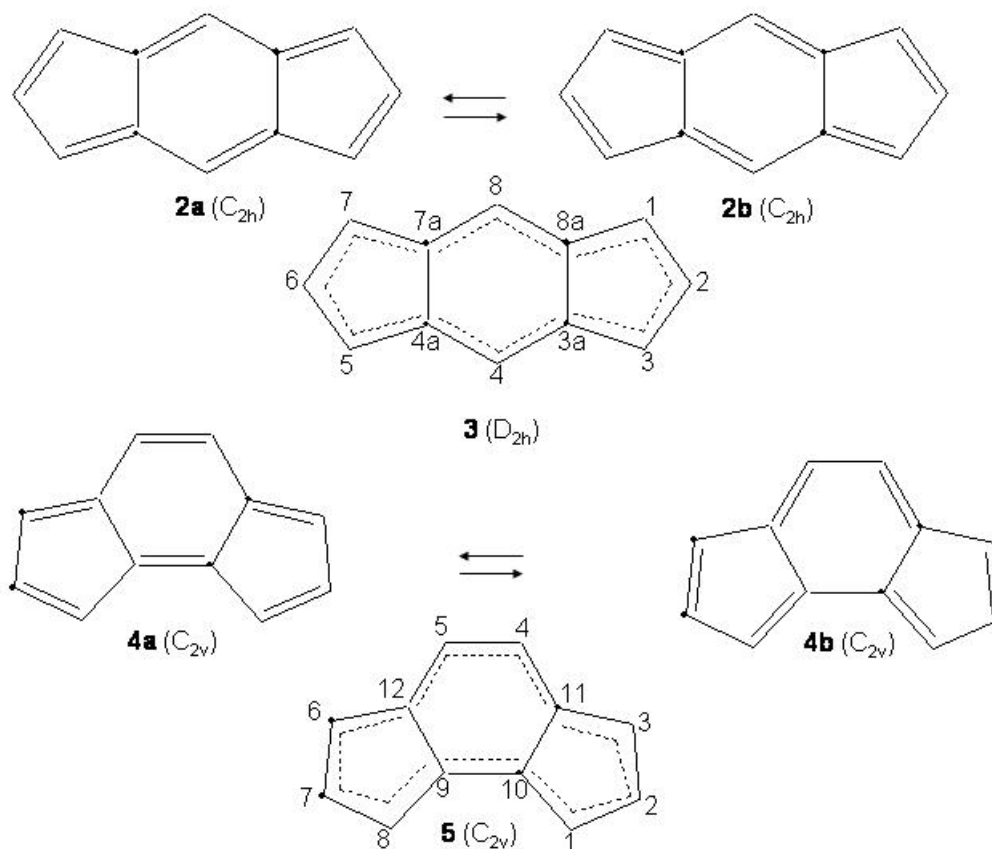


Two possible alternatives have been considered for *s*- and *as*-indacene: either a bond equalized structure of $D_{2h}/C_{2v}$ symmetry, *i.e.*, **3** and **5** of **Figure 28**, or two interconverting valence isomers of $C_{2h}/C_{2v}$ symmetry with localized bonds, *i.e.*, **2a,2b** and **4a,4b**. In the second case **3** and **5** are transition states connecting **2a** with **2b** and **4a** with **4b**, respectively. Note, however, that while **2a,2b** are degenerate configurations, **4a,4b** are structures with different energies. The two most recent *ab initio* calculations on *s*-indacene [210,211] give structural data in good agreement with each other (see **Table 11**) and small energy differences between the $D_{2h}$ and $C_{2h}$ structures, 0.7 and 0.1 kcal/mol in favor of the localized $C_{2h}$ structure. In the B3LYP/6-31G* study [211], the $D_{2h}$ structure was found to be the transition state for double bond isomerization **2a** $\rightarrow$ **2b**, the bond alternating $b_{1g}$ mode having imaginary frequency, $349i$ cm$^{-1}$. If $ZPE$ is included, the $\upsilon = 0$ energy of the $D_{2h}$ transition state is lower than the $\upsilon = 0$ energy of the localized $C_{2h}$ state by 0.6 kcal/mol. Accordingly, *s*-indacene was referred as a "quasi-delocalized" molecule. In the other study [210] single-point CASPT2 energy calculations at the MP2/6-31G* geometries lower $D_{2h}$ *s*-indacene below $C_{2h}$ by 3.1 kcal/mol. The *s*-indacene ground state has been described as due to bonding of two allyl radicals with a central benzene moiety (regarded in turn to be formed by two allyl radicals).

Although *s*-indacene is a highly reactive molecule, the 1,3,5,7 *tert*-butyl derivative is a stable compound at room temperature [30]. X-ray diffraction data have been taken at room as well as at 100 K [30,31] consistent with a symmetric $D_{2h}$ ring geometry. Coupling these data with previous results

it appears that *tert*-butyl substituents play a minor role in determining the ring structure, limited to the increase of the 1-8a bond [212]. Due to the hindered rotation of these groups around the $C_{ring} - C_{but}$ bond several conformers occur some of which are responsible of the near-infrared $S_0 \rightarrow S_1$ absorption spectrum when this molecule is dissolved in solution [212,213].

**Table 11.** Upper: ground state geometries (bondlengths, Å) of *s*- and *as*-indacene and energy difference $\Delta E$ (kcal/mol) between localized and delocalized structures of **Figure 28**. Center: ground state geometries (bondlengths, Å) of *s*-indacene (**I**), 1,3,5,7-tetramethyl-*s*-indacene (**TMI**) and 1,3,5,7-tetra-*tert*-butyl-*s*-indacene (**TTBI**). Lower: experimental ground state geometry of 1,3,5,7-tetra-*tert*-butyl-*s*-indacene and calculated geometries of the $S_2$ and $S_6$ states of *s*-indacene. The atomic numbering is indicated in **Figure 28**.

| | *s*-indacene | | | | | *as*-indacene | |
|---|---|---|---|---|---|---|---|
| | MP2/6-31G* [a] | | B3LYP/6-31G* [b] | | | MP2/6-31G* [a] | |
| | $D_{2h}$ | $C_{2h}$ | $D_{2h}$ | $C_{2h}$ | | **4a** | **4b** |
| $C_1$-$C_2$ | 1.404 | 1.439 | 1.406 | 1.432 | $C_1$-$C_2$ | 1.363 | 1.466 |
| $C_2$-$C_3$ | | 1.378 | | 1.383 | $C_2$-$C_3$ | 1.469 | 1.364 |
| $C_3$-$C_{3a}$ | 1.429 | 1.450 | 1.423 | 1.445 | $C_3$-$C_{11}$ | 1.374 | 1.462 |
| $C_1$-$C_{8a}$ | | 1.397 | | 1.400 | $C_4$-$C_{11}$ | 1.440 | 1.367 |
| $C_{3a}$-$C_4$ | 1.397 | 1.379 | 1.399 | 1.380 | $C_4$-$C_5$ | 1.366 | 1.449 |
| $C_4$-$C_{4a}$ | | 1.420 | | 1.419 | $C_9$-$C_{10}$ | 1.363 | 1.439 |
| $C_{3a}$-$C_{8a}$ | 1.437 | 1.448 | 1.448 | 1.452 | | | |
| $\Delta E$ | 0.7 | 0. | 0.1 | 0. | | 5.0 | 7.5 |

| | **I** | **TMI** | **TTBI** | **exp**[d] |
|---|---|---|---|---|
| | | B3LYP/6-31G[c] | | |
| $C_1$-$C_2$ | 1.413 | 1.413 | 1.414 | 1.406/08 |
| $C_3$-$C_{3a}$ | 1.428 | 1.437 | 1.443 | 1.438/34 |
| $C_{3a}$-$C_4$ | 1.402 | 1.400 | 1.402 | 1.394/95 |
| $C_{3a}$-$C_{8a}$ | 1.454 | 1.454 | 1.454 | 1.442 |

| | $S_0$(**TTBI, exp**[d]) | $S_2$ [e] | $S_6$ [e] |
|---|---|---|---|
| $C_1$-$C_2$ | 1.406 | 1.418 | 1.431 |
| $C_2$-$C_3$ | 1.408 | 1.414 | 1.424 |
| $C_3$-$C_{3a}$ | 1.438 | 1.445 | 1.416 |
| $C_1$-$C_{8a}$ | 1.434 | 1.441 | 1.409 |
| $C_{3a}$-$C_4$ | 1.394 | 1.413 | 1.422 |
| $C_4$-$C_{4a}$ | 1.395 | 1.416 | 1.430 |
| $C_{3a}$-$C_{8a}$ | 1.442 | 1.449 | 1.479 |

[a] calculation results [210]. [b] calculation results [211]. [c] calculation results [212]. [d] X-ray data on **TTBI** [31]. [e] semiempirical QCFF/PI results on **TTBI** [214].

1,3,5,7-tetra-*tert*-butyl-*s*-indacene fluoresces from the second excited state, a property shared by few others organic molecules among which the first and most famous is azulene [215], with fluorescence quantum yield $9 \times 10^{-5}$ and radiative decay constant $\tau_r(S_2) \approx 10$ ns [216]. There is a large energy gap between the onset of the $S_0 \rightarrow S_1$ absorption, 9270 cm$^{-1}$, and that of $S_0 \rightarrow S_2$, 18380 cm$^{-1}$ and no other energy levels are calculated in the intermediate region [214,216,217]. The relaxation dynamics of the $S_1$ and $S_2$ levels has been studied by means of picosecond transient absorption experiments [216]. Time constants of non radiative deactivation from $S_1$ and $S_2$, 18 and 2.5 ps respectively, were measured. These times are much smaller than the shortest time constants of intersystem crossing in conjugated cyclic hydrocarbons, $\tau_{ISC} \geq 10$ ns [218]. Internal conversion is the dominant relaxation process in these

cases. The $S_1 \rightarrow S_0$ internal conversion has been further characterized by the occurrence of a $S_1/S_0$ conical intersection close in energy and geometry to the $S_1$ minimum [219]. Due to this an efficient non radiative decay channel is promoted thus leading to a short $S_1$ lifetime and lack of $S_1 \rightarrow S_0$ fluorescence.

Excited states of the 1,3,5,7-tetra-*tert*-butyl-*s*-indacene have been probed by means of one-photon absorption and resonance Raman spectroscopy at low temperature [214]. As the excitation energy approaches the $S_0 \rightarrow S_2$ origin the totally symmetric Raman peaks 390, 572 and 742 cm$^{-1}$ are enhanced together with the multiplet below 300 cm$^{-1}$ (see **Figure 29**).

**Figure 29.** Pre-resonance Raman spectra of tetra-*tert*-butyl-*s*-indacene as a function of the exciting wavelength approaching the $S_0 \rightarrow S_2$ origin (bottom to top, c = $6\times10^{-4}$ M in isopentane/ether, 77K). Solvents bands are indicated by asterisks.
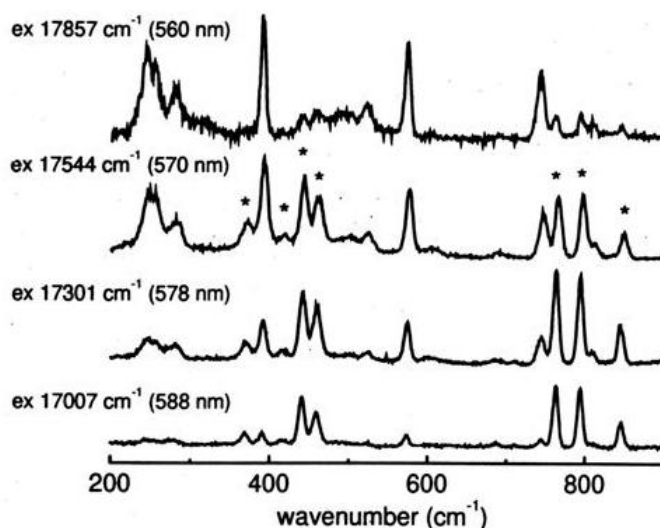


When the excitation energy is tuned across the $S_0 \rightarrow S_2$ absorption profile both resonance Raman and fluorescence signals are observed (see **Figure 30**).

The Raman enhancement profile of the 390 cm$^{-1}$ peak (corresponding to the calculated 431 cm$^{-1}$ mode) has been measured as a function of the exciting wave number and determined from the calculation of the ground and $S_2$ equilibrium structures and of the consequent Franck-Condon factor. The results are compared in **Figure 31**. Recalling the "allyl" representation of *s*-indacene, the vibrational mode (390 cm$^{-1}$, exp; 431 cm$^{-1}$, calc) describes the elongation of the two side allyl units with respect to the benzene moiety (composed of two allyl units whose CC bonds elongate), inducing the equilibrium geometry of the $S_2$ state. The structure of the $S_2$ state, having approximate $D_{2h}$ symmetry according to semiempirical methods [214], is in good agreement with expectations.

**Figure 30.** Resonance Raman and fluorescence spectra of tetra-*tert*-butyl-*s*-indacene as a function of the exciting wavenumber across the $S_0 \rightarrow S_2$ absorption region (bottom to top, c = $10^{-6}$ M in isopentane/ether, 77K). Solvents bands are indicated by asterisks.
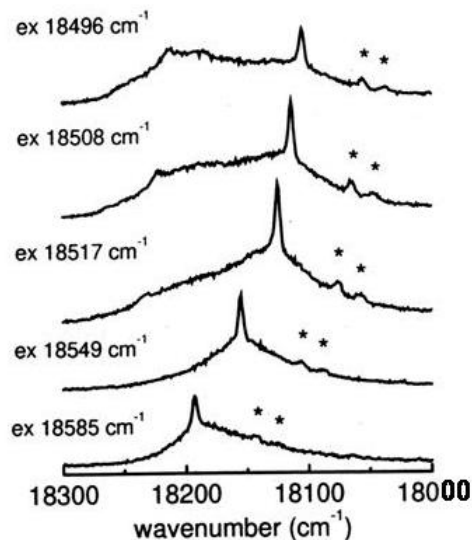


**Figure 31.** Experimental Raman enhancement factor (crosses and squares) of the 390 cm$^{-1}$ peak scanning across the $S_0 \rightarrow S_2$ origin band and the first vibronic band of tetra-*tert*-butyl-*s*-indacene and calculated factor of the corresponding 431 cm$^{-1}$ mode for the model system mono-*tert*-butyl-*s*-indacene.
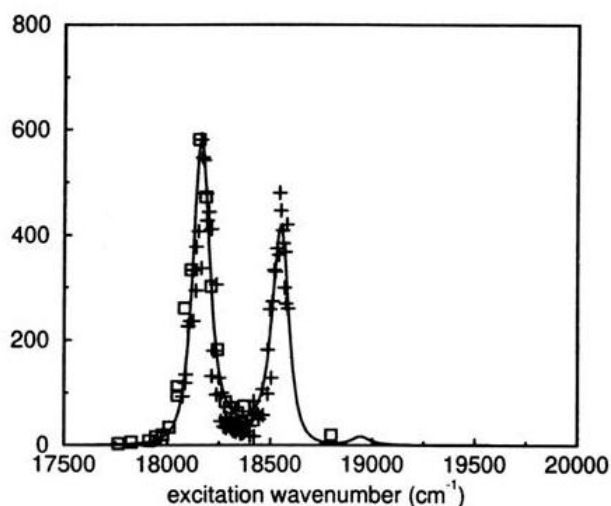


Biphenylene has been extensively investigated in the ground and lowest $\pi\pi^*$ excited states [220–226]. The infrared spectrum of biphenylene embedded in a Ar matrix was measured at 12 K, allowing the assignment of 35 fundamental modes (out of the total 54) by spectral analysis and comparison with *ab initio* calculation data [220]. As to the $\pi\pi^*$ electronic transitions, it should be recalled that one- and two-photon spectroscopy are mutually exclusive techniques since biphenylene is a centrosymmetric

molecule with $D_{2h}$ symmetry. Starting from the ground state, excited states of *ungerade* symmetry are active in one-photon spectroscopy. The second transition, $S_0 \rightarrow S_2$, is long-axis polarized [223] (see **Figure 32** for the reference system) with origin at 27690 cm$^{-1}$. At higher energy a strong absorption, equally long-axis polarized, is found at 40240 cm$^{-1}$ for biphenylene in solution [224]. Although the $S_1(B_{1g})$ state is one-photon inactive a careful analysis of the vibronically induced spectrum in the lowest absorption region [222] locates the electronic origin at 23884 cm$^{-1}$. Two-photon active states of $\pi\pi^*$ character belong to the $A_g$ and $B_{1g}$ symmetry species. The two-photon spectrum of biphenylene in **Figure 32** has been measured in the spectral range 225–370 nm combining fluorescence excitation and thermal lensing detection [225].

**Figure 32.** Two-photon excitation spectrum (lower trace) and polarization ratio $\Omega$ (upper trace) of biphenylene in cyclohexane at room temperature in the 225–370 nm spectral range.
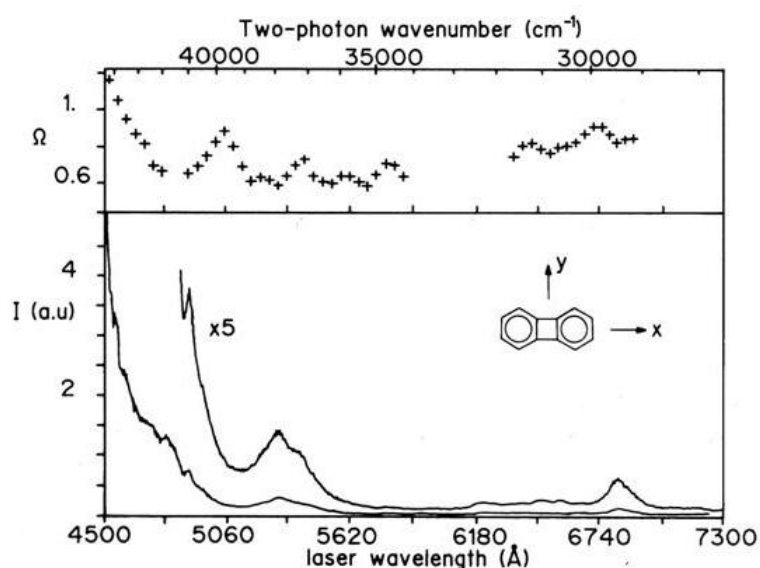


While the transition to the $S_1$ state, in principle two-photon active, is too weak to be observed, at higher energy the first excited $A_g$ state, $2A_g$, is seen around 265 nm and the second excited $B_{1g}$, $2B_{1g}$, has its onset at $\approx 225$ nm. The vibronic band structure between 340 and 310 nm is assigned to vibronically induced transitions to the second excited state. The $S_0 \rightarrow S_1$ two-photon transition has enhanced intensity in 2,3,6,7-tetra-ethylbiphenylene [226] due to the pseudoparity selection rules and to the inductive perturbation of the ring $\pi\pi^*$ density [227]. The electronic origin in the derivative is observed at $\approx 23100$ cm$^{-1}$.

### 3.3. [14]Annulene

The lowest energy isomer of [14]annulene has the structure of a distorted pyrene perimeter. The molecule is non planar and centrosymmetric but with approximate $C_{2h}$ symmetry according to X-ray data [228], as indicated in **Figure 33**. The CC bond lengths are in the range 1.350–1.407 Å without apparent alternation. Non planarity is due to the steric overcrowding of the four inner hydrogen atoms which are directed toward the center of the molecule.

**Figure 33.** Experimental [228], left, and calculated [20] (B3LYP/6-311+G**, center; BHLYP/6-311+G**, right) structures of [14]annulene. Bondlengths in Å.
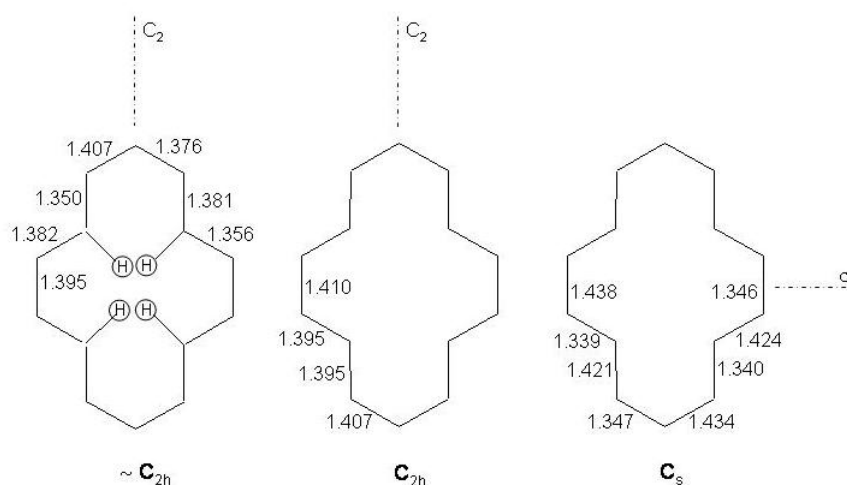


Recent density functional calculations on [14]-, [18]- and [22]annulenes have shown that the $C_{2h}$ structure of [14]annulene, though a local minimum at the B3LYP level, is a transition state when functionals like BHLYP and KMLYP, having a larger Hartree-Fock component, are chosen [20]. Using these functionals the $C_{2h}$ transition state lies 2.2 - 2.5 kcal/mol above the $C_s$ minimum. The calculated $^1H$ $NMR$ chemical shifts of the inner and outer hydrogen atoms match well the experimental values [6] assuming the $C_s$ structure for [14]annulene while this is not verified when the X-ray geometry is used. Other experimental techniques such as vibrational and electronic absorption spectroscopies should provide in principle evidences in favour of the $C_s$ structure for [14]annulenes. It has been however observed that these methods are not sensitive to the $C_{2h} \rightarrow C_s$ structural variation [20]. In the following subsection the UV absorption spectrum of [14]annulene will be compared with those of bridged [14]annulenes whose bond equalized structures are well established both on experimental and theoretical grounds.

The molecule undergoes in solution the bond shifting reaction of **Figure 34** with the equilibrium state strongly displaced toward the configurational $CTCTCTT$ isomer. The activation energy of this process was found to be 21 kcal/mol [6]. Since $\Delta$ $trans$, *i.e.*, the difference of *trans* double bonds between reactant and product, is 1, this means that one *trans* double bond isomerizes to *cis*. The reaction mechanism consists of three steps (see **Figure 35**) and requires in the final step a Möbius antiaromatic transition state [9].

Transition states of annulenes may be classified according to the Hückel or Möbius topology [229,230]. In the simple example of bond shifting in cyclobutadiene and cyclooctatetraene the number of *cis* double bonds is conserved and the interconversion process occurs through a Hückel antiaromatic transition state. In general, the number of *trans* double bonds are the reference index for bond shifting in annulenes: the reaction will occur with Hückel topology when $\Delta$ $trans$ is zero or an even number and with Möbius topology when $\Delta$ $trans$ is an odd number. For the reaction shown in **Figure 35** $\Delta$ $trans$ = 1. The reaction requires a Möbius bond shifting step and since [14]annulene is a $(4n + 2)$ $\pi$-electron system the bond equalized transition state is antiaromatic, $TS1$ in **Figure 35**. The

three step reaction $CTCTCTT \rightarrow CCTCTCT$ has an energy barrier in the bond shifting step of 19.3 kcal/mol [9].

**Figure 34.** *Cis/trans* isomerization reaction of [14]annulene in solution at room temperature.
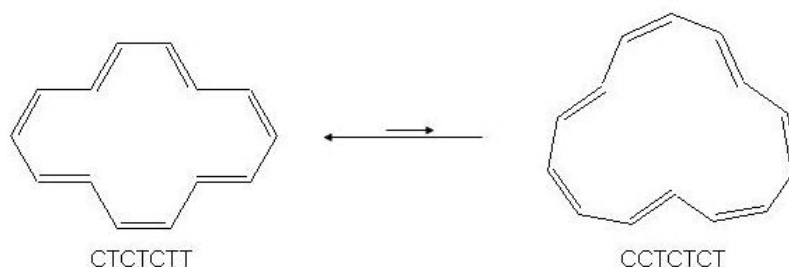


**Figure 35.** Energy profile of the *cis/trans* isomerization reaction connecting the $CTCTCTT$ and $CCTCTCT$ isomers of [14]annulene. CASPT2(14,14)/cc-pVDZ//(U)BHHLYP/6-311+G$^{**}$ results [9].
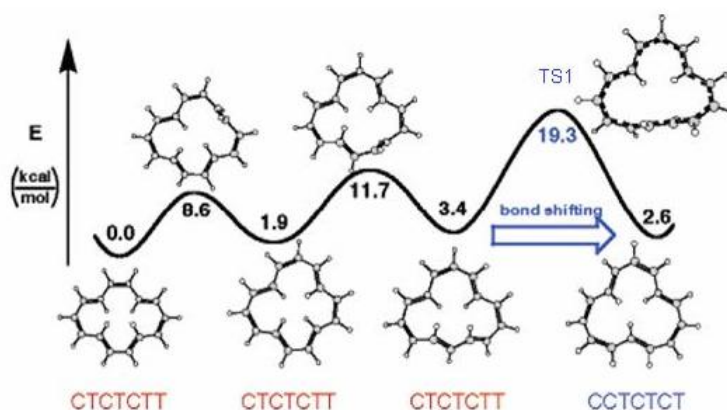


Bridged [14]Annulenes

Three types of bridged [14]annulenes have been synthesized, based on anthracene, pyrene and dicyclopentaheptalene perimeters [10]. Here we consider only the anthracene type molecules of **Figure 36**. The two methano bridges may be arranged in a *syn-* or in a *anti-* geometry: in the *syn-* isomer **6** the ring is expected to be approximately planar while in the *anti* **7** the ring takes on a polyolefinic structure [16].

The molecular framework becomes more rigid removing the two inner bridge hydrogen atoms (a) with formation of a $C_{15}$-$C_{16}$ bond in 1,6:8,13-ethanediylidene[14]annulene **8** and (b) with insertion of a methylene spacer in 1,6:8,13-propanediylidene[14]annulene **9** [231,232]. The molecular structures of **6**–**9** have been determined by X-ray diffraction [233–236]. In the *syn*-bridged [14]annulene the C-C bonds have reduced alternancy, 1.365–1.418 Å, [233] whereas alternate as single and double bonds, 1.34–1.46 Å, in the 7-methoxycarbonyl derivative of **7** [234]. Both **8** and **9** have approximate bond

equalized geometries, 1.38–1.41 Å [235,236]. These structures have been calculated with different computational methods [237–239]. It may be seen from **Table 12** that **6**, **8** and **9** have bond equalized $C_{2v}$ structures. Alternancy is associated with **7** [238]. The perimeter of **8** is appreciably planar (maximum difference between the $z$ coordinates of the ring C atoms, $\Delta \mid z_m \mid$, 0.35 Å) while **9** possesses a more bent structure ($\Delta \mid z_m \mid = 0.73$ Å). Also, the 1,6 and 8,13 non bonded atoms have distances in **8** longer than in **9** suggesting for **8** a smaller transannular interaction.

The infrared and Raman spectra of the two molecules have been measured and discussed in terms of ring and bridge modes [239], similarly to the bridged [10]annulenes case but with larger mixing between the two types of vibration.

**Figure 36.** Upper: molecular structures of *syn-* and *anti-*1,6:8,13-bismethano[14]annulene, **6**, left; **7** right, respectively, with atomic numbering. Lower: molecular structures of 1,6:8,13-ethanediylidene[14]annulene (**8**, left) and 1,6:8,13-propanediylidene[14]annulene (**9**, right).
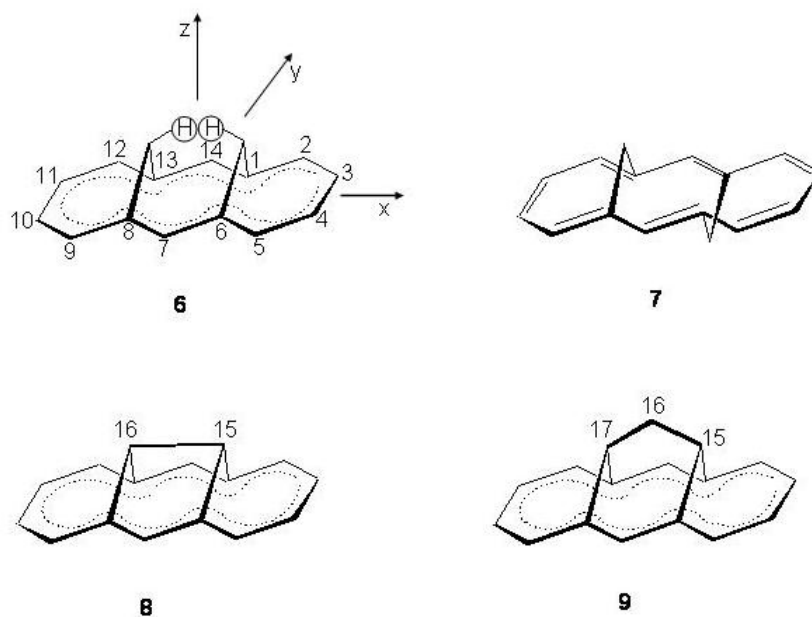


The Raman spectra depend on the excitation wavelength. In **Figure 37** the 1064 nm excitation corresponds to the normal Raman spectrum of **9**. With the 647.1 nm excitation all the Raman peaks above 800 cm$^{-1}$ show decreased intensities with respect to those below 800 cm$^{-1}$. The peaks at 251, 420 and 615 cm$^{-1}$ are assigned to modes of anthracene parentage, the lowest to an out-of-plane and the other two to in-plane modes, where the displacements of the bridgehead atoms enlarge the ring size [239]. Therefore, it has been assumed that the equilibrium geometry of the lowest excited state ($L_b$) has increased transannular distances. The analysis of high- [240] and medium-resolution [241] fluorescence spectra of the two systems confirms the hypothesis.

**Figure 37.** Raman spectra of polycrystalline 1,6:8,13-ethanediylidene[14]annulene **8** at room temperature at two excitation wavelengths, 1064 nm (upper) and 647.1 nm (lower).
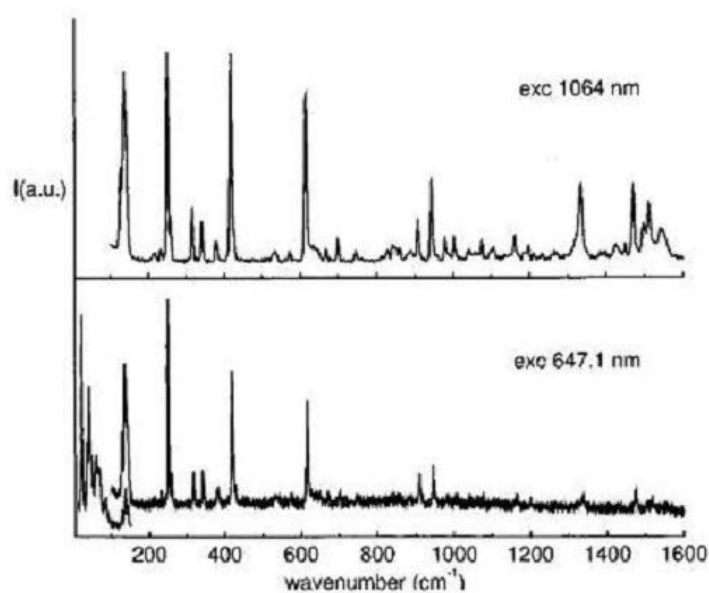


**Figure 38.** Absorption spectra of 1,6:8,13-ethanediylidene[14]annulene **8** (lower, $c = 5 \times 10^{-4}$ M in isopentane/ether, room temperature) and 1,6:8,13-propanediylidene[14]annulene **9** (upper, $c = 2 \times 10^{-5}$ M and $2 \times 10^{-3}$ M in isopentane/ether, room temperature). The excitation wavelengths of the Raman spectra are shown in the figure as vertical lines between the two spectra.
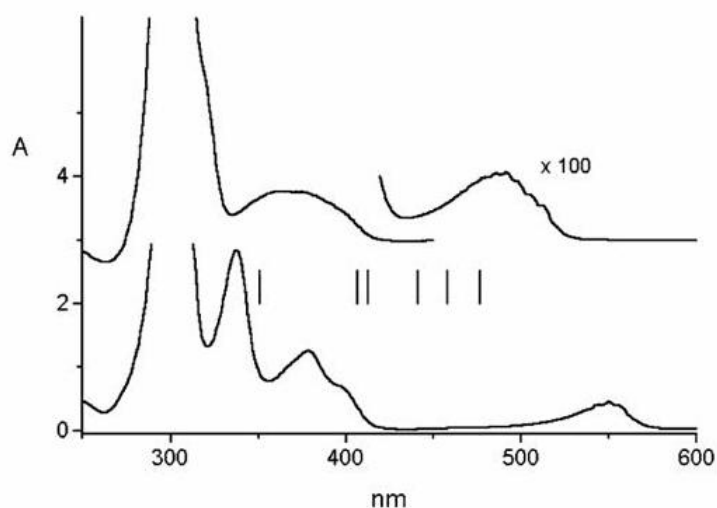


In the absorption spectra of **8** and **9**, shown in **Figure 38**, the band maxima of the lowest electronic transition shift from 480 nm in **9** to 550 nm in **8**. Reasonably, this effect is correlated with the increased ring planarity of **8** with respect to **9**. Considering also the absorption spectra of [14]annulene [242] and of dimethyldihydropyrene [243], a bridged [14]annulene with pyrene perimeter, the band maxima further

shift to $\sim 600$ nm in the first case and to $\sim 640$ nm in the second. Then, both these systems in solution are more planar than **8**.

The absorption spectra [241,244] of **8** and **9** (see **Figure 38**) offer the good opportunity to investigate about the $L_a$ and $B_a$ geometries by means of resonance Raman spectroscopy. CC stretching modes of **8** are preferentially enhanced exciting on the onset of the $L_a$ transition (see **Figure 39**) while only the 234 cm$^{-1}$ mode shows prominently with excitation at 350 nm on the foot of the $B_a$ transition.

**Figure 39.** Raman spectra of 1,6:8,13-ethanediylidene[14]annulene **8** (lower five traces) and 1,6:8,13-propanediylidene[14]annulene **9** (upper two traces), $c = 10^{-3}$ M in isopentane/ether, room temperature. The excitation wavelengths are, from bottom to top, 476.5, 457.9, 441.6, 413.1 and 406.7 nm for 1,6:8,13-ethanediylidene[14]annulene and 413.1 and 406.7 nm for 1,6:8,13-propanediylidene[14]annulene. The most intense solvent bands are indicated by asterisks in the 406.7 nm spectrum.
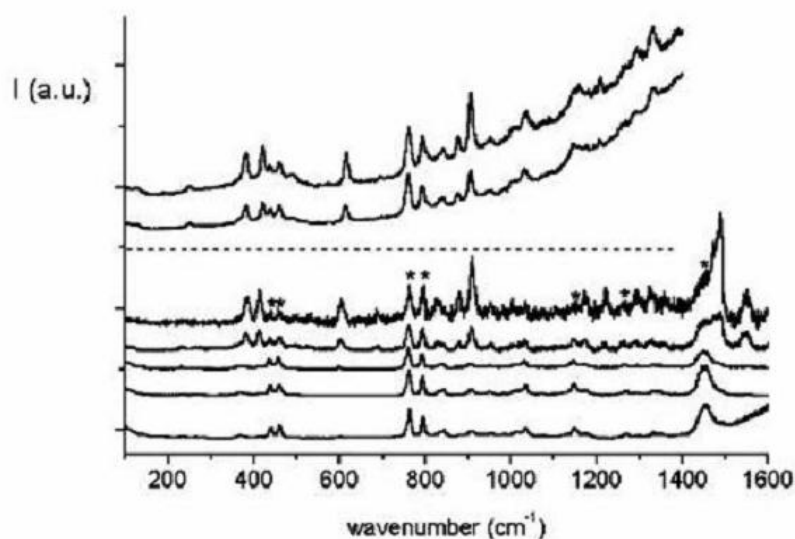


Qualitatively, the latter result points to the similarity between the $B_a$ and $L_b$ equilibrium structures. As indicated by the MCSCF/CAS(10,10) data of **Table 12**, the common feature of the two states is the increase of the transannular distances with respect to the ground state. This structural change is responsible for the strong activity of the 234 cm$^{-1}$ mode in **8** and of the 251 cm$^{-1}$ mode in **9**. On the contrary, the slight decrease of these distances in the $L_a$ together with the enhancement of bond alternation favors an anthracene-like equilibrium structure for the $L_a$ state of both molecules.

**Table 12.** Structural data (bondlengths, Å) of *syn*-1,6:8,13-bismethano[14]annulene (**6**), 1,6:8,13-ethanediylidene[14]annulene (**8**) and 1,6:8,13-propanediylidene[14]annulene (**9**). Upper row: ground state B3LYP/cc-pVDZ results [239]. Central and lower rows: geometries of the ground and of the lowest excited states (**8**, central; **9**, lower); MCSCF/CAS(10,10)/6-31G results [241].

| | ground state | | | | | |
|---|---|---|---|---|---|---|
| | **6** | | **8** | | **9** | |
| | calc | exp[a] | calc | exp[b] | calc | exp[c] |
| $C_1$-$C_2$ | 1.421 | 1.412 | 1.402 | 1.406 | 1.415 | 1.413 |
| $C_2$-$C_3$ | 1.391 | 1.370 | 1.397 | 1.381 | 1.391 | 1.387 |
| $C_3$-$C_4$ | 1.428 | 1.407 | 1.415 | 1.404 | 1.425 | 1.414 |
| $C_6$-$C_7$ | 1.406 | 1.393 | 1.403 | 1.387 | 1.404 | 1.395 |
| $C_1 \cdots C_6$ | 2.402 | 2.410 | 2.514 | 2.469 | 2.408 | 2.384 |
| $C_1$-$C_{15}$ | 1.512 | 1.498 | 1.518 | 1.524 | 1.516 | 1.517 |
| $C_{15}$-$C_{16}$ | 2.933 | 2.917 | 1.548 | 1.570 | 1.523 | 1.518 |
| $C_{15} \cdots C_{17}$ | | | | | 2.444 | 2.434 |
| H$\cdots$H | 1.686 | 1.780 | | | | |

| | **8** | | | | | |
|---|---|---|---|---|---|---|
| | $S_0$ | | $L_b$ | $L_a$ | $B_a$ | $B_b$ |
| | calc | exp[b] | | | | |
| $C_1$-$C_2$ | 1.398 | 1.406 | 1.410 | 1.384 | 1.403 | 1.417 |
| $C_2$-$C_3$ | 1.396 | 1.381 | 1.408 | 1.424 | 1.402 | 1.388 |
| $C_3$-$C_4$ | 1.391 | 1.404 | 1.383 | 1.373 | 1.400 | 1.408 |
| $C_6$-$C_7$ | 1.403 | 1.387 | 1.414 | 1.410 | 1.408 | 1.414 |
| $C_1 \cdots C_6$ | 2.508 | 2.469 | 2.554 | 2.478 | 2.552 | 2.525 |
| $C_1$-$C_{15}$ | 1.514 | 1.524 | 1.513 | 1.512 | 1.505 | 1.514 |
| $C_{15}$-$C_{16}$ | 1.547 | 1.570 | 1.545 | 1.545 | 1.539 | 1.554 |

| | **9** | | | | | |
|---|---|---|---|---|---|---|
| | $S_0$ | | $L_b$ | $L_a$ | $B_a$ | $B_b$ |
| | calc | exp[c] | | | | |
| $C_1$-$C_2$ | 1.413 | 1.413 | 1.420 | 1.392 | 1.423 | 1.418 |
| $C_2$-$C_3$ | 1.388 | 1.387 | 1.408 | 1.422 | 1.390 | 1.394 |
| $C_3$-$C_4$ | 1.404 | 1.414 | 1.388 | 1.379 | 1.411 | 1.411 |
| $C_6$-$C_7$ | 1.404 | 1.395 | 1.416 | 1.413 | 1.411 | 1.410 |
| $C_1 \cdots C_6$ | 2.408 | 2.384 | 2.479 | 2.386 | 2.440 | 2.477 |
| $C_1$-$C_{15}$ | 1.512 | 1.517 | 1.516 | 1.511 | 1.513 | 1.512 |
| $C_{15}$-$C_{16}$ | 1.520 | 1.518 | 1.522 | 1.518 | 1.522 | 1.522 |
| $C_{15} \cdots C_{17}$ | 2.443 | 2.434 | 2.443 | 2.448 | 2.451 | 2.437 |

[a] X-ray data [233]. [b] X-ray data [235], from the 15,16-dimethyl derivative of **8**. [c] X-ray data [236].

### 3.4. [16]Annulene

The synthesis of [16]annulene was first achieved starting from the dehydro[16]annulene derivative [245] and later from the cyclooctatetraene dimer [246]. At temperature below $-67°$ [16]annulene is a mixture of two configurational isomers, **10a** and **10b** of **Figure 40**, **10a** being the major (80 per cent) component [6,247]. In the solid state **10a** is the stable arrangement of [16]annulene in a nearly $S_4$ bond alternating structure [248,249]. The optimized structures of the two isomers, $CTCTCTCT$ (**10a**) and $CTCTTCTT$ (**10b**), at the BHHLYP/6-311+G$^{**}$ calculation level are reported in **Figure 40**. [16]annulenes **10a** and **10b** are the first $4n$ $\pi$ annulenes whose bond alternating structures are not overwhelmingly dominated by angle strain or steric hindrance of the inner hydrogens. In a sense,

the *UV-vis* absorption spectrum of [16]annulene should be typical of $4n$ $\pi$ systems. Two absorption bands are observed at 446 and 293 nm with strongly different extinction coefficients, both assigned to the **10a** isomer [250]. The weakest band at 446 nm has been interpreted in $S_4$ symmetry as due to the vibronically induced $2b(HOMO) \rightarrow 3b(LUMO)$ transition. The two orbitals $2b$ and $3b$ arise from splitting of the non bonding $e_{4u}$ degenerate pair due to symmetry lowering from the fully planar $D_{16h}$ to $S_4$ symmetry. The strongest band at 293 nm is due to the allowed $2b(HOMO) \rightarrow 3e(LUMO+1)$ transition. Comparing with more simple $4n$ $\pi$ systems, the first two excited states of cyclobutadiene and pentalene are of $g$ symmetry [23,26,28,29,99] (and, as a consequence, the transition to these states from the ground state not allowed) while in [16]annulene only the lowest excited state is totally symmetric (and then the $S_0 \rightarrow S_1$ transition not allowed). The difference follows from a property of cyclobutadiene and pentalene not shared by [16]annulene, *i.e.*, the occurrence of low energy doubly-excited configurations determining the second excited state in these molecules.

**Figure 40.** The structures of the $CTCTCTCT$ (**10a** and $CTCTTCTT$ (**10b** [16]annulene isomers calculated at the BHHLYP/6-311+G$^{**}$ level [8]. Selected bondlengths (Å) and dihedral angles (◦) are shown.
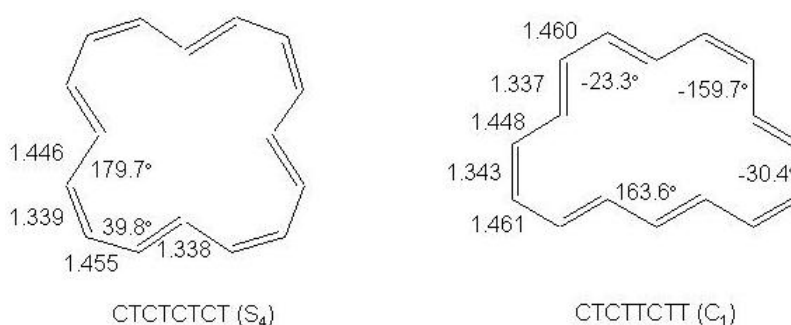


A large number of [16]annulene isomers has been computationally discovered [251,252]. In **Figure 41** the dynamical processes characterizing **10a** and **10b** are shown [253]. These include (a) the configurational change **10a** $\rightarrow$ **10b** or $CTCTCTCT \rightarrow CTCTTCTT$ with activation energy 10.3 kcal/mol, (b) the conformational change **10a** $\rightarrow$ **10a′** and **10b** $\rightarrow$ **10b′** with activation energy 9.2 and 8.2 kcal/mol, respectively, and (c) the bond shifting **10a** $\rightarrow$ **10a″** and **10b** $\rightarrow$ **10b″**, $E_a \approx$ 8.2–8.8 kcal/mol [6]. These processes have been investigated [8] optimizing structures by means of density functional methods, B3LYP/6-311+G$^{**}$ and BHHLYP/6-311+G$^{**}$, and calculating single-point energies with the CCSD(T)/cc-pVDZ//B3LYP/6-311+G$^{**}$ or CCSD(T)/cc-pVDZ//BHHLYP/6-311+G$^{**}$ procedure.

**Figure 41.** Conformational (**10a** → **10a′**; **10b** → **10b′**), configurational (**10a** → **10b**) and bond shift (**10a** → **10a″**; **10b** → **10b″**) processes in [16]annulene.
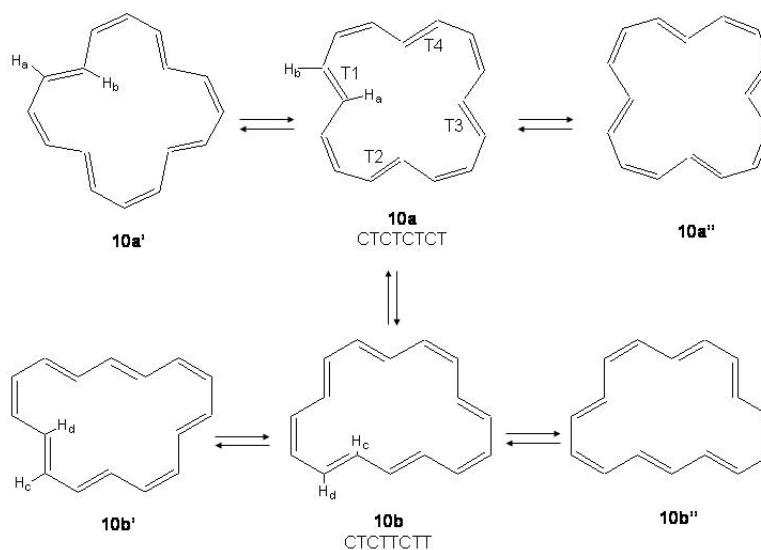


The **10a** isomer lies below **10b** by ≈ 1 kcal/mol, in agreement with experimental data at low temperature [254]. The conformational change **10a** → **10a′** occurs in a stepwise mechanism following two different pathways with calculated activation energies 8 - 10 kcal/mol. If the indicated *trans* double bonds of **10a** are called $T1$, $T2$, $T3$ and $T4$ consecutively, in one case the rotation around $T1$ is followed by that around the adjacent $T2$ *trans* double bond, in the other by that around the opposite $T3$ *trans* double bond. The configurational change **10a** → **10b** occurs with isomerization of one *trans* double bond to *cis* and then with Möbius topology. The key step of the process is a twist-coupled bond shifting during which a Möbius aromatic transition state is crossed [8]. The overall process then consists of (1) the conformational change around a *trans* double bond, (2) the Möbius step and (3) the final conformational change to **10b**. The highest activation barrier is found for the second step and ranges from 16.7 kcal/mol (BHHLYP/6-311+G**) to 6.9 kcal/mol (B3LYP/6-311+G**).

**Figure 42.** Schematic view of the synthetic strategy used to stabilize the $C_2$ Möbius structure of [16]annulene [255].
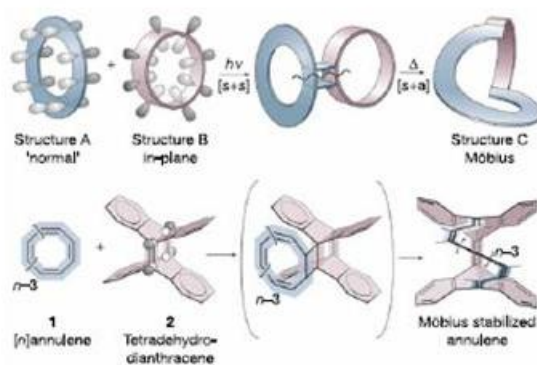
Recently, the synthesis of a stabilized [16]annulene isomer with Möbius topology has been reported by cycloaddition of a normal aromatic structure with a "belt-like" in-plane structure, as schematically depicted in **Figure 42** [229,255,256]. While the Möbius rings of parent [16]annulene are at higher energies with respect to **10a** and **10b** [257], the stabilization imposed by the belt reverses the energy ordering placing two Möbius rings, of $C_1$ and $C_2$ symmetry, at the lowest and nearly equal energy [255]. The synthesized Möbius ring lies $\sim 2$ kcal/mol above and has the structure $anti - tZcZcZt$ shown in **Figure 43** with $C_2$ symmetry [255]. It has been argued [258] about aromaticity of this system, on the basis of the bond alternation resulting from crystal data [255] and of large dihedral angles inhibiting the overlap between $\pi$ orbitals. In contrast, the principal component analysis performed on the 153 most stable structures of [16]annulenes and the 25 most stable Möbius stabilized [16]annulenes indicates that the compound of **Figure 43** belongs to the cluster of aromatic Möbius [16]annulene systems [256]. A detailed account of the discussion about aromaticity of the Möbius [16]annulene of **Figure 43** can be found elsewhere [230].

**Figure 43.** Structure of $anti - tZcZcZt$ [16]annulene in the Möbius topology. Bondlengths in Å are from X-ray data [255]. Dihedral angles ($\circ$) are from DFT calculations (B3LYP/6-31G\*) [255]. Nomenclature: the $anti$ configuration is relative to the two H atoms at the quinoid double bonds; $c$ and $t$ denote the *s-cis* or *s-trans* geometry between two adjacent double bonds; $E$ and $Z$ the stereochemistry of the three central double bonds. For the sake of clarity the benzo groups fused with bonds marked with a $b$ are omitted [230].
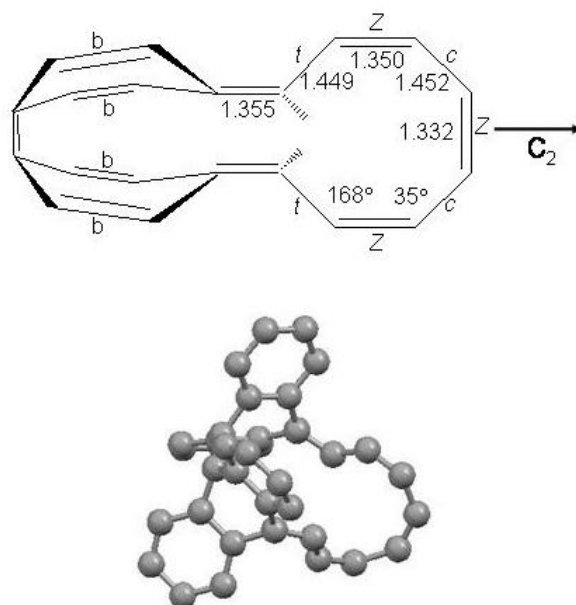


## 3.5.  *[18]Annulene*

The molecule occupies a special position in the annulene series being the next higher homologue [259] of benzene which allows, though does not require, the highly symmetrical $D_{6h}$ structure. According to X-ray diffraction data at room and 111 K [260,261] the planar strainless $D_{6h}$ geometry of [18]annulene

has twelve *transoid* and six *cisoid* CC bonds, 1.385 and 1.405 Å long, respectively [261], without bond alternation (see **Figure 44**).

> **Figure 44.** The structure of [18]annulene: left, experimental [260,261], in parentheses, and calculated B3LYP/6-311+G$^{**}$ [20] CC bond lengths; right, calculated [20] KMLYP/6-311+G$^{**}$ CC bond lengths in $C_2$ symmetry. Bond lengths in Å. The calculated structure on the right is slightly non planar with $C_2$ axis as indicated. No dihedral angle has been reported [20].
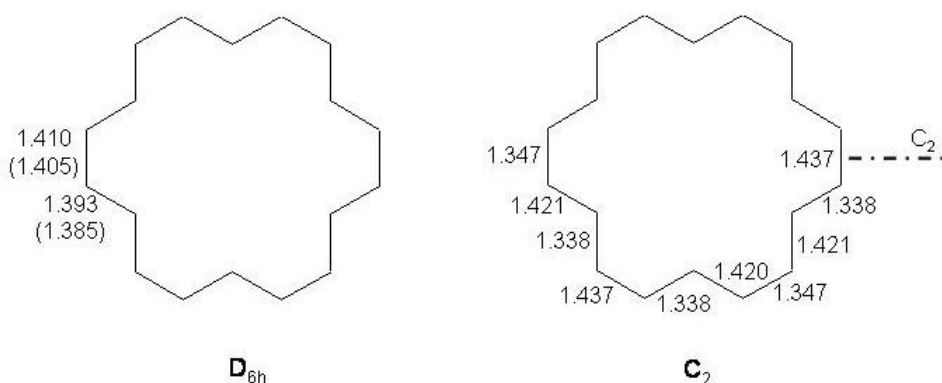


Along the years it has been debated about the stability of the bond alternating $D_{3h}$ structure with respect to $D_{6h}$. In fact, semiempirical and *ab initio* HF calculations indicate a greater stability of the former structure [112,262,263]. On the contrary, using density functional and MP2 methods to take into account the correlation energy the $D_{6h}$ structure is preferred with calculated bond lengths in substantial agreement with experimental data [19,264,265]. More recently, a bold statement has been advanced challenging the currently accepted structural information on [18]annulene [20]. On the basis of the gross disagreement between observed and calculated proton chemical shifts assuming the $D_{6h}$ geometry and, in addition, considering that correlated methods overestimate delocalization in annulenes [173,174], functionals having a larger HF component, such as KMLYP and BHHLYP, have been used. With both functionals the $D_{6h}$ geometry results to be a transition state between equivalent minima structures of $C_2$ symmetry (see **Figure 44**). The proton chemical shifts of the inner and outer hydrogen atoms calculated starting from the $C_2$ structure have been found in excellent agreement with experiment [6,266]. Static and dynamic crystal disorder may explain, according to this study [20], the difference with respect to the X-ray indications. For example, it has been noted that a 50/50 superposition of the two $C_2$ structures is close to the reported X-ray data [260,261] and therefore in principle this possibility cannot be excluded. Second, since the calculated barrier between the two interconverting minima is around 3 kcal/mol, the symmetrization of [18]annulene should take place rapidly even at 111 K, resulting in a time-average $D_{6h}$ structure [20].

The proposed failure of crystallographic studies to determine the structure of [18]annulene has been subjected to critical reconsiderations [267]. First, the superposition of two $D_{3h}$ (or $C_2$) bond alternating structures with $\Delta r = 0.1$ Å between $C - C$ and $C = C$ bondlengths and rotated 60° gives an orientational disorder in the crystal of the order of 0.0025 Å$^2$ for the twelve outer C atoms. In contrast with benzene,

a disorder effect of this size can be detected, for instance performing variable temperature neutron diffraction studies [108]. Second, the experimental proton chemical shifts are relative to [18]annulene in solution. Given the small energy difference between the $C_2$ and $D_{6h}$ structures, packing interactions in the crystal may favor the planar non alternating $D_{6h}$ structure. It has been concluded [267] that further experimental and computational effort should be made in order to confirm the $C_2$ structure for [18]annulene.

Finally, although spectroscopic data do not allow the unequivocal assignment of the [18]annulene structure among geometrical alternatives [20], it is worth noting the better agreement with experimental results of infrared[164] and *UV-vis* [268] spectroscopy when calculations are made starting from the delocalized $D_{6h}$ rather than from the localized $D_{3h}$ structure [268,269]. Taking advantage of the occurrence of the inversion center for $D_{6h}$ symmetry and of its absence for $C_2$ symmetry, a careful comparison of the infrared and near-infrared Raman spectra of the [18]annulene crystal at very low temperature appears to be highly recommended in order to solve the structural issue.

### 3.6. Porphyrins

Porphyrin and substituted porphyrins are molecules of enormous interest for their role in biological processes such as light absorption in green plants and oxygen transport in aerobic organisms [270]. They are also chemical structures of relevance by their own and accordingly in this Section results on structures and decay mechanisms of porphyrin and closely related species will be presented and discussed in relation to the annulene character of the macrocycle. Diprotonated porphyrin has a non planar structure mimicking that of non planar porphyrinic prosthetic groups [271]. Tetraoxaporphyrin dication, the oxygen analogue of porphyrin, has the highly symmetrical $D_{4h}$ structure [272,273] which may be modulated through five redox stages [274]. The structural parameters of the three molecular species have been the object of a large number of computational studies all of which indicate that the stable forms of porphyrin and tetraoxaporphyrin have $D_{2h}$ and $D_{4h}$ geometries, respectively, when electron correlation is taken into account [275–282]. The experimental [272,283,284] and calculated [275] bondlengths of the three macrocycles are reported in **Figure 45**.

As to the diprotonated species, the structure of **Figure 45** is the lowest energy conformer with $D_{2d}$ symmetry. Other two stable conformers with approximate $C_{2h}$ and $C_s$ symmetry, the so-called quasi-wave and quasi-ruffled isomers [285], have been found by calculations [275,286] $\approx 5$ kcal/mol above the $D_{2d}$ conformer. In qualitative discussions on porphyrins the concept of main conjugation path embedded in the macrocycle and responsible of the electronic absorption has been advanced [287,288]. The proposal may be useful also to estimate how the perturbation introduced by the $>O$, $>NH$ and $>N^-$ groups affect the macrocycle structure. The oxo bridge, $>O$, has the weakest effect on the outer ring as evidenced by the fact that the CO distance is close to the single C-O bond. Tetraoxaporphyrin dication may thus be considered a slightly perturbed [20]annulene system with 18 $\pi$ electrons. Also the $D_{2d}$ structure of diprotonated porphyrin, though not planar, has ring bondlengths appreciably similar to those of tetraoxaporphyrin with a growing interaction of the macrocycle with the $>NH$ bridges (the CN distance is roughly intermediate between single and double CN bonds). On the other hand, a quantitative determination of the main conjugation path in the porphyrin macrocycle has been proposed on the basis of structural data relative to a quite large number of porphyrin derivatives [289]. The porphyrin $\pi$ system

consists of the two pyrrole rings and of the "internal cross", *i.e.*, the [16]annulene dianion with 18 $\pi$ electrons [289].

**Figure 45.** Calculated (B3LYP/cc-pVDZ) [275] and (in parentheses) experimental bond lengths (Å) [272,283,284] of the stable structures of porphyrin (PH$_2$, $D_{2h}$), diprotonated porphyrin (PH$_4^{2+}$, $D_{2d}$) and tetraoxaporphyrin dication (TOXP$^{2+}$, $D_{4h}$). The experimental bond lengths are in the three cases average values of distances symmetrically equivalent in $D_{2h}$, $D_{2d}$ and $D_{4h}$ symmetry, respectively. The reference axis system is also shown on the top of the Figure.
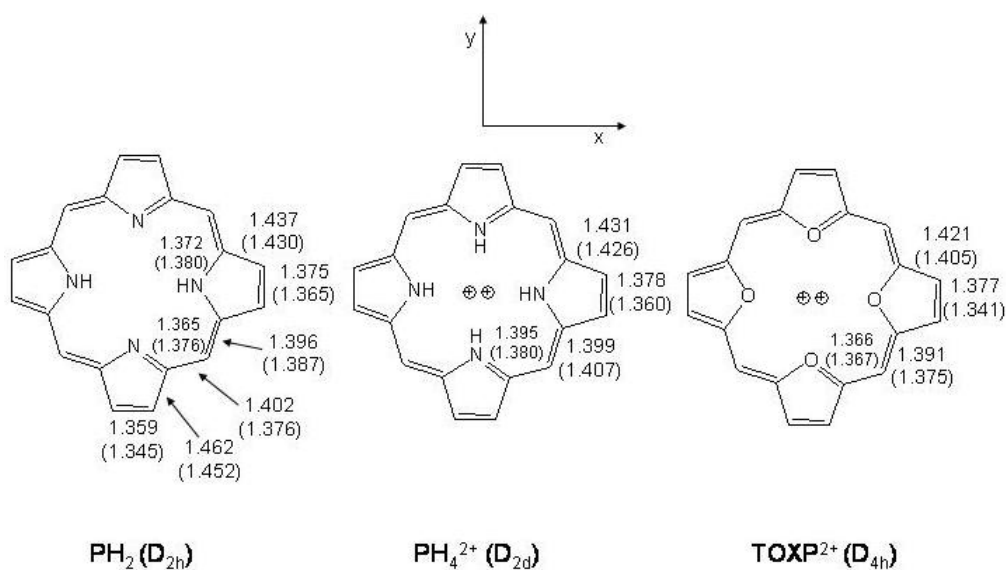


**Figure 46.** Raman spectra of PH$_2$ in benzene (c = $7 \times 10^{-4}$ M) and of PH$_4^{2+}$ in HCl solution (c = $3 \times 10^{-4}$ M) at room temperature excited at 406.7 nm. The asterisks mark solvent bands. In the inset the experimentally observed spectrum of PH$_4^{2+}$.
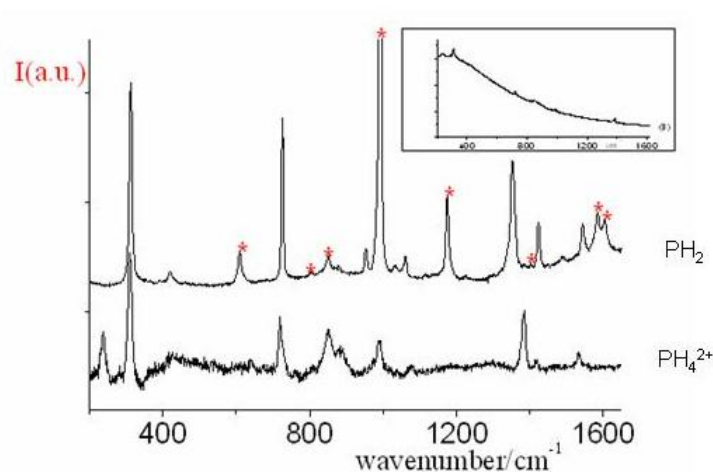


A large amount of vibrational data have been acquired on porphyrin from normal and resonance Raman [290,291], infrared [292] and fluorescence/phosphorescence [293] spectroscopies and the

assignment of the fundamental modes has been established in great detail [290,294]. The infrared and Raman spectra of the tetraoxa- and diprotonated porphyrin have been equally obtained and completely assigned making use of *ab initio* calculated frequencies and intensities and correlation with porphyrin [275]. The near resonance Raman spectra of porphyrin and diprotonated porphyrin excited at 406.7 nm and the normal Raman spectrum of tetraoxaporphyrin exciting at 785 nm are reported in **Figure 46** and **Figure 47**, respectively.

**Figure 47.** Raman spectrum of TOXP$^{2+}$ as polycrystalline sample at room temperature excited at 785 nm. The asterisks mark solvent bands of the ClO$_4^-$ counterion. In the inset the experimentally observed spectrum of TOXP$^{2+}$.
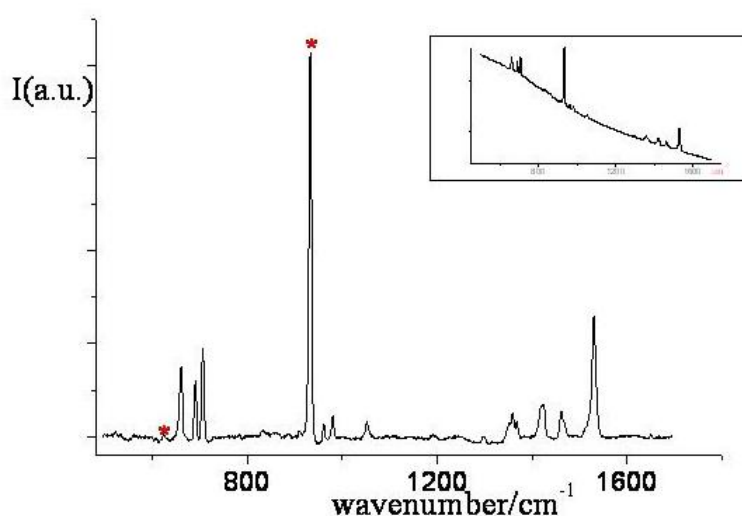


The absorption spectra of the three macrocycles may be qualitatively interpreted on the basis of the main conjugation path. The conjugation path of the [20]annulene dication represents the suitable choice for the tetraoxa- and diprotonated porphyrin [288]. By means of the PMO theory [57] it is found that the >O and >NH perturbations split the doubly-degenerate HOMO orbitals of the regular [20]annulene polygon into two orbitals of different energy, HOMO and HOMO-1, while shift uniformly the doubly-degenerate LUMO orbitals to higher energies. Two transitions are expected, HOMO → LUMO and HOMO-1 → LUMO, which correspond to the weak $Q$ and intense $B$ (or Soret) bands of **Figure 48**.

The strong perturbation due to the >N$^-$ bridges further splits the LUMO orbitals into a doublet, thus giving the well known four-orbital model of porphyrins [295,296]. Four electronic transitions are expected, all of them active in one-photon spectroscopy, the two at lower energy denoted $Q_x$, $Q_y$ while the two higher $B_x$, $B_y$ coalesce in a single band (see **Figure 48**). A quantitative treatment of the vertical excitation energies for the three molecules can only be performed with *ab initio* calculation methods [297–303]. The results from three recent calculations relative to porphyrin and presented in **Table 13** differ from experiment [299,304] by no more than 0.2 - 0.3 eV not only for the $Q_x$, $Q_y$ and $B_x$, $B_y$ pairs but also for the weak transitions, usually denoted $N_x$, $N_y$ and $L_y$, and observed at higher energies with respect to the Soret band.

**Figure 48.** Absorption spectra of $PH_2$, $PH_4^{2+}$ and $TOXP^{2+}$ solutions, c $\approx 10^{-5}$ M, room temperature, from bottom to top. The solvents are benzene/cyclohexane 1:10 for $PH_2$, benzene/cyclohexane 1:10 added with $CF_3COOH$ (5 % in volume) for $PH_4^{2+}$, concentrated $HClO_4$ for $TOXP^{2+}$. Vertical arrows indicate pump wavelengths in our pump-probe experiments in the three cases.
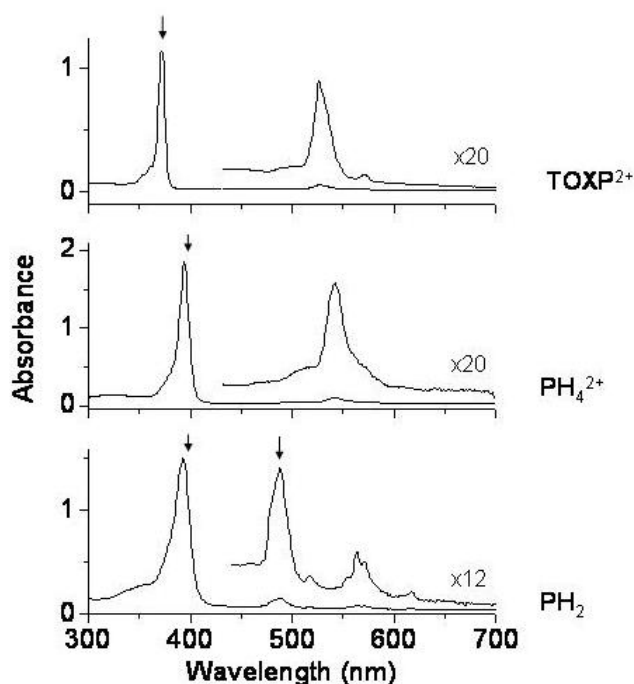


Exciting into the Soret absorption band of tetraoxaporphyrin as indicated in **Figure 48** radiative and non radiative decay processes are promoted [305,306]. The fluorescence emissions from the first and second excited state, $Q \to S_0$ and $B \to S_0$, are easily observed with quantum yield 0.11 and 0.035, respectively [305]. The upper state fluorescence is favored by the sharpness of the Soret band having a considerably high extinction coefficient and by the absence of intermediate states in the large energy gap between $B$ and $Q$. The $B$ lifetime could only be estimated to be $\leq 100$ ps, due to the instrumental resolution of the time-resolved fluorescence apparatus, and indirectly evaluated from quantum yield and radiative time constant to be $\approx 40$ ps. Transient absorption pump-probe experiments have been set up in the femtosecond time domain [306] following experimental procedures described in detail [160,307,308] in order to characterize the non-radiative relaxation channels from the $B$ state. In general, transient absorbances $\Delta A$ arise from four different contributions [307], excited state absorption (ESA), stimulated emission (SE), stimulated Raman gain (SRG) and bleaching (B). All these contributions are clearly seen in the transient spectrum of **Figure 49**.

The decay kinetics of the 405 and 425 nm ESA bands in **Figure 50** identifies a single rise time of 25 ps, interpreted as the time constant of the population increase in the $Q$ state. Successively, the transient absorbance decays with time constant 7.2 ns, *i.e.*, the lifetime of the $Q$ state. By comparison with the estimated $B$ lifetime, $\approx 40$ ps, it has been concluded that, within the experimental error, all the tetraoxaporphyrin molecules excited into the $B$-state decay by internal conversion into the $Q$ state.

**Table 13.** Transition energies and oscillator strengths ($\Delta E$, eV; $f$) of porphyrin to the lowest excited states, $\pi\pi^*$ unless otherwise specified. Exp: gas-phase [304] and solution band maxima $\Delta E$ [299] and $f$ values [300]. Calculated transition energies under all other headings: DF/SCI results [299] (reference system as in Figure 33); TD/DFT, results [298]; CASPT2 results [297].

| Exp | | | | | DF/SCI | | | TD/DFT | | CASPT2 | |
| gas | | sol | | | | | | | | | |
| $\Delta E$ | | $\Delta E$ | $f$ | | $\Delta E$ | $f$ | ass. | $\Delta E$ | $f$ | $\Delta E$ | $f$ |
|---|---|---|---|---|---|---|---|---|---|---|---|
| 1.98 | $Q_x$ | 2.01 | 0.02 | | 2.26 | $< 10^{-4}$ | $1B_{3u}$ | 2.24 | 0.0002 | 1.63 | 0.0004 |
| 2.42 | $Q_y$ | 2.38 | 0.07 | | 2.41 | $< 10^{-4}$ | $1B_{2u}$ | 2.39 | 0.00004 | 2.11 | 0.002 |
| 3.33 | $B_x;B_y$ | 3.13 | 1.15 | | 3.30 | 0.42 | $2B_{3u}$ | 3.27 | 0.40 | 3.08 | 0.91 |
| | | | | | 3.47 | 0.63 | $2B_{2u}$ | 3.45 | 0.61 | 3.12 | 0.70 |
| | | | | | 3.39 | – | $1B_{1g}$ | | | | |
| | | | | | 3.57 | – | $2A_g$ | | | | |
| 3.65 | N | 3.47 | 0.19 | | 3.73 | 0.51 | $3B_{2u}$ | 3.70 | 0.55 | 3.42 | 0.46 |
| | | 3.66 | 0.14 | | 3.83 | 0.78 | $3B_{3u}$ | 3.79 | 0.82 | 3.53 | 0.83 |
| | | | | | 4.01 | – | $2B_{1g}$ | | | | |
| | | | | | 4.03 | – | $1A_u(n\pi^*)$ | | | | |
| | | | | | 4.05 | – | $1B_{2g}(n\pi^*)$ | | | | |
| | | | | | 4.09 | 0.001 | $1B_{1u}(n\pi^*)$ | | | | |
| | | | | | 4.09 | – | $1B_{3g}(n\pi^*)$ | | | | |
| | | | | | 4.22 | – | $3B_{1g}$ | | | | |
| | | | | | 4.23 | – | $3A_g$ | | | | |
| 4.25 | $L_y$ | 4.09 | 0.17 | | 4.33 | 0.12 | $4B_{2u}$ | 4.29 | 0.12 | $3.96(L_y)$ | 0.34 |
| | | | | | | | | | | $4.04(L_x)$ | 0.20 |
| | | | | | 4.41 | – | $4A_g$ | | | | |
| 4.65 | $L_x$ | | | | 4.44 | 0.11 | $4B_{3u}$ | 4.40 | 0.11 | | |
| | | | | | 4.65 | – | $4B_{1g}$ | | | | |
| | | | | | 4.80 | – | $5A_g$ | | | | |
| 5.50 | M | | | | 5.14 | 0.14 | $5B_{3u}$ | | | | |

The transient absorption from the $Q_x;Q_y$ bands and the relaxation dynamics from the Soret band have been investigated in substituted porphyrins [309–312]. In tetraphenylporphyrin the internal conversions $(B_x, B_y) \rightarrow Q_y$ and $Q_y \rightarrow Q_x$ take place in less than 50 and 100 fs, respectively [310,311]. Later, three decay channels are activated; (a) intramolecular vibrational redistribution by dephasing and elastic collision with the solvent with time constants 100–200 fs and 1.4 ps, (b) thermal equilibration by energy transfer to the solvent in the temporal range 10–20 ps and (c) intersystem crossing $Q_x \rightarrow T_1$ with time constant 12 ns. In another experiment [312], exciting into the $Q_x;Q_y$ bands of the tetra-$p$-tolyl derivative of porphyrin and probing with infrared pulses, states of *gerade* symmetry in the vicinity of the Soret band have been observed by transient absorption spectroscopy.

Going to the unsubstituted molecule, the non radiative processes follow a decay pattern similar to that of tetraphenylporphyrin [306]. The femtosecond transient absorption results on porphyrin are presented in **Figure 51** while **Figure 52** shows the decay kinetics of the 412 nad 465 nm ESA bands.

After the unresolvably short $(B_x, B_y) \rightarrow Q_y$ internal conversion the $Q_y \rightarrow Q_x$ process is observed with time constant 140–150 fs, a rise/decay time for the 412/465 nm ESA band. As expected, this time constant is slightly longer than in substituted porphyrins. Also the subsequent fast processes with time constants 1.8 ps and 25 ps slow down in porphyrin with respect to the tetraphenyl derivative [311].

**Figure 49.** Transient absorption spectra of TOXP$^{2+}$ (c = $6 \times 10^{-6}$ M in concentrated HClO$_4$, room temperature) in the spectral range 400–600 nm exciting at 370 nm with femtosecond pulses. The transient spectra are plotted as a function of the delay time between pump and probe pulses. The ESA, SRG, B and SE symbols identify transient bands due to excited state absorption, stimulated Raman gain of the solvent, bleaching and stimulated emission, respectively. Solid line, temporal coincidence between pump and probe pulses; long dashed, dashed-dotted, dashed-doubly dotted, 5, 20 and 200 ps delay times, respectively; vertical arrow up, intensity increase with time. Inset: transient absorption spectra at 200 ps and 1.5 ns delay times.
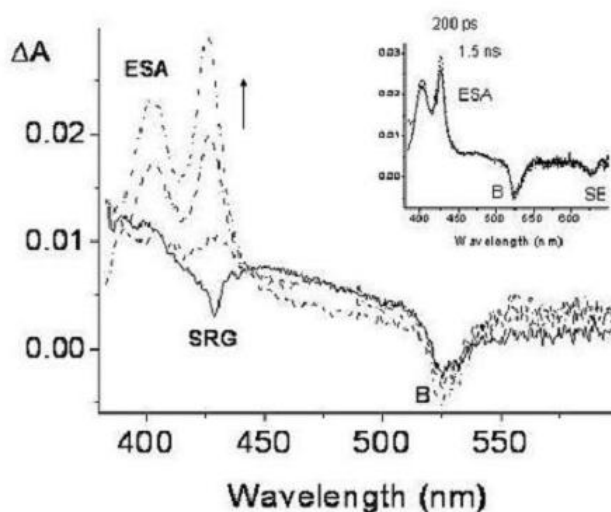


**Figure 50.** Transient absorbance of TOXP$^{2+}$ as a function of the delay time in the same experimental conditions detailed in Figure 37 and probing at 425 nm (lower) and 405 nm (upper). The insets of the two panels show the transient absorbances at the probe wavelengths 425 and 405 nm for long delay times.
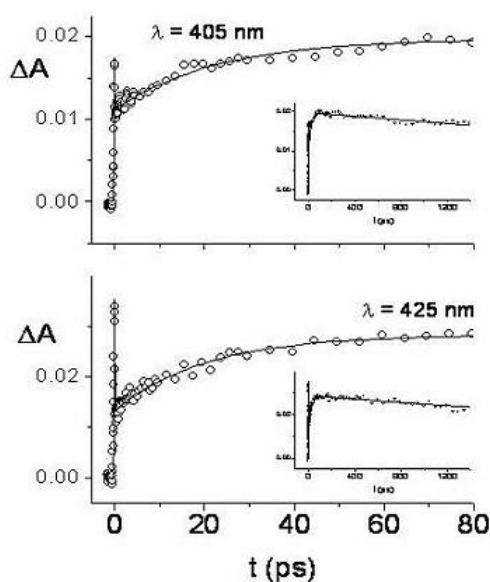
**Figure 51.** Transient absorption spectra of $PH_2$ ($c = 3 \times 10^{-5}$ M in benzene/cyclohexane 1:10, room temperature) in the spectral range 400–600 nm exciting at 400 nm with femtosecond pulses. The transient spectra are plotted as a function of the delay time between pump and probe pulses. The ESA, SRG, B and SE symbols identify transient bands due to excited state absorption, stimulated Raman gain of the solvent, bleaching and stimulated emission, respectively. Lower panel: transient spectra in the first 5 ps; solid line, temporal coincidence between pump and probe pulses; long dashed, short dashed, dotted lines, 200 fs, 1 ps, 5 ps delay times, respectively; vertical arrows up and down, intensity increase and decrease with time. Upper panel: transient spectra after 5 ps delay time; solid, dotted, short dashed, dash-dotted lines; 5, 20, 100, 500 ps delay times, respectively. Inset of the upper panel: transient absorption spectrum at 1.5 ns delay time.
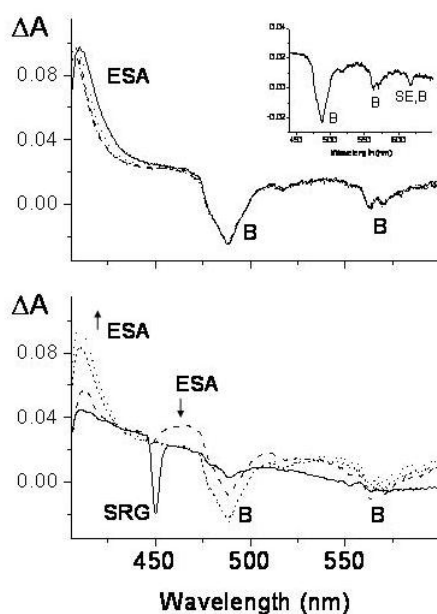


Diprotonated porphyrin is a case more complex than porphyrin and tetraoxaporphyrin. Although the energy gap between the $B$ and $Q$ states of the diprotonated species is comparable to that of tetraoxaporphyrin, efficient decay processes are promoted due either to the torsional flexibility of the non planar structure [313–315] or to the formation of the complex with the trifluoroacetic acid used for the preparation of the diprotonated species, *i.e.*, $(PH_4^{2+})(CF_3COO^-)_2$, as suggested in similar cases [316]. The complex has charge transfer states interspersed between $B$ and $Q$ and provides a deactivation mechanism more efficient than the direct $B \rightarrow Q$ internal conversion channel. According to the B3LYP/cc-pVDZ calculation the molecular complex isomerizes between the two equivalent $A_1$ and $A_2$ structures of **Figure 53**, expressed as $(PH_2)(CF_3COOH)_2$ , with an activation barrier of 0.05 eV ($\approx$ 1.1 kcal/mol).

**Figure 52.** Transient absorbance of PH$_2$ as a function of the delay time in the same experimental conditions detailed in Figure 39 and probing at 465 nm (lower) and 412 nm (upper). In the lower panel the cross-correlation gaussian profile (FWHM = 160 fs) between pump and probe pulses is also reported as dashed line. The insets of the two panels show the transient absorbances at the probe wavelengths 412 and 465 nm for long delay times.
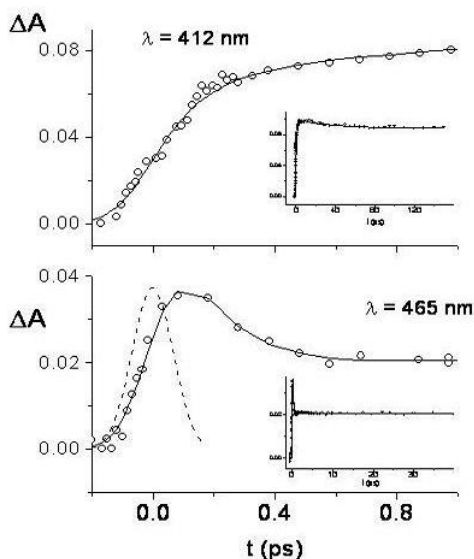


**Figure 53.** The complex of diprotonated porphyrin with trifluoroacetic acid according to B3-LYP/cc-pVDZ calculations. A$_1$, A$_2$: (PH$_2$)(CF$_3$COOH)$_2$ tautomers. B: (PH$_4$$^{2+}$)(CF$_3$COO$^-$)$_2$ transition structure. For the sake of clarity, the four central hydrogen atoms are evidentiated as violet balls for the three structures and their distances (Å) from the closest oxygen atoms are indicated. Bottom: schematic diagram of the potential energy responsible for interconversion of A$_1$ and A$_2$ structures through the transition structure B. The energy barrier is estimated to be 0.05 eV ($\approx$ 1.1 kcal/mol).
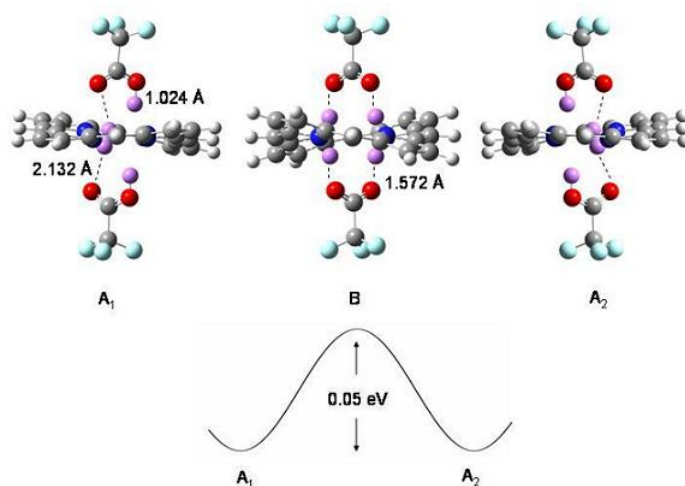
### 3.7. *Porphycenes*

Porphycene **1** ([18]porphyrin-(2.0.2.0), see **Figure 54**) is the structural isomer of porphyrin **2** ([18]porphyrin-(1.1.1.1)) first synthesized [317] in a series including corrphycene ([18]porphyrin-(2.1.0.1)) [318] and hemiporphycene ([18]porphyrin-(2.1.1.0)) [319]. Porphycenes have attracted much attention since their synthesis [320]. Three ground state isomeric structures of porphycene differing for the inner hydrogen positions are *trans*, *cis-A* and *cis-B* (see **Figure 54**). Their energies were estimated using *ab-initio* calculations methods with the *trans* geometry more stable than *cis-A* by few kcal/mol [281,321]. The *cis-B* structure was calculated at much higher energy [321]. Infrared and Raman spectra have been measured [322] and compared with calculated vibrational data of the *trans* and *cis-A* isomers [281,321,322].

The *UV-vis* absorption spectra of porphycene and of a large number of porphycene derivatives have been comprehensively investigated applying the charged 18-electron [20]annulene planar model for a qualitative discussion of the $Q$ and Soret bands [288]. Unlike the porphyrin case, by perturbing the [20]annulene ring with $> NH$ and $> N^-$ bridges such that to obtain porphycene, one of the two degenerate $LUMO$ orbitals of the model perimeter shifts to higher energy while the second has unaltered energy. Further, the effect of perturbation on the two degenerate $HOMO$ orbitals is approximately equal so that they remain accidentally degenerate. Accordingly, the two $Q$ transitions of porphycene, $HOMO \rightarrow LUMO$ and $HOMO - 1 \rightarrow LUMO$, are much closer in porphycene than in porphyrin (see **Figure 55** and compare with **Figure 48**, bottom) [288].

**Figure 54.** Top: the structures of porphycene **1** and porphyrine **2**. Bottom: the inner hydrogen migration in porphycene.
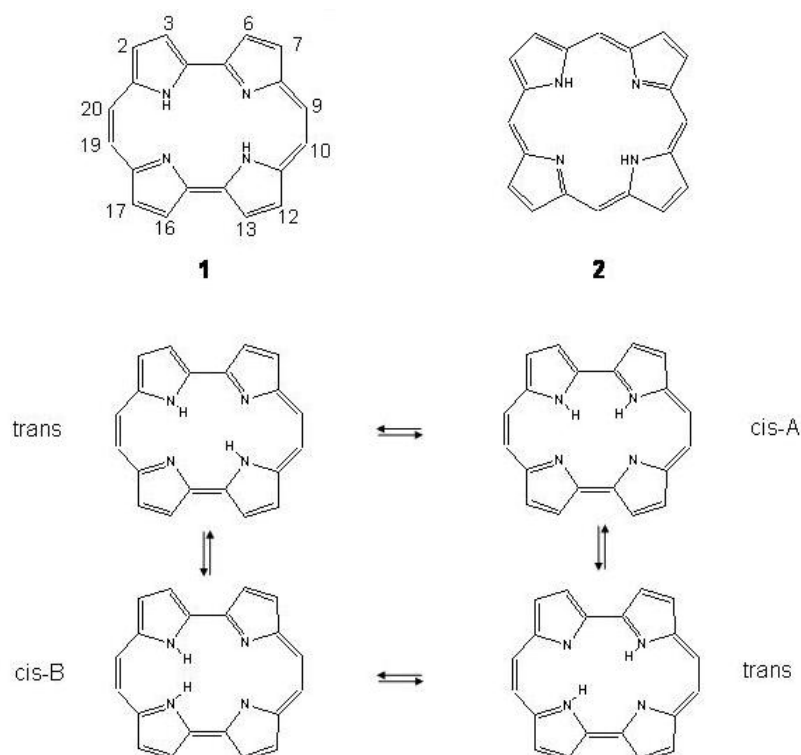
The inner hydrogen migration between *trans* structures (see **Figure 54**, bottom) is common to porphyrin and porphycene [288]. Ground and excited state tautomerism in porphycene has been experimentally investigated by several techniques [323–326]. While this process has a stepwise mechanism in porphyrin [327], in porphycene the tautomerism has been described as a synchronous double hydrogen tunneling activated by a low frequency mode whose displacement affects the NH···N distances [320]. By supersonic jet spectroscopy the tunneling splitting has been observed in the fluorescence excitation spectrum of the isolated molecule in the region of the (0-0) transition [325]. Also, the inner hydrogen transfer between the *trans* and the *cis-B* geometry is related to the efficient radiationless deactivation in excited porphycene [328]. It has been in fact proposed that crossing of the potential energy curves of the ground and lowest excited states for these two isomers occurs along the hydrogen transfer coordinate, thus giving origin to a conical intersection at a geometry close to that of the lowest *cis-B* excited state [328]. Additional information on excited state dynamics and relaxation in electronically excited porphycene is provided by transient absorption spectroscopy [329]. Similarly to the porphyrin case, the relaxation scheme for the molecule in solution excited into the Soret band involves ultrafast intramolecular decay processes and a slower thermal equilibration with the surrounding solvent.

**Figure 55.** Fluorescence (right) and fluorescence excitation (left) spectra of porphycene in poly(vinyl butyral) film at 20 K.
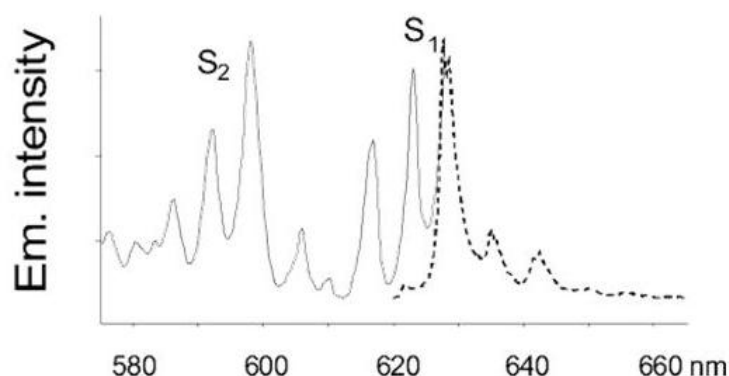


## 4. Summary

In this paper the most significant structural aspects of annulene and model annulene systems relative to the ground and lowest excited states have been reviewed. The research activity of our group has been centered on one side on antiaromatic systems such as pentalene and *s*-indacene, and on the other on aromatic bridged annulenes and porphyrins. More recently, energy levels and decay mechanisms have been studied in planar and non planar porphyrins. The relaxation processes have been probed by means of time-resolved picosecond fluorescence and transient absorption femtosecond spectroscopy. Radiative and non radiative processes have been observed in unsubstituted porphyrin, diprotonated porphyrin and tetraoxaporphyrin dication describing the decay channels activated after excitation in the Soret band.

In an effort to present our results in the context of the aromaticity/antiaromaticity theory and to provide basic notions on the structural properties of annulenes the review has supplemented additional information also on these systems. A common feature of higher annulenes is the occurrence of non

planar isomers and of thermal or photochemical valence isomerization among them. Two other fields of intense activity are worth mentioning. The design, almost entirely theoretical until now, of molecules exhibiting Möbius topology has stimulated growing interest in the chemistry of large annulenes. Möbius transition states have been proposed and computationally justified for the isomerization processes in these systems. The first Möbius ring has been synthesized, thus making feasible the direct comparison between experiment and theory. On the other hand, the structural transition from the delocalized to a localized valence tautomeric form in the series of $[4n + 2]$ annulenes is a second issue giving evidence of the distortive nature of $\pi$ electrons in conjugated systems. In this respect the discussion on the delocalized/localized ground state structure of [18]annulene takes on particular importance.

The review has covered in depth as much as possible the structural properties of aromatic/antiaromatic systems. Given the amplitude of the aromaticity subject, these properties do not exhaust the theme. As an example, the magnetic criteria of aromaticity have not been tackled, for which more complete reports are recommended [4,330,331].

## Acknowledgments

## References

1.  Sondheimer, F. The annulenes. *Acc. Chem. Res.* **1972**, *5*, 81-91.
2.  Lloyd, D. *Non-benzenoid Conjugated Carbocyclic Compounds*; Elsevier: Amsterdam, The Netherland, 1984.
3.  Balaban, A.T.; Banciu M.; Ciorba,V. In *Annulenes, Benzo-, Hetero-, Homo-Derivatives and their Valence Isomers*; CRC Press: Boca Raton, FL, USA, 1987; Volume 1.
4.  Minkin, V.I.; Glukhovtsev, M.N.; Simkin, B.Ya. *Aromaticity and Antiaromaticity*; John Wiley and Sons: New York, NY, USA, 1994.
5.  Shaik, S.S.; Hiberty, P.C. *A Chemist's Guide to Valence Bond Theory*; John Wiley and Sons: New York, NY, USA, 2008.
6.  Oth, J.F.M. Conformational Mobility and Fast Bond Shift in the Annulenes. *Pure Appl. Chem.* **1971**, *25*, 573-622.
7.  Castro, c.; Karney, W.L.; Valencia, M.A.; Vu, C.M.H.; Pemberton, R.P. Möbius Aromaticity in [12]Annulene: Cis-Trans Isomerization via Twist-Coupled Bond Shifting. *J. Am. Chem. Soc.* **2005**, *127*, 9704-9705.
8.  Pemberton, R.P.; McShane, C.M.; Castro, C.; Karney, W.L. Dynamic Processes in [16]Annulene: Möbius Bond-Shifting Routes to Configuration Change. *J. Am. Chem. Soc.* **2006**, *128*, 16692-16700.

9.  Moll, J.K.; Pemberton, R.P.; Gutierrez, M.G.; Castro, C.; Karney, W.L. Configuration Change in [14]Annulene Requires Möbius Antiaromatic Bond Shifting. *J. Am. Chem. Soc.* **2007**, *129*, 274-275.

10. Garratt, P.J. *Aromaticity*; John Wiley and Sons: New York, NY, USA, 1986.

11. Fray, G.I.; Saxton, R.G. *The Chemistry of Cyclooctatetraene and Its Derivatives*; Cambridge University press: Cambridge, UK, 1978.

12. Schleyer, P.v.R. Introduction: Aromaticity. *Chem. Rev.* **2001**, *101*, 1115-1117.

13. Schleyer, P.v.R. Introduction: Delocalization - Pi and Sigma. *Chem. Rev.* **2005**, *105*, 3433-3435.

14. Kertesz, M.; Choi, C.H.; Yang, S. Conjugated Polymers and Aromaticity. *Chem. Rev.* **2005**, *105*, 3448-3481.

15. Kennedy, R.D.; Lloyd, D.; McNab, H. Annulenes, 1980-2000. *J. Chem. Soc., Perkin Trans.* **2002**, *1*, 1601-1621.

16. Vogel, E.Recent Advances in the Chemistry of Bridged Annulenes. *Pure Appl. Chem.* **1982**, *54*, 1015-1039.

17. Shaik, S.; Shurki, A.; Danovich, D.; Hiberty, P.C. A Different Story of $\pi$-Delocalization - The Distortivity of $\pi$-Electrons and Its Chemical Manifestations. *Chem. Rev.* **2001**, *101*, 1501-1539.

18. Longuet-Higgins, H.C.; Salem, H.C. The Alternation of Bond Lengths in Long Conjugated Chain Molecules. *Proc. R. Soc. London* **1959**, *A251*, 172-185.

19. Choi, C.H.; Kertesz, M. Bond Length Alternation and Aromaticity in Large Annulenes. *J. Chem. Phys.* **1998**, *108*, 6681-6688.

20. Wannere, C.S.; Sattelmeyer, K.W.; Schaefer, H.F., III; Schleyer, P.v.R. Aromaticity: the Alternating C-C Bond Length Structures of [14]-, [18]-, and [22]Annulene. *Angew. Chem. Int. Ed. Engl.* **2004**, *43*, 4200-4206.

21. Breslow, R. Antiaromaticity. *Acc. Chem. Res.* **1973**, *6*, 393-398.

22. Wiberg, K.B. Antiaromaticity in Monocyclic Conjugated Carbon Rings. *Chem. Rev.* **2001**, *101*, 1317-1331.

23. Bally, T.; Masamune, S. Cyclobutadiene. *Tetrahedron* **1980**, *36*, 343-370.

24. Maier, G. Tetrahedrane and Cyclobutadiene. *Angew. Chem. Int. Ed. Engl.* **1988**, *27*, 309-332.

25. Mo, Y.; Schleyer, P.v.R. An Energetic Measure of Aromaticity and Antiaromaticity Based on the Pauling-Wheland Resonance Energies. *Chem. Eur. J.* **2006**, *12*, 2009-2020.

26. Bally, T. Cyclobutadiene: the Antiaromatic Paradigm? *Angew. Chem. Int. Ed. Engl.* **2006**, *45*, 6616-6619.

27. Hafner, K.; Suss, H.U. 1,3,5-Tri-*tert*-Butylpentalene. A Stabilized Planar 8$\pi$-Electron System. *Angew. Chem. Int. Ed. Engl.* **1973**, *12*, 575-577.

28. Bally, T.; Chai, S.; Neuenschwander, M.; Zhu, Z. Pentalene: Formation, Electronic and Vibrational Structure. *J. Am. Chem. Soc.* **1997**, *119*, 1869-1875.

29. Falchi, A.; Gellini, C.; Salvi, P.R.; Hafner, K. Fluorescence of Antiaromatic Systems: an Experimental and Theoretical Study of 1,3,5-Tri-*tert*-Butylpentalene. *J. Phys. Chem. A* **1998**, *102*, 5006-5012.

30. Hafner, K.; Stowasser, B.; Krimmer, H.P.; Fisher, S.; Bohm, M.C.; Lindner, H.J. Synthesis and Properties of 1,3,5,7-Tetra-*tert*-Butyl-*s*-Indacene. *Angew. Chem. Int. Ed. Engl.* **1986**, *25*, 630-635.

31. Dunitz, J.D.; Krüger, C.; Irngartinger, H.; Maverick, E.F.; Wang, Y.; Nixdorf, M. Equilibrium Structure, Stabilized Transition State, or Disorder in the Crystal? Studies of the Antiaromatic Systems Tetra-*tert*-Butyl-*s*-Indacene and Tetra-*tert*-Butylcyclobutadiene. *Angew. Chem. Int. Ed. Engl.* **1988**, *27*, 387-389.

32. Spitler, E.L.; Johnson, C.A., II; Haley, M.M. Renaissance of Annulene Chemistry. *Chem. Rev.* **2006**, *106*, 5344-5386.

33. Marsden, J.A.; Palmer, G.J.; Haley, M.M. Synthetic Strategies for Dehydrobenzo[*n*]annulenes. *Eur. J. Org. Chem.* **2003**, 2355-2369.

34. Gorelik, M.V. Current State of Aromaticity Problem. *Usp. Khim.* **1990**, *58*, 197-228.

35. Ziegler, L.D.; Hudson, B.S. In *The Vibronic Spectroscopy of Benzene: Old Problems and New Techniques*; Lim, E.C., Ed.; Academic Press: New York, NY, USA, 1982; Volume 5, pp. 41-200.

36. Hassenruck, K.; Martin, H.D.; Walsh, R. Consequences of Strain in $(CH)_8$ Hydrocarbons. *Chem. Rev.* **1989**, *89*, 1125-1146.

37. Klärner, F.G. About the Aromaticity of Planar Cyclooctatetraene. *Angew. Chem. Int. Ed. Engl.* **2001**, *40*, 3977-3981.

38. Mulder, J.J.C. The $\pi$-Electron System of Monocyclic Polyenes $C_{2n}H_{2n}$ with Alternating Single and Double Bonds. *J. Chem. Educ.* **1998**, *75*, 594-595.

39. Heilbronner, E. Why Do Some Molecules Have Symmetry Different from that Expected? *J. Chem. Educ.* **1989**, *66*, 471-478.

40. Eyring, H.; Walter, J.; Kimball, G. *Quantum Chemistry*; John Wiley and Sons: New York, NY, USA, 1944.

41. Lennard-Jones, J.E.; Turkevich, J. The Electronic Structure of some Polyenes and Aromatic Molecules. *Proc. R. Soc. London* **1937**, *A158*, 297-305.

42. Pearson, R.G. A Symmetry Rule for Predicting Molecular Structures. *J. Am. Chem. Soc.* **1969**, *91*, 4947-4955.

43. Binsch, G.; Heilbronner, E.; Murrell, J.N. The Theory of Double Fixation in Conjugated Hydrocarbons. *Mol. Phys.* **1966**, *11*, 305-320.

44. Nakajima, T. Quantum Chemistry of Nonbenzenoid Cyclic Conjugated Hydrocarbons. *Topics Curr. Chem.* **1972**, *32*, 340-1022.

45. Berry, R.S. Zero-Point Vibrations in Benzene. *J. Chem. Phys.* **1961**, *35*, 2253-2254.

46. Shaik, S.S.; Bar, R. How Important Is Resonance in Organic Species? *Nouv. J. Chim.* **1984**, *8*, 411-420.

47. Epiotis, N.D. Application of Molecular Orbital-Valence Bond Theory in Chemistry. *Pure Appl. Chem.* **1983**, *55*, 229-236.

48. Shaik, S.S.; Hiberty, P.C. When Does Electronic Delocalization Become a Driving Force of Molecular Shape and Stability? The "Aromatic" Sextet. *J. Am. Chem. Soc.* **1985**, *107*, 3089-3095.

49. Shaik, S.S.; Hiberty, P.C.; Lefour, J.M.; Ohanessian, G. Is Delocalization a Driving Force in Chemistry? Benzene, Allyl Radical, Cyclobutadiene, and Their Isoelectronic Species. *J. Am. Chem. Soc.* **1987**, *109*, 363-374.

50. Shaik, S.S.; Hiberty, P.C.; Ohanessian, G.; Lefour, J.M. When Does Electronic Delocalization Become a Driving Force of Chemical Bonding? *J. Phys. Chem.* **1988**, *92*, 5086-5094.

51. Hiberty, P.C.; Danovich, D.; Shurki, A.; Shaik, S. Why Does Benzene Posses a $D_{6h}$ Symmetry? A Quasiclassical State Approach for Probing $\pi$-Bonding and Delocalization Energies. *J. Am. Chem. Soc.* **1995**, *117*, 7760-7768.

52. Shaik, S.; Zilberg, S.; Haas, Y. A Kekule-Crossing Model for the "Anomalous" Behaviour of the $b_{2u}$ Modes of Aromatic Hydrocarbons in the Lowest Excited $^1B_{2u}$ State. *Acc. Chem. Res.* **1996**, *29*, 211-218.

53. Jug, K.; Hiberty, P.C.; Shaik, S. $\sigma - \pi$ Energy Separation in Modern Electronic Theory for Ground States of Conjugated Systems. *Chem. Rev.* **2001**, *101*, 1477-1500.

54. Jug, K.; Koster, A.M.Influence of $\sigma$ and $\pi$ Electrons on Aromaticity. *J. Am. Chem. Soc.* **1990**, *112*, 6772-6777.

55. Streitwieser, A. *Molecular Orbital Theory for Organic Chemists*; Wiley: New York, NY, USA, 1961.

56. Dewar, M.J.S. *The Molecular Orbital Theory of Organic Chemistry*; McGraw-Hill: New York, NY, USA, 1969.

57. Dewar, M.J.S.; Dougherty, R.C. *PMO Theory in Organic Chemistry*. Plenum: New York, NY, USA, 1975.

58. Mo, Y.; Hiberty, P.C.; Schleyer, P.v.R. How To Properly Compute the Resonance Energy Within the *Ab Initio* Valence Bond Theory - A Response to the ZHJVL Paper. *Theor. Chem. Acc.*, in press.

59. Dewar, M.J.S.; Gleicher, G.J. Ground State of Conjugated Molecules. Allowance for Molecular Geometry. *J. Am. Chem. Soc.* **1965**, *87*, 685-696.

60. Dewar, M.J.S.; de Llano, C. Ground State of Conjugated Molecules. Improved Treatment of Hydrocarbons. *J. Am. Chem. Soc.* **1969**, *91*, 789-795.

61. Hess, B.A., Jr.; Schaad, L.J. Hückel Molecular Orbital $\pi$ Resonance Energies. A New Approach. *J. Am. Chem. Soc.* **1971**, *93*,305-310.

62. Schaad, L.J.; Hess, B.A., Jr. Hückel Theory and Aromaticity. *J. Chem. Ed.* **1974**, *51*, 640-643.

63. Schaad, L.J.; Hess, B.A., Jr. Dewar Resonance Energy. *Chem. Rev.* **2001**, *101*, 1465-1476.

64. Hohlneicher, G.; Packschies, L.; Weber, J. On the $\sigma,\pi$-Energy Separation of the Aromatic Stabilization Energy of Cyclobutadiene. *Phys. Chem. Chem. Phys.* **2007**, *9*, 2517-2530.

65. Kollmar, H. Direct Calculation of Resonance Energies of Conjugated Hydrocarbons with *ab Initio* MO Methods. *J. Am. Chem. Soc.* **1979**, *101*, 4832-4840.

66. George, P.;Trachtman, M.; Bock, C.W.; Brett, A.M. An Alternative Approach to the Problem of Assessing Stabilization Energies in Cyclic Conjugated Hydrocarbons. *Theoret. Chim. Acta (Berl.)* **1975**, *38*, 121-129.

67. George, P.; Trachtman, M.; Bock, C.W.; Brett, A.M. Homodesmotic Reactions for the Assessment of Stabilization Energies in Benzenoid and Other Conjugated Cyclic Hydrocarbons. *J. Chem. Soc., Perkin Trans.* **1976**, *II*, 1222-1227.

68. George, P.; Bock, C.W.; Trachtman, M. The Evaluation of Empirical Resonance Energies as Reaction Enthalpies with Particular Reference to Benzene. *J. Chem. Ed.* **1984**, *61*, 225-227.

69. George, P. A Critique of the Resonance Energy Concept with Particular Reference to Nitrogen Heterocycles, Especially Porphyrins. *Chem. Rev.* **1975**, *75*, 85-111.

70. Deniz, A.A.; Peters, K.S.; Snyder, G.J. Experimental Determination of the Antiaromaticity of Cyclobutadiene. *Science* **1999**, *286*, 1119-1122.

71. Fattahi, A.; Liz, L.; Thian, Z.; Kan, S.R. The Heat of Formation of Cyclobutadiene. *Angew. Chem. Int. Ed. Engl.* **2006**, *45*, 4984-4988.

72. Kovacevic, B.; Baric, D.; Maksic, Z.B.; Müller, T. Dominant Role of the $\pi$ Framework in Cyclobutadiene. *J. Phys. Chem. A* **2004**, *108*, 9126-9133.

73. Hochstrasser, R.M.; Sung, H.N.; Wessel, J.E. Moderate-Resolution Study of the Two-Photon Spectrum of the $^1B_{2u}$ State of Benzene-$h_6$ and Benzene-$d_6$. *Chem. Phys. Lett.* **1974**, *24*, 7-10.

74. Friedrich, D.M.; McClain, W.M. Polarization and Assignment of the Two-Photon Spectrum of Benzene Vapor. *Chem. Phys. Lett.* **1975**, *32*, 541-549.

75. Wunsch, L.; Metz, F.; Neusser, H.J.; Schlag, E.W. Two-photon Spectroscopy in the Gas Phase: Assignments of Molecular Transitions in Benzene. *J. Chem. Phys.* **1977**, *66*, 386-400.

76. Hochstrasser, R.M.; Sung, H.N.; Wessel, J.E. Moderate-Resolution Two-Photon Spectrum of the Naphthalene Crystal and Naphthalene in Durene. *Chem. Phys. Lett.* **1974**, *24*, 168-171.

77. Mikami, N.; Ito, M. Two-Photon Excitation Spectra of Naphthalene-$h_8$ and -$d_8$: Vibronic Coupling Involving the Ground State. *Chem. Phys.* **1977**, *23*, 141-152.

78. Marconi, G.; Orlandi, G. Vibronic Activity of $b_{2u}$ Modes in the Two-Photon Spectrum of Naphthalene. *J. Chem. Soc., Faraday Trans.* **1982**, *78*, 565-572.

79. Salvi, P.R.; Marconi, G. On the Nature of the Two Low-Lying Singlet States of Anthracene: Vibronic Activity in the Two-Photon Excitation Spectrum. *J. Chem. Phys.* **1986**, *84*, 2542-2555.

80. Wolf, J.; Hohlneicher, G. High-Resolution One- and Two-Photon Spectra of Matrix-Isolated Anthracene. *Chem. Phys.* **1994**, *181*, 185-208.

81. Bree, A.; Leyderman, A.; Salvi, P.R.; Taliani, C. A Study of the Two-Photon Spectrum and Vibronic Coupling in the First System of Pyrene. *Chem. Phys.* **1986**, *110*, 211-225.

82. Liem, N.Q.; Marconi, G.; Salvi, P.R. Two-Photon Vibronic Transitions in Crystalline Chrysene. *Chem. Phys.* **1990**, *144*, 425-435.

83. Catani, L.; Gellini, C.; Moroni, L.; Salvi, P.R. Two-Photon Fluorescence Excitation Spectrum of 1,6-Methano-[10]Annulene. *J. Phys. Chem. A* **2000**, *104*, 6566-6572.

84. Borden, W.T.; Davidson, E.R. Effects of Electron Repulsion in Conjugated Hydrocarbon Diradicals. *J. Am. Chem. Soc.* **1977**, *99*, 4587-4594.

85. Voter, A.F.; Goddard, W.A., III. The Generalized Resonating Valence Bond Description of Cyclobutadiene. *J. Am. Chem. Soc.* **1986**, *108*, 2830-2837.

86. Fratev, F.; Monev, V.; Janoschek, R. *Ab Initio* Study of Cyclobutadiene in Excited States: Optimized Geometries, Electronic Transitions and Aromaticities. *Tetrahedron* **1982**, *38*, 2929-2932.

87. Jafri, J.A.; Newton, M.D. Potential Energy Surfaces of Cyclobutadiene: *Ab Initio* SCF and CI calculations for the Low-Lying Singlet and Triplet States. *J. Am. Chem. Soc.* **1978**, *100*, 5012-5017.

88. Agren, H.; Correia, N.; Flores-Riveros, A.; Jensen, H.J.A. Direct Restricted-Step MCSCF Calculations on the Structure and Spectrum of Cyclobutadiene. *Int. J. Quantum Chem.* **1986**, *19*, 237-246.

89. Nakamura, K.; Osamura, Y.; Iwata, S. Second-Order Jahn-Teller Effect of Cyclobutadiene in Low-Lying States. An MCSCF Study. *Chem. Phys.* **1989**, *136*, 67-77.

90. Balkova', A.; Bartlett, R.J. A Multireference Coupled-Cluster Study of the Ground State and Lowest Excited States of Cyclobutadiene. *J. Chem. Phys.* **1994**, *101*, 8972-8987.

91. Eckert-Maksic, M.; Vazdar, M.; Barbatti, M.; Lischka, H.; Maksic, Z.B. Automerization Reaction of Cyclobutadiene and its Barrier Height: An *ab initio* Benchmark Multireference Average-Quadratic Coupled Cluster Study. *J. Chem. Phys.* **2006**, *125*, 064310: 1-9 .

92. Salvi, P.R.; Gellini, C. Recent Studies on Antiaromatic Molecules. *Trends Chem. Phys.* **1997**, *6*, 215-245.

93. Kollmar, H.; Staemmler, V. A Theoretical Study of the Structure of Cyclobutadiene. *J. Am. Chem. Soc.* **1977**, *99*, 3583-3587.

94. Borden, W.T.; Davidson, E.R.; Hart, P. The Potential Surfaces for the Lowest Singlet and Triplet States of Cyclobutadiene. *J. Am. Chem. Soc.* **1978**, *100*, 388-392.

95. Herzberg, G. *Electronic Spectra of Polyatomic Molecules*; Van Nostrand: New York, NY, USA, 1975.

96. Whitman, D.W.; Carpenter, B.K. Limits on the Activation Parameters for Automerization of Cyclobutadiene-1,2-$d_2$. *J. Am. Chem. Soc.* **1982**, *104*,6473-6474.

97. Carpenter, B.K. Heavy-Atom Tunnelling as the Dominant Pathway in a Solution-Phase Reaction? Bond Shift in Antiaromatic Annulenes. *J. Am. Chem. Soc.* **1983**, *105*, 1700-1701.

98. Carski, P.; Bartlett, R.J.; Fitzgerald, G.; Noga, J.; Spirko, V. *Ab Initio* Calculations on the Energy of Activation and Tunnelling in the Automerization of Cyclobutadiene. *J. Chem. Phys.* **1988**, *89*, 3008-3015.

99. Levchenko, S.V.; Krylov, A.I. Equation-of-Motion Spin-Flip Coupled-Cluster Model with Single and Double Substitutions: Theory and Application to Cyclobutadiene. *J. Chem. Phys.* **2004**, *120*, 175-185.

100. Wörner, H.J.; Merkt, F. Diradicals, Antiaromaticity, and the Pseudo-Jahn-Teller Effect: Electronic and Rovibronic Structures of the Cyclopentadienyl Cation. *J. Chem. Phys.* **2007**, *127*, 034303:1-16.

101. Baird, N.C. Quantum Organic Photochemistry. Resonance and Aromaticity in the Lowest $^3\pi\pi^*$ State of Cyclic Hydrocarbons. *J. Am. Chem. Soc.* **1972**, *94*, 4941-4948.

102. Gogonea, V.; Schleyer, P.v.R.; Schreiner, P.R. Consequences of Triplet Aromaticity in $4n\pi$-Electron Annulenes: Calculation of Magnetic Shieldings for Open-Shell Species. *Angew. Chem. Int. Ed. Engl.* **1998**, *37*, 1945-1948.

103. Cox, E.G.; Cruickshank, D.W.J.; Smith, J.A.S. The Crystal Structure of Benzene at -3 °C. *Proc. R. Soc. London, Ser A.* **1958**, *247*, 1-21.

104. Bacon, G.E.; Curry, N.A.; Wilson, S.A. A Crystallographic Study of Solid Benzene by Neutron Diffraction. *Proc. R. Soc. London, Ser A.* **1964**, *279*, 98-110.

105. Kimura, K.; Kubo, M. Application of Least-Squares Method to Gaseous Benzene in Electron Diffraction Investigations. *J. Chem. Phys.* **1960**, *32*, 1776-1780.

106. Langseth, A.; Stoicheff, B.P. High Resolution Raman Spectroscopy of Gases: VI. Rotational Spectrum of Symmetric Benzene-$d_3$. *Can. J. Phys.* **1956**, *34*, 350-353.

107. Ermer, O. Concerning the Structure of Benzene. *Angew. Chem. Int. Ed. Engl.* **1987**, *26*, 782-784.

108. Bürgi, H.-B.; Capelli, S.C. Getting More out of Crystal-Structure Analyses. *Helv. Chim. Acta* **2003**, *86*, 1625-1640.

109. Jeffrey, G.A.; Ruble, J.R.; McMullan, R.K.; Pople, J.A. The Crystal Structure of Deuterated Benzene. *Proc. R. Soc. Lond., Sect. A* **1987**, *414*, 47-57.

110. Janoschek, R. Back to the Structure of Benzene. *Angew. Chem. Int. Ed. Engl.* **1987**, *26*, 1298.

111. Almlöf, J.; Faegri, K. Basis Set Effects in Hartree-Fock Studies on Aromatic Molecules: Hartree-Fock Calculations of Properties in Benzene and Hexafluorobenzene. *J. Chem. Phys.* **1983**, *79*, 2284-2294.

112. Haddon, R.C.; Raghavachari, K. Comparative Molecular Orbital Study of [6]-, [10]-, and [18]Annulenes and the Bridged [10]Annulenes. *J. Am. Chem. Soc.* **1985**, *107*, 289-298.

113. Goodman, L.; Ozkabak, A.G.; Thakur, S.N. A Benchmark Vibrational Potential Surface: Ground-State Benzene. *J. Phys. Chem.* **1991**, *95*, 9044-9058.

114. Handy, N.C.; Maslen, P.E.; Atoms, R.D.; Murray, C.W.; Laming, G. The Harmonic Frequencies of Benzene. *Chem. Phys. Lett.* **1992**, *197*, 506-515.

115. Orlandi, G.; Palmieri, P.; Tarroni, R.; Zerbetto, F.; Zgierski, M.Z.The $S_0(1A_g) - S_1(1B_{2u})$ Vibronic Transition in Benzene: An *ab initio* Study. *J. Chem. Phys.* **1994**, *100*, 2458-2464.

116. Bohm, M.C.; Schulte, J.; Ramirez, R. Excited State Properties of $C_6H_6$ and $C_6D_6$ Studied by Feynman Path Integral - *Ab Initio* Simulations. *J. Phys. Chem. A* **2002**, *106*, 3169-3180.

117. Karadakov, P.B. Ground- and Excited-State Aromaticity and Antiaromaticity in Benzene and Cyclobutadiene. *J. Phys. Chem. A* **2008**, *112*, 7303-7309.

118. Moran, D.; Simmonett, A.C.; Leach, F.E., III.; Allen, W.D.; Schleyer,P.v.R.; Schaefer, H.F., III. Popular Theoretical Methods Predict Benzene and Arenes To Be Nonplanar. *J. Am. Chem. Soc.* **2006**, *128*, 9342-9343.

119. Osamura, Y. The Molecular Structure of the Lowest Triplet State of Benzene: Quinoid or Anti-Quinoid? *Chem. Phys. Lett.* **1988**, *145*, 541-544.

120. Buma, W.J.; van der Waals, J.H.; van Hemert, M.C.Conformational Instability of the Lowest Triplet State of the Benzene Nucleus. The Unsubstituted Molecule. *J. Chem. Phys.* **1990**, *93*, 3733-3745.

121. Callomon, J.H.; Dunn, T.M.; Mills, I.M. Rotational Analysis of the 2600 Angstrom Absorption System of Benzene. *Philos. Trans. R. Soc. London, Sez. A* **1966**, *259*, 499-532.

122. Lombardi, J.R.; Wallenstein, R.; Haensch, T.W.; Friedrich, D.M. High Resolution Two-Photon Spectroscopy in the $^1B_{2u}$ State of Benzene. *J. Chem. Phys.* **1976**, *65*, 2357.

123. Kato, S. A Theoretical Study on the Mechanism of Internal Conversion of $S_1$ Benzene. *J. Chem. Phys.* **1988**, *88*, 3045-3056.

124. Nakajima, T.; Toyota, A.; Kataoka, M. Geometrical Structures of Electronically Excited States of Conjugated Hydrocarbons. *J. Am. Chem. Soc.* **1982**, *104*, 5610-5616.

125. Malar, E.J.P.; Jug, K. Excited States of Benzene and Its Derivatives. *J. Phys. Chem.* **1984**, *88*, 3508-3516.

126. Meisl, M.; Janoschek, R. The Dynamics of Low-Lying Excited States of Benzene: the Biradical Structure of the $S_2$ State. *J. Chem. Soc., Chem. Commun.* **1986**, 1066-1067.

127. Nakashima, N.; Inoue, H.; Sumitani, M.; Yoshihara, K. Laser Flash Photolysis of Benzene. III. $S_n \leftarrow S_1$ Absorption of Gaseous Benzene. *J. Chem. Phys.* **1980**, *73*, 5976-5980.

128. Hay, P.J.; Shavitt, I. *Ab Initio* Configuration Interaction Studies of the $\pi$-Electron States of Benzene. *J. Chem. Phys.* **1974**, *60*, 2865-2877.

129. Matos, J.M.; Roos, B.O.; Malmqvist, P.A. A CASSCF-CCI Study of the Valence and Lower Excited States of the Benzene Molecule. *J. Chem. Phys.* **1987**, *86*, 1458-1466.

130. Kitao, O.; Nakatsuji, H. Cluster Expansion of the Wave Function. Valence and Rydberg Excitations and Ionizations of Benzene. *J. Chem. Phys.* **1987**, *87*, 1169-1182.

131. Ghigo, G.; Roos, B.O.; Malmqvist, P.A. A Modified Definition of the Zeroth-Order Hamiltonian in Multiconfigurational Perturbation Theory (CASPT2). *Chem. Phys. Lett.* **2004**, *396*, 142-149.

132. Devarajan, A.; Gaenko, A.V.; Khait, Y.G.; Hoffmann, M.R. Generalized van Vleck Perturbation Theory (GVVPT2) Study of the Excited States of Benzene and the Azabenzenes. *J. Phys. Chem. A* **2008**, *112*, 2677-2682.

133. Craig, M.; Berry, R.S. Covalent and Ionic Character in Ground and Excited States of Benzene. *J. Am. Chem. Soc.* **1967**, *89*, 2801-2805.

134. Buma, W.J.; van der Waals, J.H.; van Hemert, M.C. Conformational Instability of the Lowest Triplet State of Benzene: The Result of *Ab Initio* Calculations. *J. Am. Chem. Soc.* **1989**, *111*, 86-87.

135. de Groot, M.S.; van der Waals, J.H. Paramagnetic Resonance in Phosphorescent Aromatic Hydrocarbons. *Mol. Phys.* **1963**, *6*, 545-562.

136. de Groot, M.S.; Hesselman, I.A.M.; van der Waals, J.H. Electron Resonance of Phosphorescent Benzene in a Single Crystal. *Mol. Phys.* **1967**, *13*, 583-586.

137. Burland, D.M.; Castro, G.; Robinson, G.W.J. Experimental Observation of Singlet-Triplet Absorption in Pure Crystalline Benzene. *J. Chem. Phys.* **1970**, *52*, 4100-4108.

138. Hochstrasser, R.M.; Wessel, J.E.; Zewail, A.H. Zeeman Effect Studies of the Triplet States of Benzene. *J. Chem. Phys.* **1971**, *55*, 3596-3597.

139. Karle, I.L. An Electron Diffraction Investigation of Cyclooctatetraene and Benzene. *J. Chem. Phys.* **1952**, *20*, 65-70.

140. Bastiansen, O.; Hedberg, L.; Hedberg, K. Reinvestigation of the Molecular Structure of 1,3,5,7-Cyclooctatetraene by Electron Diffraction. *J. Chem. Phys.* **1957**, *27*, 1311-1317.

141. Tratteberg, M. The Molecular Structure of 1,3,5,7-Cyclo-Octatetraene. *Acta Chem. Scand.* **1966**, *20*, 1724-1726.

142. Bordner, J.; Parker, R.G.; Stanford, R.H. The Crystal Structure of Octamethylcyclooctatetraene. *Acta Crystallogr. B* **1972**, *28*, 1069-1075.

143. Claus, K.H.; Kruger, C. Structure of Cyclooctatetraene at 129 K. *Acta Crystallogr. C* **1988**, *44*, 1632-1634.

144. Kummli, D.S.; Lobsiger, S.; Frey, H.M.; Leutwyler, S.; Stanton, J.F. Accurate Determination of the Structure of Cyclooctatetraene by Femtosecond Rotational Coherence Spectroscopy and *Ab Initio* Calculations. *J. Phys. Chem. A* **2008**, *112*, 9134-9143.

145. Paquette, L.A. The Current View of Dynamic Change within Cyclooctatetraenes. *Acc. Chem. Res.* **1993**, *26*, 57-62.

146. Anet, F.A.L. The Rate of Bond Change in Cyclooctatetraene. *J. Am. Chem. Soc.* **1962**, *84*, 671-672.

147. Hrovat, D.A.; Borden, W.T. CASSCF Calculations Find That a $D_{8h}$ Geometry Is the Transition State for Double-Bond Shifting in Cyclooctatetraene. *J. Am. Chem. Soc.* **1992**, *114*, 5879-5881.

148. Andres, J.L.; Castano, O.; Morreale, A.; Palmeiro, R.; Gomperts, R. Potential Energy Surface of Cyclooctatetraene. *J. Chem. Phys.* **1998**, *108*, 203-207.

149. Smith, L.R. Schemes and Transformations in the $(CH)_8$ Series. *J. Chem. Educ.* **1978**, *55*, 569-570.

150. Balaban, A.T.; Banciu, M. Schemes and Transformations in the $(CH)_{2k}$ Series. Valence Isomers of [8]- and [10]-Annulene. *J. Chem. Educ.* **1984**, *61*, 766-770.

151. Wenthold, P.G.; Hrovat, D.A.; Borden, W.T.; Lineberger, W.T. Transition-State Spectroscopy of Cyclooctatetraene. *Science* **1996**, *272*, 1456-1459.

152. Castano, O.; Frutos, L.M.; Palmeiro, R.; Notario, R.; Andres, J.L.; Gomperts, R.; Blancafort, L.; Robb, M.A. The Valence Isomerization of Cyclooctatetraene to Semibullvalene. *Angew. Chem. Angew. Int. Ed. Engl.* **2000**, *39*, 2095-2097.

153. Castano, O.; Notario, R.; Gomperts, R.; Abboud, J.L.M.; Palmeiro, R.; Andres, J.L. Heats of Formation of 1,3,5,7-Cyclooctatetraene and Bicyclo[4.2.0]octa-2,4,7-triene. A High-Level *Ab Initio* Study. *J.Phys. Chem. A* **1998**, *102*, 4949-4951.

154. Jiao, H.J.; Nagelkerke, R.; Kurtz, H.A.; Williams, R.V.; Borden, W.T.; Schleyer,P.v.R. Annelated Semibullvalenes: A Theoretical Study of How They "Cope" with Strain. *J. Am. Chem. Soc.* **1997**, *119*, 5921-5929.

155. Garavelli, M.; Bernardi, F.; Moliner, V.; Olivucci, M. Intrinsically Competitive Photoinduced Polycyclization and Double-Bond Shift through a Boatlike Conical Intersection. *Angew. Chem. Angew. Int. Ed. Engl.* **2001**, *40*, 1466-1468.

156. Garavelli, M.; Bernardi, F.; Cembran, A.; Castano, O.; Frutos, L.M.; Merchan, M.; Olivucci, M. Cyclooctatetraene Computational Photo- and Thermal Chemistry: A Reactivity Model for Conjugated Hydrocarbons. *J. Am. Chem. Soc.* **2002**, *124*, 13770-13789.

157. Falchi, A.; Gellini, C.; Salvi, P.R.; Hafner, K. Vibrational and Electronic Properties of Antiaromatic Systems: A Spectroscopic Study of 1,3,5-Tri-*tert*-Butylpentalene. *J. Phys. Chem.* **1995**, *99*, 14659-14666.

158. Zywietz, T.K.; Jiao, H.; Schleyer, P.v.R.; de Meijere, A. Aromaticity and Antiaromaticity in Oligocyclic Annelated Five-Membered Ring Systems. *J. Org. Chem.* **1998**, *63*, 3417-3422.

159. Kitschke, B.; Lindner, H.J. The Crystal and Molecular Structure of Two Substituted Pentalenes. *Tetrahedron Lett.* **1977**, *29*, 2511-2514.

160. Bussotti, L.; Foggi, P.; Gellini, C.; Moroni, L.; Salvi, P.R. The Transient Absorption of 1,3,5-Tri-*tert*-Butylpentalene. *PCCP* **2001**, *3*, 3027-3033.

161. Falchi, A.; Gellini, C.; Salvi, P.R.; Hafner, K. Reply to Comment on "Fluorescence of Antiaromatic Systems: An Experimental and Theoretical Study of 1,3,5-Tri-*tert*-Butylpentalene. *J. Phys. Chem. A* **2000**, *104*, 1078.

162. Bischof, P.; Gleiter, R.; Hafner, K.; Knauer, K.H.; Spanget-Larsen, J.; Süss, H.U. Das Photoelektronen- und Elektronenspektrum des 1,3,5-Tri-*tert*-Butylpentalenes. Hinweis auf Bindungsalternanz im Grundzustand. *Chem.Ber.* **1978**, *111*, 932-938.

163. Sondheimer, F.; Gaoni, Y. Unsaturated Macrocyclic Compounds. XV Cyclotetradecaheptaene. *J. Am. Chem. Soc.* **1960**, *82*, 5765-5766.

164. Sondheimer, F.; Wolovsky, R.; Amiel, Y. Unsaturated Macrocyclic Compounds. The Synthesis of the Fully Conjugated Macrocyclic Polyenes Cyclooctatetraene ([18]Annulene), Cyclotetracosadodecaene ([24]Annulene), and Cyclotriacontapentadecaene ([30]Annulene). *J. Am. Chem. Soc.* **1962**, *84*, 274-284.

165. Vogel, E.; Roth, H.D. The Cyclodecapentaene System. *Angew. Chem. Int. Ed. Engl.* **1964**, *3*, 228-229.

166. Vogel, E.; Klug, W.; Breuer, A. 1,6-Methano[10]Annulene. *Org. Synth. Coll. Vol. 6* **1988**, *54*, 731-732.

167. van Tammelen, E.E.; Burkoth, T.L. Cyclodecapentaene. *J. Am. Chem. Soc.* **1967**, *89*, 151-152.

168. Masamune, S.; Seidner, R.T. [10]Annulene. *J. Chem. Soc., Chem. Commun.* **1969**, 542-544.

169. Masamune, S.; Hojo, K.; Bigam, G.; Rabenstein, D.L. The Geometry of [10]Annulenes. *J. Am. Chem. Soc.* **1971**, *93*, 4966-4968.

170. Farnell, L.; Kao, J.; Radom, L.; Schaefer, H.F., III. Structures and Stabilities of Isomeric [10]Annulenes. *J. Am. Chem. Soc.* **1981**, *103*, 2147-2151.

171. Xie, Y.; Schaefer, H.F., III.; Liang, G.; Bowen, J.P. [10]Annulene: the Wealth of Energetically Low-Lying Structural Isomers of the Same $(CH)_{10}$ Connectivity. *J. Am. Chem. Soc.* **1994**, *116*, 1442-1449.

172. Sulzbach, H.M.; Schleyer,P.v.R.; Jiao, H.; Xie, Y.; Schaefer, H.F., III. A [10]Annulene Isomer May Be Aromatic, After All! *J. Am. Chem. Soc.* **1995**, *117*, 1369-1373.

173. Sulzbach, H.M.; Schaefer, H.F., III.; Klopper, W.; Lüthi, H.P. Exploring the Boundary between Aromatic and Olefinic Character: Bad News for Second-Order Perturbation Theory and Density Functional Schemes. *J. Am. Chem. Soc.* **1996**, *118*, 3519-3520.

174.  King, R.A.; Crawford, T.D.; Stanton, J.F.; Schaefer, H.F., III. Conformations of [10]Annulene: More Bad News for Density Functional Theory and Second-Order Perturbation Theory. *J. Am. Chem. Soc.* **1999**, *121*, 10788-10793.

175.  Price, D.R.; Stanton, J.F. Computational Study of [10]Annulene NMR Spectra. *Org. Lett.* **2002**, *4*, 2809-2811.

176.  Orlova, G.; Goddard, J.D. Practical Failures from the Inclusion of Exact Exchange: How Much Exact Exchange Is Appropriate? *Mol. Phys.* **2002**, *100*, 483-497.

177.  Sancho-Garcia, J.C. Assessment of Recently Developed Multicoefficient Strategies for the Treatment of π-Conjugated Molecules. *J. Phys. Chem. A* **2005**, *109*, 3470-3475.

178.  Bettinger, H.F.; Sulzbach, H.M.; Schleyer, P.v.R.; Schaefer, H.F., III. Aza[10]annulene: Next Higher Aromatic Analogue of Pyridine. *J. Org. Chem.* **1999**, *64*, 3278-3280.

179.  Fokin, A.A.; Jiao, H.; Schleyer, P.v.R. From Dodecahedrapentaene to the "[*n*]Trannulenes". A New In-Plane Aromaticity Family. *J. Am. Chem. Soc.* **1998**, *120*, 9364-9365.

180.  Burley, G.A. Trannulenes with "In-Plane" Aromaticity: Candidates for Harvesting Light Energy. *Angew. Chem. Int. Ed.* **2005**, *44*, 3176-3178.

181.  Wei, X.W.; Darwish, A.D.; Boltalina, O.V.; Hitchcock, P.B.; Street, J.M.; Taylor, R. The Remarkable Stable Emerald Green $C_{60}F_{15}[CBr(CO_2Et)_2]_3$: The First [60]Fullerene That Is also the First [18]Trannulene. *Angew. Chem. Int. Ed.* **2001**, *40*, 2989-2992.

182.  Troshin, P.; Lyubovskaya, R.N.; Ioffe, I.N.; Shustova, N.B.; Kemnitz, E.; Troyanov, S.I. Synthesis and Structure of the Highly Chlorinated [60]fullerene $C_{60}Cl_{60}$ with a Drum-Shaped Carbon Cage. *Angew. Chem. Int. Ed.* **2005**, *44*, 234-237.

183.  Canteenwala, T.; Padmawar, P.A.; Chiang, L.Y. Intense Near-Infrared Optical Absorbing Emerald Green [60]Fullerene. *J. Am. Chem. Soc.* **2005**, *127*, 26-27.

184.  Burley, G.A.; Avent, A.G.; Boltalina, O.V.; Gol'dt, I.V.; Guldi, D.M.; Marcaccio, M.; Paolucci, F.; Paolucci, D.; Taylor, R. A Light-Harvesting Fluorinated Fullerene Donor-Acceptor Ensemble: Long-Lived Charge Separation. *Chem. Comm.* **2003**, 148-149.

185.  Schleyer, P.v.R.; Jiao, H.; Sulzbach, H.M.; Schaefer, H.F., III. Highly Aromatic Planar *all-cis*-[10]Annulene Derivatives. *J. Am. Chem. Soc.* **1996**, *118*, 2093-2094.

186.  Navarro-Vazquez, A.; Schreiner, P.R. 1,2-Didehydro[10]annulenes: Structures, Aromaticity, and Cyclizations. *J. Am. Chem. Soc.* **2005**, *127*, 8150-8159.

187.  Bianchi, R.; Pilati, T.; Simonetta, M. Structure of 1,6-Methano[10]Annulene. *Acta Cryst.* **1980**, *B36*, 3146-3148.

188.  Dobler, M.; Dunitz, J.D. Die Kristallstruktur der 1,6-Methano-cyclodecapentaen-2-carbonsäure. *Helv. Chim. Acta* **1965**, *48*, 1429-1440.

189.  Bürgi, H.B.; Schefter, E.; Dunitz, J.D. Chemical Reaction Paths - VI: A Pericyclic Ring Closure. *Tetrahedron* **1975**, *31*, 3089-3092.

190.  Bailey, N.A.; Mason, R. The Molecular Structure of 1,6-Epoxy[10]Annulene. *Chem. Comm.* **1967**, 1039-1040.

191.  Bianchi, R.; Morosi, G.; Mugnoli, A.; Simonetta, M. The Influence of Substituents on the Equilibrium Bisnorcaradiene - [10]Annulene. The Crystal and Molecular Structure of 11,11-Dimethyltricyclo[4,4,1,0]undeca-2,4,7,9-tetraene. *Acta Cryst.* **1973**, *B29*, 1196-1208.

192. Bianchi, R.; Pilati, T.; Simonetta, M. The Influence of Substituents on the Equilibrium Bisnorcaradiene - [10]Annulene. The Crystal and Molecular Structure of 11-Methyltricyclo[4,4,1,0]undeca-2,4,7,9-tetraene-11-carbonitrile. *Acta Cryst.* **1978**, *B34*, 2157-2162.

193. Vogel, E.; Scholl, T.; Lex, J.; Hohlneicher, G. Norcaradiene Valence Tautomer of a 1,6-Methano[10]Annulene: Tricyclo [4.4.1.0]undeca-2,4,7,9-tetraene-11,11-dicarbonitrile. *Angew. Chem. Int. Ed. Engl.* **1982**, *21*, 869-870.

194. Neidlein, R.; Wirth, W.; Gieren, A.; Lamm, V.; Hubner, T. 2,5,7,10-Tetrakis(trimethylsilyl)-1,6-methano[10]annulene, a Fluxional Valence Tautomer with Cyclopolyolefin Structure. *Angew. Chem. Int. Ed. Engl.* **1985**, *24*, 587-588.

195. Gellini, C.; Salvi, P.R.; Vogel, E. Ground State of 1,6-Bridged [10] Annulenes: Infrared and Raman Spectra and Density Functional Calculations. *J. Phys. Chem. A* **2000**, *104*, 3110-3116.

196. Jiao, H.; van Eikema Hommes, N.J.R.; Schleyer, P.v.R. Can Bridged 1,6-X-[10]Annulenes (X= $SiH_2$, $SiMe_2$, PH and S) Exist? *Org. Lett.* **2002**, *4*, 2393-2396.

197. Choi, C.H.; Kertesz, M. New Interpretation of the Valence Tautomerism of 1,6-Methano[10]annulenes and Its Application to Fullerene Derivatives. *J. Phys. Chem. A* **1998**, *102*, 3429-3437.

198. Catani, L.; Gellini, C.; Salvi, P.R. Excited States of 1,6-Methano[10]annulene: Site Selection Fluorescence and Fluorescence Excitation Spectroscopy on $S_1$. *J. Phys. Chem. A* **1998**, *102*, 1945-1953.

199. Giugni, A.; Eramo, R.; Cavalieri, S.; Pietraperzia, G.; Becucci, M.; Gellini, C.; Moroni, L.; Salvi, P.R. The Jet Cooled $S_0 \rightarrow S_1$ Excitation Spectrum of 1,6-Epoxy-[10]annulene. *Chem. Phys. Lett.* **200**, *330*, 315-324.

200. Blattmann, H.R.; Boll, W.A.; Heilbronner, E.; Hohlneicher, G.; Vogel, E.; Weber, J.P. Die Elektronenzustände von Perimeter-$\pi$-Systemen: I. Die Elektronenspektren 1,6-überbrückter [10]-Annulene. *Helv. Chim. Acta* **1966**, *49*, 2017-2038.

201. Dewey, H.J.; Deger, H.; Frölich, W.; Dick, B.; Klingensmith, K.A.; Hohlneicher, G.; Vogel, E.; Michl, J. Excited States of Methano-Bridged [10]-, [14]-, and [18]Annulenes. Evidence for Strong Transannular Interaction, and Relation to Homoaromaticity. *J. Am. Chem. Soc.* **1980**, *102*, 6412-6417.

202. Klingensmith, K.A.; Puttmann, W.; Vogel, E.; Michl, J. Applications of MCD Spectroscopy: MO Ordering and Transannular Interaction in 1,6-Methano[10]annulenes from Analysis of Substituent Effects. *J. Am. Chem. Soc.* **1983**, *105*, 3375-3380.

203. Seiler, R.; Kensy, U.; Dick, B. Fluorescence Excitation and UV-UV Double-Resonance Spectroscopy of the $S_0 \rightarrow S_1(L_b)$ Transition of 1,6-Methano[10]annulene Cooled in a Supersonic Jet. *PCCP* **2001**, *3*, 5373-5382.

204. Nakano, H.; Yamanishi, M.; Hirao, K.Multireference Møller-Plesset Method: Accurate Description of Electronic States and Their Chemical Interpretation. *Trends Chem. Phys.* **1997**, *6*, 167-214.

205. Oth, J.F.M.; Röttele, H.; Schröder, G. [12]Annulene. *Tetrahedron Lett.* **1970**, 61-66.

206. Oth, J.F.M.; Gilles, J.M.; Schröder, G. Configuration and Conformational Mobility of [12]Annulene from NMR Studies at Various Temperatures. *Tetrahedron Lett.* **1970**, 67-72.

207. Kiesewetter, M.K.; Gard, M.N.; Reiter, R.C.; Stevenson, C.D. Reactions Involving Di-*trans*-[12]Annulenes. *J. Am. Chem. Soc.* **2006**, *128*, 15618-15624.

208. Castro, C.; Karney, W.L.; Vu, C.M.H.; Burkhardt, S.E.; Valencia, M.A. Computational Evaluation of the Evidence for Tri-*trans*-[12]Annulene. *J. Org. Chem.* **2005**, *70*, 3602-3609.

209. Braten, M.N.; Castro, C.; Herges, R.; Köhler, F.; Karney, W.L. The [12]Annulene Global Minimum. *J. Org. Chem.* **2008**, *73*, 1532-1535.

210. Hertwig, R.H.; Holthausen, M.C.; Koch, W.; Maksic, Z.B. *Ab Initio* MO and Approximate Density Functional Theory Studies on the Lowest Singlet and Triplet States of $s$- and $as$-Indacene. *Int. J. Quantum Chem.* **1995**, *54*, 147-159.

211. Nendel, M.; Goldfuss, B.; Houk, K.N.; Hafner, K. $s$-Indacene, a Quasi-Delocalized Molecule with Mixed Aromatic and Anti-Aromatic Character. *J. Mol. Struct. (THEOCHEM)* **1999**, *461*, 23-28.

212. Moroni, L.; Gellini, C.; Salvi, P.R. The Conformational Isomerism of 1,3,5,7-Tetra-*tert*-butyl-indacene. *J. Mol. Struct. (THEOCHEM)* **2004**, *677*, 1.

213. Gellini, C.; Cardini, G.; Salvi, P.R.; Marconi, G.; Hafner, K. The Ground State of Antiaromatic 1,3,5,7-Tetra-*tert*-butyl-$s$-indacene. *J. Phys. Chem.* **1993**, *97*, 1286-1293.

214. Gellini, C.; Angeloni, L.; Salvi, P.R.; Marconi, G. Excited States of $s$-Indacene. *J. Phys. Chem.* **1995**, *99*, 85-93.

215. Beer, M.; Longuet-Higgins, H.C. Anomalous Light Emission of Azulene. *J. Chem. Phys.* **1955**, *23*, 1390-1392.

216. Klann, R.; Bäuerle, R.J.; Laermer, F.; Elsaesser, T.; Niemeyer, M.; Lüttke, W. Radiationless Processes in Antiaromatic Molecules: the Photophysics of $s$-Indacene Studied by Ultrashort Light Pulses. *Chem. Phys. Lett.* **1990**, *169*, 172-178.

217. Gellini, C.; Salvi, P.R.; Hafner, K. Fluorescence Emission and Conformational Changes of 1,3,5,7-Tetra-$t$-butyl-$s$-indacene (TTBI). *J. Phys. Chem.* **1993**, *97*, 8152-8157.

218. Birks, J.B. *Photophysics of Aromatic Molecules*. Wiley-Interscience, New York, 1970.

219. Bearpark, M.J.; Celani, P.; Jolibois, F.; Olivucci, M.; Robb, M.A.; Bernardi, F. Characterization of the Indacene $S_0/S_1$ Conical Intersection: an MMVB and CASSCF Study. *Mol. Phys.* **1999**, *96*, 645-652.

220. Kautz, I.; Koch, T.; Malsch, K.; Hohlneicher, G. Ground State Vibrations of Biphenylene: Experiment and Theory. *J. Mol. Struct. (THEOCHEM)* **1997**, *417*, 223-236.

221. Zanon, I. Near Ultra-Violet Absorption Spectrum of Biphenylene. *J. Chem. Soc. Faraday Trans. II* **1973**, *69*, 1164-1171.

222. Nickel, B.; Hertzberg, J. Prompt Fluorescence from Biphenylene in Liquid Solution: Absence of Detectable $S_2 \rightarrow S_0$ Fluorescence and Its Implications, Vibrational Structure and Polarization of $S_1 \rightarrow S_0$ Fluorescence, and Orientational Relaxation of Molecules in $S_1$. *Chem. Phys.* **1989**, *132*, 219-234.

223. Hochstrasser, R.M. Electronic Absorption Spectrum of Diphenylene in Substitutional Solid-Solid Solution. *J. Chem. Phys.* **1960**, *33*, 950-951.

224. Yamaguchi, H.; Ata, M.; Mc Omie, J.W.F.; Barton, J.W.; Baumann, H. Electronic Spectra of Biphenylene and Diazabiphenylenes. *J. Chem. Soc. Faraday Trans. II* **1983**, *79*, 599-609.

225. Bich, V.T.; Bini, R.; Salvi, P.R.; Marconi, G. Two-Photon Spectroscopy of Antiaromatic Molecules: the Case of Biphenylene. *Chem. Phys. Lett.* **1990**, *175*, 413-418.

226. Gellini, C.; Salvi, P.R.; Orlic, N. Inductive Effects in Alternants Hydrocarbons: the Two-Photon Spectra of Biphenylene and 2,3,6,7-Tetra-ethyl-biphenylene. *Chem. Phys. Lett.* **1995**, *246*, 335-340.

227. Callis, P.R.; Scott, T.W.; Albrecht, A.C. Perturbation Selection Rules for Multiphoton Electronic Spectroscopy of Neutral Alternant Hydrocarbons. *J. Chem. Phys.* **1983**, *78*, 16-22.

228. Chiang, C.C.; Paul, I.C. Crystal and Molecular Structure of [14]Annulene. *J. Am. Chem. Soc.* **1972**, *94*, 4741-4743.

229. Herges, R. Topology in Chemistry: Designing Möbius Molecules. *Chem. Rev.* **2006**, *106*, 4820-4842.

230. Rzepa, H.S. Möbius Aromaticity and Delocalization. *Chem. Rev.* **2005**, *105*, 3697-3715.

231. Vogel, E.; Reel, H. Bent [14]Annulenes. Synthesis of 1,6:8,13-Ethanediylidene[14]annulene. *J. Am. Chem. Soc.* **1972**, *94*, 4388-4389.

232. Vogel, E.; Vogel, A.; Kübbeler, H.K.; Sturm, W. 1,6:8,13-Propanediylidene[14]annulene. *Angew. Chem. Int. Ed. Eng.* **1970**, *9*, 514-516.

233. Destro, R.; Pilati, T.; Simonetta, M. *syn*-1,6:8,13-Bismethano[14]annulene. *Acta Cryst.* **1977**, *B33*, 940-942.

234. Gramaccioli, C.M.; Mimun, A.S.; Mugnoli, A.; Simonetta, M. Crystal and Molecular Structure of 7-Methoxycarbonyl-*anti*-1,6:8,13-dimethano[14]annulene. *J. Am. Chem. Soc.* **1973**, *95*, 3149-3154.

235. Bianchi, R.; Casalone, G.; Simonetta, M. 15,16-Dimethyl-1,6:8,13-Ethanediylidene[14]annulene. *Acta Cryst. B* **1975**, *31*, 1207-1209.

236. Gavezzotti, A.; Mugnoli, A.; Raimondi, M.; Simonetta, M. Crystal and Molecular Structure of 1,6:8,13-Propane-1,3-Diylidene[14]Annulene. *J. Chem. Soc. Perkin Trans. II* **1972**, 425-431.

237. Nendel, M.; Houk, K.N.; Tolbert, L.M.; Vogel, E.; Jiao, H.; Schleyer, P.v.R. The Bond Localization Energies in the Aromatic Bismethano[14]annulenes. *Angew. Chem. Int. Ed. Engl.* **1997**, *36*, 748-750.

238. Nendel, M.; Houk, K.N.; Tolbert, L.M.; Vogel, E.; Jiao, H.; Schleyer, P.v.R. Bond Alternation and Aromatic Character in Cyclic Polyenes: Assessment of Theoretical Methods for Computing the Structures and Energies of Bismethano[14]annulenes. *J. Phys. Chem. A* **1998**, *102*, 7191-7198.

239. Moroni, L.; Gellini, C.; Salvi, P.R.; Liu, C.J.; Vogel, E. Vibrational Spectra and Density Functional Calculations of Bridged [14]Annulenes with an Anthracene Perimeter. *J. Phys. Chem. A* **2002**, *106*, 6554-6562.

240. Klingensmith, K.A.; Dewey, H.J.; Vogel, E.; Michl, J. Vibrational Structure of the $^1L_b$ Transition of 1,6:8,13-Ethano[14]annulene. Transannular Interaction, the "Mystery Band", and the Kekule Vibration. *J. Am. Chem. Soc.* **1989**, *111*, 1539-1546.

241. Moroni, L.; Gellini, C.; Salvi, P.R.; Vogel, E. Excited States of Bridged [14]Annulenes. *J. Phys. Chem. A* **2004**, *108*, 8279-8286.

242. Baumann, H.; Oth, J.F.M. The Low-Temperature UV/VIS Absorption Spectrum of [14]Annulene. *Helv. Chim. Acta* **1995**, *78*, 679-692.

243. Blattmann, H.R.; Boekelheide, V.; Heilbronner, E.; Weber, J.P. 10. Die Elektronenzustände von Perimeter-π-Systemen II. Das Elektronenspektrum des *trans*-15,16-Dimethyl-dihydropyrens. *Helv. Chim. Acta* **1967**, *50*, 68-84.

244. Kolc, J.; Michl, J.; Vogel, E. Excited States of Bridged [14]Annulenes with Anthracene Perimeter: Absorption, Polarized Emission, Linear Dichroism, and Magnetic Circular Dichroism. *J. Am. Chem. Soc.* **1976**, *98*, 3935-3948.

245. Sondheimer, F.; Gaoni, Y. Unsaturated Macrocyclic Compounds. XXIV. Synthesis of Four Completely Conjugated Sixteen-Membered Ring Cyclic Systems. *J. Am. Chem. Soc.* **1961**, *83*, 4863-4864.

246. Schröder, G.; Oth, J.F.M. Zu Kenntnis des [16]Annulens. *Tetrahedron Lett.* **1966**, 4083-4088.

247. Oth, J.F.M.; Gilles, J.M. Mobilite Conformationelle et Isomerie de Valence Rapide Reversible dans le [16]Annulene. *Tetrahedron Lett.* **1968**, 6259-6264.

248. Johnson, S.M.; Paul, I.C. Crystal and Molecular Structure of [16]Annulene. *J. Am. Chem. Soc.* **1968**, *90*, 6555-6556.

249. Johnson, S.M.; Paul, I.C.; King, G.S.D. [16]Annulene: the Crystal and Molecular Structure. *J. Chem. Soc. B* **1970**, 643-649.

250. Oth, J.F.M.; Baumann, H.; Gilles, J.M.; Schröder, G. The Radical Anion and the Dianion of [16]Annulene. *J. Am. Chem. Soc.* **1972**, *94*, 3498-3512.

251. Martin-Santamaria, S.; Lavan, B.; Rzepa, H.S. Hückel and Möbius Aromaticity and Trimerous Transition State Behaviour in the Pericyclic Reactions of [10], [14], [16] and [18]Annulenes. *J. Chem. Soc., Perkin Trans.* **2000**, *2*, 1415-1417.

252. Lee, H.L.; Li, W.K. Computational Study on the Electrocyclic Reactions of [16]Annulene. *Org. Biomol. Chem.* **2003**, *1*, 2748-2754.

253. Schröder, G.; Martin, W.; Oth, J.F.M. Thermal and Photochemical Behaviour of a [16]Annulene. *Angew. Chem. Int. Ed. Engl.* **1967**, *6*, 870-871.

254. Oth, J.F.M.; Anthoine, G.; Gilles, J.M. Le Dianion du [16]Annulene. *Tetrahedron Lett.* **1968**, 6265-6270.

255. Ajami, D.; Oeckler, O.; Simon, A.; Herges, R. Synthesis of a Möbius Aromatic Hydrocarbon. *Nature* **2003**, *426*, 819-821.

256. Ajami, D.; Hess, K.; Köhler, F.; Näther, C.; Oeckler, O.; Simon, A.; Yamamoto, C.; Okamoto, Y.; Herges, R. Synthesis and Properties of the First Möbius Annulenes. *Chem. Eur. J.* **2006**, *12*, 5434-5445.

257. Castro, C.; Isborn, C.M.; Karney, W.L.; Mauksch, M.; Schleyer, P.v.R. Aromaticity with a Twist: Möbius [4n]Annulenes. *Org. Lett.* **2002**, *4*, 3431-3434.

258. Castro, C.; Chen, Z.; Wannere, C.S.; Jiao, H.; Karney, W.L.; Mauksch, M.; Puchta, R.; van Eikema Hommes, N.J.R.; Schleyer, P.v.R. Investigation of a Putative Möbius Aromatic Hydrocarbon. The Effect of Benzannelation on Möbius [4n]Annulene Aromaticity. *J. Am. Chem. Soc.* **2005**, *127*, 2425-2432.

259. Sondheimer, F.; Wolovsky, R. The Synthesis of Cyclooctadecanonaene, a New Aromatic System. *Tetrahedron Lett.* **1959**, 3-6.

260. Bregman, J.; Hirshfeld, F.L.; Rabinovich, D.; Schmidt, G.M.J. The Crystal Structure of [18]Annulene. X-Ray Study. *Acta Crystallogr.* **1965**, *19*, 227-234.

261. Gorter, S.; Rutten-Keulemans, E.; Krever, M.; Romers, C.; Cruickshank, D.W.J. [18]Annulene, $C_{18}H_{18}$, Structure, Disorder and Hückel's $4n + 2$ Rule. *Acta Crystallogr. B* **1995**, *51*, 1036-1045.

262. Dewar, M.J.S.; Haddon, R.C.; Student, P.J. MINDO/3 Study of [18]Annulene. *J. Chem. Soc. Chem. Commun.* **1974**, 569-570.

263. Dewar, M.J.S.; McKee, M.L. Aspects of Cyclic Conjugation. *Pure Appl. Chem.* **1980**, *52*, 1431-1441.

264. Jiao, H.; Schleyer, P.v.R. Is Kekulene Really Superaromatic? *Angew. Chem. Int. Ed. Engl.* **1996**, *35*, 2383-2386.

265. Baldridge, K.K.; Siegel, J.S. *Ab Initio* Density Functional vs Hartree Fock Predictions for the Structure of [18]Annulene: Evidence for Bond Localization and Diminished Ring Currents in Bicycloannelated [18]Annulenes. *Angew. Chem. Int. Ed. Engl.* **1997**, *36*, 745-748.

266. Stevenson, C.D.; Kurth, T.L. Isotopic Perturbations in Aromatic Character and New Closely Related Conformers Found in [16]- and [18]Annulene. *J. Am. Chem. Soc.* **2000**, *122*, 722-723.

267. Ermer, O. Concerning the Structure of [18]Annulene. *Helv. Chim. Acta* **2005**, *88*, 2262-2266.

268. Baumann, H.; Oth, J.F.M. The Low Temperature UV/VIS Absorption Spectrum of [18]Annulene. *Helv. Chim. Acta* **1982**, *65*, 1885-1893.

269. Choi, C.H.; Kertesz, M.; Karpfen, A. Do Localized Structures of [14]- and [18]Annulenes Exist? *J. Am. Chem. Soc.* **1997**, *119*, 11994-11995.

270. Gouterman, M. *The Porphyrins*; Dolphin, D., Ed.; Academic Press: New York, NY, USA, 1978; Volume I-VII.

271. Shelnutt, J.A.; Song, X.Z.; Ma, J.G.; Jia, S.L.; Jentzen, W.; Medforth, C.J. Nonplanar Porphyrins and Their Significance in Proteins. *Chem. Soc. Rev.* **1998**, *27*, 31-41.

272. Vogel, E.; Haas, W.; Knipp, B.; Lex, J.; Schmickler, H. Tetraoxaporphyrin Dication. *Angew. Chem. Int. Ed. Engl.* **1988**, *27*, 406-409.

273. Vogel, E. Novel Porphyrinoid Macrocycles and Their Metal Complexes. *J. Heterocyclic Chem.* **1996**, *33*, 1461-1487.

274. Bachmann, A.; Gerson, F.; Gescheidt, G.; Vogel, E. Five Redox Stages of Tetraoxaporphyrin: a UV/Visible/Near-IR, ESR, and MO-Theoretical Study. *J. Am. Chem. Soc.* **1992**, *114*, 10855-10860.

275. Jelovica, I.; Moroni, L.; Gellini, C.; Salvi, P.R.; Orlic, N. Structural and Vibrational Properties of Tetraoxaporphyrin Dication, the Oxygen Analogue of Porphyrin, and of Isoelectronic Diprotonated Porphyrin. *J. Phys. Chem. A* **2005**, *109*, 9935-9944.

276. Almlöf, J.; Fischer, T.H.; Gassman, P.G.; Ghosh, A.; Haser, M. Electron Correlation in Tetrapyrroles. *Ab Initio* Calculations on Porphyrin and the Tautomers of Chlorin. *J. Phys. Chem.* **1993**, *97*, 10964-10970.

277. Kozlowski, P.M.; Zgierski, M.Z.; Pulay, P. An Accurate In-Plane Force Field for Porphine. A Scaled Quantum Mechanical Study. *Chem. Phys. Lett.* **1995**, *247*, 379-385.

278. Ghosh, A.; Almlöf, J. Structure and Stability of *cis*-Porphyrin. *J. Phys. Chem.* **1995**, *99*, 1073-1075.

279. Merchan, M.; Orti, E.; Roos, B.O. Ground State Free Base Porphin: $C_{2v}$ or $D_{2h}$ Symmetry? A Theoretical Contribution. *Chem. Phys. Lett.* **1994**, *221*, 136-144.

280. Reimers, J.R.; Lu, T.X.; Crossley, M.J.; Hush, N.S. The Mechanism of Inner-Hydrogen Migration in Free Base Porphyrin: *Ab Initio* MP2 Calculations. *J. Am. Chem. Soc.* **1995**, *117*, 2855-2861.

281. Malsch, K.; Roeb, M.; Karuth, V.; Hohlneicher, G. The Importance of Electron Correlation for the Ground State Structure of Porphycene and Tetraoxaporphyrin-Dication. *Chem. Phys.* **1998**, *227*, 331-348.

282. Wan, J.; Ren, Y.; Wu, J.; Xu, X. Time-Dependent Density Functional Theory Investigation of Electronic Excited States of Tetraoxaporphyrin Dication and Porphycene. *J. Phys. Chem. A* **2004**, *108*, 9453-9460.

283. Chen, B.M.L.; Tulinsky, A.J. Redetermination of the Structure of Porphine. *J. Am. Chem. Soc.* **1972**, *94*, 4144-4151.

284. Cheng, B.; Munro, O.Q.; Marques, H.M.; Scheidt, W.R. An Analysis of Porphyrin Molecular Flexibility - Use of Porphyrin Diacids. *J. Am. Chem. Soc.* **1997**, *119*, 10732-10742.

285. Ravikanth, M.; Chandrashekar, T.K. Nonplanar Porphyrins and Their Biological Relevance: Ground and Excited State Dynamics. *Struct. Bond.* **1995**, *82*, 105-188.

286. Chen, D.M.; Liu, X.; He, T.J.; Liu, F.C. Density Functional Theory Investigation of Porphyrin Diacid: Electronic Absorption Spectrum and Conformational Inversion. *Chem. Phys.* **2003**, *289*, 397-407.

287. Vogel, E.; Balci, M.; Pramod, K.; Koch, P.; Lex, J.; Ermer, O. 2,7,12,17-Tetrapropylporphycene - Counterpart of Octaethylporphyrin in the Porphycene Series. *Angew. Chem. Int. Ed. Engl.* **1987**, *26*, 928-931.

288. Waluk, J.; Müller, M.; Swiderek, P.; Köcher, M.; Vogel, E.; Hohlneicher, G.; Michl, J. Electronic States of Porphycenes. *J. Am. Chem. Soc.* **1991**, *113*, 5511-5527.

289. Cyranski, M.K.; Krygowski, T.M.; Wisiorowski, M.; van Eikema Hommes, N.J.R.; Schleyer, P.v.R. Global and Local Aromaticity in Porphyrins: an Analysis Based on Molecular Geometries and Nucleus-Independent Chemical Shifts. *Angew. Chem. Int. Ed. Engl.* **1998**, *37*, 177-180.

290. Kozlowski, P.M.; Jarzecki, A.A.; Pulay, P.; Li, X.Y.; Zgierski, M.Z. Vibrational Assignment and Definite Harmonic Force Field for Porphine. 2. Comparison with Nonresonance Raman Data. *J. Phys. Chem.* **1996**, *100*, 13985-13992.

291. Plus, R.; Lutz, M. Study of Band IV of Porphin by Resonance Raman Spectroscopy. *Spectrosc. Lett.* **1974**, *7*, 73-84.

292. Radziszewski, J.G.; Nepras, M.; Balaji, V.; Waluk, J.; Vogel, E.; Michl, J. Polarized Infrared Spectra of Photooriented Matrix-Isolated Free-Base Porphyrin Isotopomers. *J. Phys. Chem.* **1995**, *99*, 14254-14260.

293. Radziszewski, J.G.; Waluk, J.; Nepras, M.; Michl, J. Fourier Transform Fluorescence and Phosphorescence of Porphine in Rare Fas Matrices. *J. Phys. Chem.* **1991**, *95*, 1963-1969.

294. Kozlowski, P.M.; Jarzecki, A.A.; Pulay, P. Vibrational Assignment and Definite Harmonic Force Field for Porphine. 1. Scaled Quantum Mechanical Results and Comparison with Empirical Force Field. *J. Phys. Chem.* **1996**, *100*, 7007-7013.

295. Gouterman, M. In *The Porphyrins*; Dolphin, D., Ed.; Academic Press: New York, NY, USA, 1978; Volume III, pp. 1-165.

296. Gouterman, M. Study of the Effects of Substitution on the Absorption Spectra of Porphin. *J. Chem. Phys.* **1959**, *30*, 1139-1161.

297. Serrano-Andres, L.; Merchan, M.; Rubio, M.; Roos, B.O. Interpretation of the Electronic Absorption Spectrum of Free Base Porphin by Using Multiconfigurational Second-order Perturbation Theory. *Chem. Phys. Lett.* **1998**, *295*, 195-203.

298. Sundholm, D. Interpretation of the Electronic Absorption Spectrum of Free- Base Porphin Using Time-Dependent Density-Functional Theory. *PCCP* **2000**, *2*, 2275-2281.

299. Moroni, L.; Gellini, C.; Salvi, P.R.; Marcelli, A.; Foggi, P. Excited States of Porphyrin Macrocycles. *J. Phys. Chem. A* **2008**, *112*, 11044-11051.

300. Nagashima, U.; Takada, T.; Ohno, K. *Ab Initio* SCF-CI Calculation on Free Base Porphin and Chlorin; Theoretical Analysis on Intensities of the Absorption Spectra. *J. Chem. Phys.* **1986**, *85*, 4524-4529.

301. Nakatsuji, H.; Hasegawa, J.; Hada, M. Excited and Ionized States of Free Base Porphin Studied by the Symmetry Adapted Cluster-Configuration Interaction (SAC-CI) Method. *J. Chem. Phys.* **1996**, *104*, 2321-2329.

302. Nooijen, M.; Bartlett, R.J. Similarity Transformed Equation-of-Motion Coupled-Cluster Study of Ionized, Electron Attached, and Excited States of Free Base Porphin. *J. Chem. Phys.* **1997**, *106*, 6449-6455.

303. Tokita, Y.; Hasegawa, J.; Nakatsuji, H. SAC-CI Study on the Excited and Ionized States of Free-Base Porphin: Rydberg Excited States and Effect of Polarization and Rydberg Functions. *J. Phys. Chem. A* **1998**, *102*, 1843-1849.

304. Edwards, L.; Dolphin, D.H.; Gouterman, M.; Adler, A.D. Porphyrins XVII. Vapor Absorption Spectra and Redox Reactions: Tetraphenylporphins and Porphin. *J. Mol. Spectry* **1971**, *38*, 16-32.

305. Marcelli, A.; Foggi, P.; Moroni, L.; Gellini, C.; Salvi, P.R.; Badovinac, I.J.; Relaxation Properties of Porphyrin, Diprotonated Porphyrin, and Isoelectronic Tetraoxaporphyrin Dication in the $S_2$ State. *J. Phys. Chem. A* **2007**, *111*, 2276-2282.

306. Marcelli, A.; Foggi, P.; Moroni, L.; Gellini, C.; Salvi, P.R. Excited-State Absorption and Ultrafast Relaxation Dynamics of Porphyrins, Diprotonated Porphyrin, and Tetraoxaporphyrin Dication. *J. Phys. Chem. A* **2008**, *112*, 1864-1872.

307. Neuwhal, F.V.R.; Bussotti, L.; Foggi, P. In *Transient Absorption Spectroscopy with UV-Visible Sub-Picosecond Pulses*; Global Research Network: Trivandrum, India, 2000; Volume 1, pp. 77-94.

308. Foggi, P.; Neuwahl, F.V.R.; Moroni, L.; Salvi, P.R. $S_1 \to S_n$ and $S_2 \to S_n$ Absorption of Azulene: Femtosecond Transient Spectra and Excited State Calculations. *J. Phys. Chem. A* **2003**, *107*, 1689-1696.

309. Rodriguez, J.; Kirmaier, C.; Holten, D. Optical Properties of Metalloporphyrin Excited States. *J. Am. Chem. Soc.* **1989**, *111*, 6500-6506.

310. Akimoto, S.; Yamazaki, T.; Yamazaki, I.; Osuka, A. Excitation Relaxation of Zinc and Free-Base Porphyrin Probed by Femtosecond Fluorescence Spectroscopy. *Chem. Phys. Lett.* **1999**, *309*, 177-182.

311. Baskin, J.S.; Yu, H.Z.; Zewail, A.H. Ultrafast Dynamics of Porphyrins in the Condensed Phase: Free Base Tetraphenylporphyrin. *J. Phys. Chem. A* **2002**, *106*, 9837-9844.

312. Schalk, O.; Brands, H.; Balaban, T.S.; Unterreiner, A.N. Near-Infrared Excitation of the *Q* Band in Free Base and Zinc Tetratolyl-porphyrins. *J. Phys. Chem. A* **2008**, *112*, 1719-1729.

313. Gentemann, S.; Medforth, C.J.; Forsyth, T.P.; Nurco, D.J.; Smith, K.M.; Fajer, J.; Holten, D. Photophysical Properties of Conformationally Distorted Metal-Free Porphyrins. Investigation into the Deactivation Mechanism of the Lowest Excited Single State. *J. Am. Chem. Soc.* **1994**, *116*, 7363-7368.

314. Gentemann, S.; Nelson, N.Y.; Jaquinod, L.; Nurco, D.J.; Leung, S.H.; Medforth, C.J.; Smith, K.M.; Fajer, J.; Holten, D. Variations and Temperature Dependence of the Excited State Properties of Conformationally and Electronically Perturbed Zinc and Free Base Porphyrins. *J. Phys. Chem. B* **1997**, *101*, 1247-1254.

315. Chirvony, V.S.; van Hoek, A.; Galievski, V.A.; Sazanovich, I.V.; Schaafsma, T.J.; Holten, D. Comparative Study of the Photophysical Properties of Nonplanar Tetraphenylporphyrin and Octaethylporphyrin Diacids. *J. Phys. Chem. B* **2000**, *104*, 9909-9917.

316. Avilov, I.V.; Panarin, A.Y.; Chirvony, V.S. Quantum-Chemical and Experimental Kinetical Investigation of the Porphyrin Diacids: Role of the Counterions in Non-Radiative Deactivation of the Excited Electronic States. *Chem. Phys. Lett.* **2004**, *389*, 352-358.

317. Vogel, E.; Köcher, M.; Schmickler, H.; Lex, J.Porphycene - A Novel Porphyrin Isomer. *Angew. Chem. Int. Ed. Engl.* **1986**, *25*, 257-259.

318. Sessler, J.L.; Brucker, E.A.; Weghorn, S.J.; Kisters, M.; Schaefer, M.; Lex, J.; Vogel, E. Corrphycene: A New Porphyrin Isomer. *Angew. Chem. Int. Ed. Engl.* **1994**, *33*, 2308-2312.

319. Vogel, E.; Broering, M.; Wighorn, S.J.; Scholz, P.; Deponte, R.; Lex, J.; Schmickler, H.; Schaffner, K.; Braslavski, S.E.; Mueller, M.; Poerting, S.; Sessler, J.L.; Fowler, C. Octaethylhemiporphycene: Synthesis, Molecular Structure and Photophysics. *Angew. Chem. Int. Ed. Engl.* **1997**, *36*, 1651-1654.

320. Waluk, J. Ground- and Excited-State Tautomerism in Porphycenes. *Acc. Chem. Res.* **2006**, *39*, 945-952.

321. Kozlowski, P.M.; Zgierski, M.Z.; Baker, J. The Inner-Hydrogen Migration and Ground-State Structure of Porphycene. *J. Chem. Phys.* **1998**, *109*, 5905-5913.

322. Malsch, K.; Hohlneicher, G. The Force Field of Porphycene: a Theoretical and Experimental Approach. *J. Phys. Chem. A* **1997**, *101*, 8409-8416.

323. Waluk, J.; Vogel, E. Distance Dependence of Excited-State Double Proton Transfer in Porphycenes Studied by Fluorescence Polarization. *J. Phys. Chem.* **1994**, *98*, 4530-4535.

324.  Wehrle, B.; Limbach, H.H.; Köcher, M.; Ermer, O.; Vogel, E. ^{15}N-CPMAS-NMR Study of the Problem of NH Tautomerism in Crystalline Porphine and Porphycene. *Angew. Chem. Int. Ed. Engl.* **1987**, *26*, 934-936.

325.  Sepiol, J.; Stepanenko, Y.; Vdovin, A.; Mordzinski, A.; Vogel, E.; Waluk, J. Proton Tunnelling in Porphycene Seeded in a Supersonic Jet. *Chem. Phys. Lett.* **1998**, *296*, 549-556.

326.  Piwonski, H.; Stupperich, C.; Hartschuh, A.; Sepid, J.; Meixner, A.; Waluk, J. Imagin of Tautomerism in a Single Molecule. *J. Am. Chem. Soc.* **2005**, *127*, 5302-5303.

327.  Braun, J.; Schlabach, M.; Wehrle, B.; Köcher, M.; Vogel, E.; Limbach, H.H. NMR Study of the Tautomerism of Porphyrin Including the Kinetic HH/HD/DD Isotope Effects in the Liquid and the Solid State. *J. Am. Chem. Soc.* **1994**, *116*, 6593-6604.

328.  Sobolewski, A.L.; Gil, M.; Dobkowski, J.; Waluk, J. On the Origin of Radiationless Transitions in Porphycenes. *J. Phys. Chem. A* **2009**, *113*, 7714-7716.

329.  Fita, P.; Radzewicz, C.; Waluk, J. Electronic and Vibrational Relaxation of Porphycene in Solution. *J. Phys. Chem. A* **2008**, *112*, 10753-10757.

330.  Gomes, J.A.N.F.; Mallion, R.B. Aromaticity and Ring Currents. *Chem. Rev.* **2001**, *101*, 1349-1383.

331.  Chen, Z.; Wannere, C.S.; Corminboeuf, C.; Puchta, R.; Schleyer, P.v.R. Nucleus-Independent Chemical Shifts (NICS) as an Aromaticity Criterion. *Chem. Rev.* **2005**, *105*, 3842-3888.